Expression and function of the connexin43G138R mutation in mice causing oculodentodigital dyplasia (ODDD) in human

Dissertation

zur

Erlangung des Doktorgrades (Dr. rer. nat.)

der

Mathematisch-Naturwissenschaftlichen Fakultät

der

Rheinischen Friedrich-Wilhelms-Universität Bonn

vorgelegt von

Radoslaw Dobrowolski

aus

Radom

Bonn, 2008

Angefertigt mit Genehmigung der Mathematisch-Naturwissenschaftlichen Fakultät
der Rheinischen Friedrich-Wilhems-Universität Bonn

Erscheinungsjahr: 2008

Erstgutachter: Prof. Dr. Klaus Willecke

Zweigutachter: Prof. Dr. Karl-Heinz Scheidtmann

Fachnahes Mitglied: Prof. Dr. Dieter Fürst

Fachangrenzendes Mitglied: PD Dr. Gerhild van Echten-Deckert

Tag der Promotion: 15.07.2008 (entspricht dem Tag der mündl. Prüfung)

Erklärung

Hiermit versichere ich, dass diese Dissertation von mir selbst und ohne unerlaubte Hilfe angefertigt worden ist. Es wurden keine anderen als die angegebenen Hilfsmittel benutzt. Ferner erkläre ich, dass die vorliegende Arbeit an keiner anderen Universität als Dissertation eingereicht wurde.

Bonn, März 2008

.....
Radoslaw Dobrowolski

Danksagung

Herrn Prof. Dr. Klaus Willecke danke ich insbesondere für die Überlassung des interessanten Themas, die eingeräumten Freiheiten bei der Bearbeitung der Fragestellungen und die stete Unterstützung beim Aufbau von Kooperationen.

Herrn Prof. Dr. Karl-Heinz Scheidtmann danke ich für die Übernahme des Koreferates.

Herrn Prof. Dr. Dieter Fürst und Frau PD Dr. Gerhild van Echten-Deckert danke ich für die Bereitschaft der Promotionskommission als fachnahes und fachangrenzendes Mitglied zur Verfügung zu stehen.

Für die freundliche und erfolgreiche Kooperation sowie das Vermitteln neuer Techniken möchte ich mich bei den folgenden Mitgliedern auswärtiger Arbeitsgruppen bedanken: Dr. Philipp Sasse, Dr. Jan W. Schrickel, Dr. Alexander Ghanem, Dr. Clemens Troatz, Prof. Dr. Bernd Fleischmann, Prof. Dr. Thorsten Lewalter, PD Dr. Klaus Tiemann, Dr. Peter Bedner, Dr. Martin Theis, Dipl. Biol. Hildegard Lechner (Bonn), Dr. Mindaugas Rackauskas, Prof. Dr. Feliksas F. Bukauskas (New York), Dr. Jung-Sun Kim (Seoul), Dr. Marcus Watkins, Prof. Dr. Roberto Civitelli (St. Louis) und Hartmann Hartz (München).
Den ehemaligen und jetztigen Mitarbeitern des Instituts für Genetik danke ich für stete Diskussions- und Hilfsbereitschaft bei wissenschaflichen und technischen Fragen. Hierbei möchte ich besonders Dr. Markus Kretz, Dipl. Biol. Thorsten Höher, Dipl. Biol. Robert Requardt und Dipl. Biol. Oliver Tress hervorheben. Darüberhinaus möchte ich mich für die herzliche Atmosphäre bei allen Mitarbeitern des Labors 712 bedanken, insbesondere jedoch bei Indra Lübkemeier und Marina Frank.
Insbesondere möchte ich mich bei Gerda Hertig für die hervorragende technische Unterstützung bedanken. Annette Sommershof danke ich für die erfolgreiche Zusammenarbeit an den mutanten Cx43 HeLa-Zellen. Für die Hilfe bei der Erzeugung und Pflege Cx43 transgener Tiere danke ich Dr. Joachim Degen.
Ein besonderer Dank gilt natürlich meiner Familie, die mich in jeder Situation uneingeschränkt unterstützt hat.

Table of contents

1. Introduction

1.1 Gap junctions

Proper organic function and organization require cellular interaction and communication. Cells communicate via diverse mechanisms, i.e. ligands and their receptors, mediators, second messengers, electrical impulses and / or gap junctions. Gap junctions, tight junctions and desmosomes connect cells to each other, whereas gap junctions enable the intercellular communication. This communication coordinate physiological processes in many tissues, for example the synchronized contraction of cardiomyocytes in the heart. Gap junctions are intercellular conduits formed between adjacent cells, allowing direct metabolic and electrical coupling of contacting cells by diffusional exchange of metabolites, ions, and second messengers up to 1.8 kDa in molecular mass (c.f. Willecke et al., 2002; Neijssen et al., 2005). Generally, gap junctions are characterized by adjacent cell membranes narrowed down to 2-4 nm instead of the usual 20-30 nm (Revel and Karnovsky, 1967).

Gap junction mediated communication is described in almost all cell types in mammals except differentiated skeletal muscle, erythrocytes, thrombocytes and sperm cells (Gilula et al., 1978). However, the precursors of these cells express gap junctions. The other gene family in vertebrates which was suggested to be analogous to connexin gap junction channels are pannexins (Bruzzone et al., 2003), however these channels seem not to be capable to form intercellular channels but assembled into functional cell surface channels (Penuela et al., 2007). In invertebrates innexins generate gap junctions (Bauer et al., 2005). The following introduction is focused on connexins which also are the subject of this PhD thesis.

1.1.1 Structure of gap junction channels

Each cell contributes a hemichannel (or connexon) composed of six protein subunits, termed connexins. Connexins are transmembrane proteins characterized by a cytoplasmic amino terminus, four transmembrane domains, two extracellular and one cytoplasmic loop and a regulatory carboxy terminal region. Connexins oligomerize to connexons, also

called ‘‘hemichannels’’ which can dock to each other in contacting plasma membranes and form intercellular conduits. Different connexin isoforms that are coexpressed in the same cell can aggregate to homomeric channels, i.e. they consist of the same Cx isoforms within the single hemichannel. Heteromeric channels, i.e. different Cx isoforms are expressed within the single hemichannel. Homotypic channels, i.e. both hemichannels have the same Cx isoform composition and heterotypic channels, i.e. both hemichannels are composed of different Cx isoforms (Kumar and Gilula, 1996; Brink et al., 1997) (Fig. 1.1).

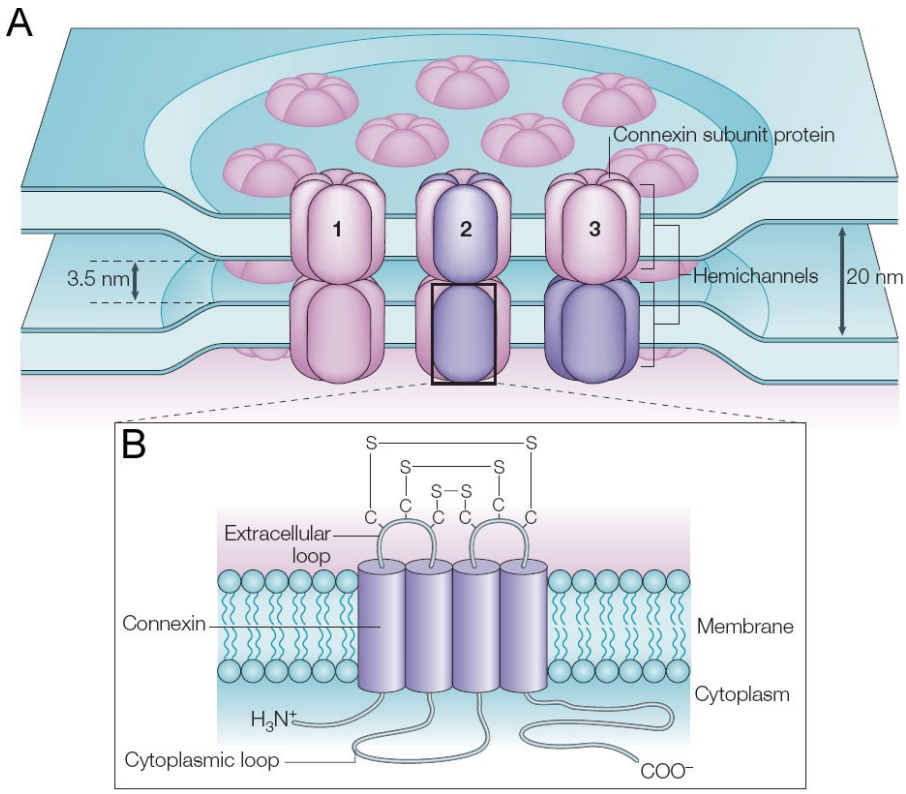

Figure 1.1: Organization and topology of gap junction plaques. (A) Two hemichannels in plasma membranes of two adjacent cells can dock to each other forming a gap junctional channel. Connexons (hemichannels) consist of six connexin subunits of the same connexin isoform (1, homomeric) or different connexin isoforms (2, heteromeric). Gap junctions containing two identical connexons are called homotypic (1, 2), those composed of different connexons are termed heterotypic (3). (B) Connexins are transmembrane proteins containing four transmembrane domains, an amino-terminal domain, cytoplasmic loop and carboxy-terminal domain and two extracellular loops. The extracellular loops are connected by disulfide bonds (S-S) between the highly conserved cystein residues. (Söhl et al., 2005)

1.1.2 Functions of gap junction channels and hemichannels

Gap junction channels (GJC) allow mutual intercellular diffusion of ions, second messengers or metabolites and are assumed to be necessary for normal embryogenesis and maintenance of organ functions in the mammalian organism (Bennett & Verselis, 1992). These channels facilitate electric and metabolic communication between cells of the cardiovascular, the central nervous system and other tissues. GJCs allow the diffusional exchange of metabolites such as sugars, amino acids, nucleotides and ions (Bennett and Verselis 1992) or second messengers such as cAMP, Ca^{2+}, NAD^{+} or IP_3 between contacting cells (Bruzzone et al., 2001). Thereby gap junction channels composed of different connexin isoforms can exhibit different permeability to molecules such as cAMP or inositol-1,4,5-trisphosphate (Niessen et al., 2000; Bedner et al., 2006). Also permeation of small peptides up to a molecular mass of 1.8 kDa was recently reported which provides a mechanism of antigen acquisition for crosspresentation during immune responses (Neijssen et al., 2005).

During the last few years, the physiological role of unopposed gap junctional hemichannels (connexons) has become a focus of gap junctional research (Bennett et al., 2003; Ebihara, 2003; Stout et al., 2004; Spray et al., 2006). Recent data suggest that unpaired hemichannels can transiently open under cellular stress, i.e. hypoxia (Evans et al., 2006). These hemichannels have been proposed to be also permeable to second messengers such as ATP or NAD^{+}, indicating their potential involvement in cellular signaling (Bruzzone et al., 2001; Evans et al., 2006; Stout et al., 2002) (Fig. 1.2). However, the molecular identity of hemichannels and their physiological role are still controversially discussed (Spray et al., 2006). For example, besides connexin hemichannels, also pannexins and the purinergic P2X7 receptor have been suggested to be involved in the cellular release of ATP (Spray et al., 2006).

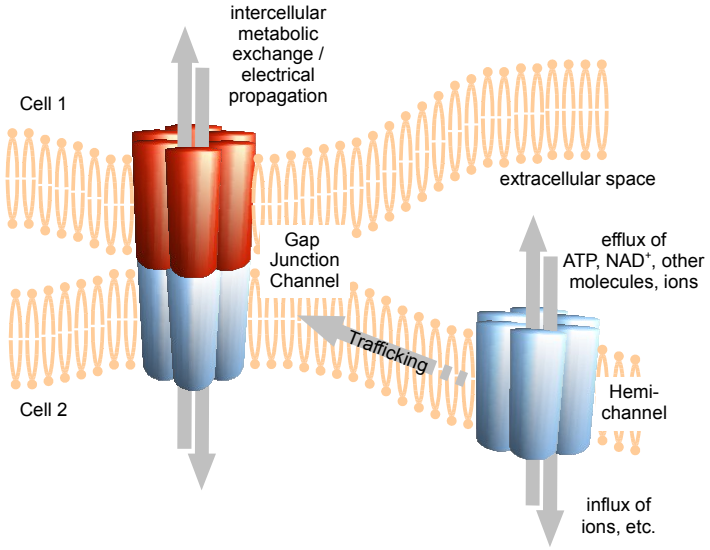

Figure 1.2: Proposed functions of gap junction channels and hemichannels. Gap junctions mediate intercellular communication by allowing exchange of small molecules like metabolites or second messengers up to 1.8 kDa molecular mass. Connexons or hemichannels on their way to a gap junction plaque can open transiently, mediating efflux of ATP, NAD^+, ions or second messengers and influx of Ca^{2+} and other ions.

1.1.3 Regulation of gap junction channels

In general three factors are known which regulate the extent of gap junctional coupling: the open probability of a channel, the single channel conductance and the number of gap junction channels. The open probability can be regulated by several factors. The increase of cytoplasmic Ca^{2+} concentration, for example as a consequence of an injury of neighboring cell closes the channels (Rose and Löwenstein, 1975). An acidification of intercellular milieu has the same effect, whereas the pH-sensitivity is specific for each connexin isoform (Wang et al., 1996; Stergiopoulos et al., 1999). The third possibility of posttranslationally regulate the open probability of a gap junction channel is the phosphorylation, whose effect depends on the site involved (Lampe and Lau, 2004; Solan et al., 2007). Recently, phosphorylation of serine residue S365 has been described as a gatekeeper event for Cx43 containing channels, which may represent a mechanism to prevent cells from ischemia (Solan et al., 2007). Additionally, intermolecular interactions can influence the channel function (Toyofuku et al., 1998; Giepmans et al., 2001; van Zeijl et al., 2007). A number of catalytic and non-catalytic proteins serve as interaction

partners of connexins, for example, the zonula occludens 1 (ZO-1) protein. Recently, ZO-1 was described to be essential for the regulation of Cx43 containing channels by phosphatidylinositol bisphosphate hydrolyzing receptors (PLCß3) (Fig. 1.3).

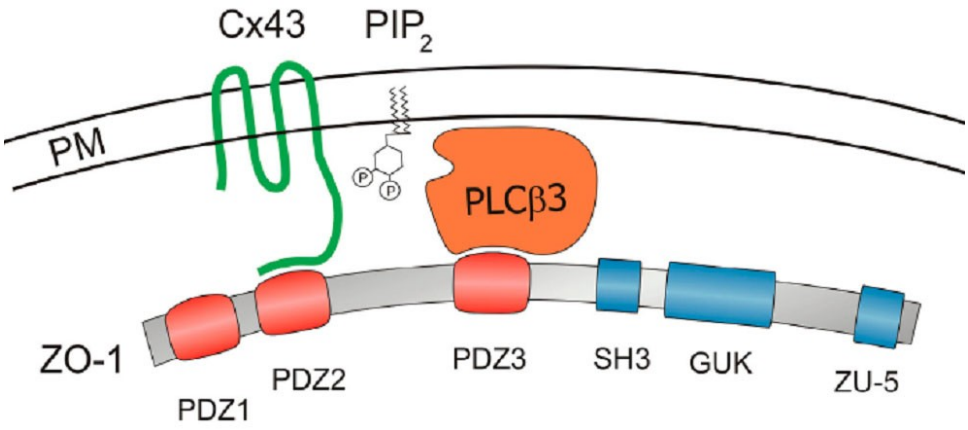

Figure 1.3: Proposed model for ZO-1 dependent regulation of gap junctional coupling in fibroblasts. ZO-1 binds to Cx43 via its PDZ2 domain and to PLCß3 via its PDZ3 domain assembling the two proteins into a complex and mediating gap junction channel phosphorylation by PLCß3. Phosphatidylinositol bisphosphate (PIP_2) is a crucial substrate for this reaction. (van Zeijl et al., 2007).

The regulation of gap junctional coupling by the number of gap junction channels thereby depends on the connexin expression, the trafficking of hemichannels to the membrane and the protein turnover (Musil et al., 2000; Evans and Martin, 2002).

1.2 Connexins in human and mouse

Until now, 21 human and 20 mouse genes have been described (Söhl and Willecke, 2004) coding for connexin proteins. The orthologous genes in mouse and man exhibit different degrees of protein sequence identity varying from 68% (between mouse Cx39 to the human Cx40.1) to 99% (Cx43 and Cx45 in both species). Connexins with high sequence identity also show a similar expression pattern among the different species (Söhl et al., 2003).

1.3 Connexin associated human disease

Mutations in connexin genes lead to alterations in important biological functions of gap junction channels and hemichannels, disturbing intercellular communication (Laird, 2006) and / or modifying hemichannel activity (Lai et al., 2006, Dobrowolski et al., 2007) thus causing and aggravating symptoms of hereditary human disorders. These diseases (Table 1.1) can be divided into seven major classes: neuropathic or myelin disorders, non syndromic and syndromic deafness, skin diseases, cataracts, oculodentodigital dysplasia and idiopathic atrial fibrillation. Connexin32 (Cx32) mutations were first described to be associated with the X-linked Charcot-Marie-Tooth disease (Bergoffen et al., 1993). Currently more than 270 mutations in the Cx32 gene are known to cause this disease. The second neuropathic connexin disorder is the Pelizaeus-Merzbacher-like disease, caused by nine known recessive mutations in the Cx47 gene (Uhlenberg et al., 2004, Bugiani et al., 2006, Wolf et al., 2007, Salviati et al., 2007). Non-syndromic deafness is the most frequent phenotype of connexin linked diseases with mutations in Cx26, Cx30 or Cx31 (http://davinci.crg.es/deafness/index.php). In addition, some mutations in Cx26 and Cx31 lead to syndromic deafness, i.e. deafness accompanied by skin disorders like palmoplantar keratoderma (Richard et al., 1998, Uyguner et al., 2002) and palmoplantar hyperkeratosis (Heathcote et al., 2000), mutilating keratoderma (Vohwinkel syndrome) (Maestrini et al., 1999), keratitis and ichthyosis (KID) (Richard et al., 2002) or erythrokeratodermia variabilis (EKV) (Lopez-Bigas et al., 2001). The associated skin disorders also occur alone leading to hidrotic ectodermal dysplasia (Clouston syndrome) (Lamartine et al., 2000) and EKV as a result of connexin30, 30.3 or 31 mutations (Richard, 2000, Macari et al., 2000). Pathological mutations of connexins in the lens (Cx46 and Cx50) are one of the genetic reasons for the development of zonular pulverulent cataracts (Shiels et al., 1998, Mackay et al., 1999), whereas mutations in Cx43, which is expressed in many cell types, cause the rare oculodentodigital dysplasia (ODDD). More than 30 mutations harboring point mutations, codon duplications, and a frame shift in the Cx43 coding DNA were reported to lead to the pleiotropic phenotype of ODDD (Paznekas et al., 2003). A new link between human diseases and connexins has recently been reported. Gollob et al. (2007) described four mutations in Cx40 gene causing idiopathic atrial fibrillation, thereby underlining the importance of gap junctional

function in cardiac physiology.

Human connexin gene protein	***Human disease***	***Mouse connexin gene protein***	***Phenotype of connexin null mutated mouse***
GJA1 Cx43	Oculodentodigital dysplasia (ODDD)	*Gja1* Cx43	Cardiac dysmorphogenesis (postnatal lethality)
GJA3 Cx46	Zonular pulverulent cataract-3 (CZP3)	*Gja3* Cx46	Zonular nuclear cataracts
GJA4 Cx37	Predisposition to arterosclerosis	*Gja4* Cx37	Female Sterility
GJA5 Cx40	Idiopathic atrial fibrillation	*Gja5* Cx40	Atrial arrhythmias
GJA6P ---	---	*Gja6* Cx33	---
GJA8 Cx50	Zonular pulverulent cataract-1 (CZP1)	*Gja8* Cx50	Microphthalmia, congenital cataracts
GJA9 Cx59	---	---	---
GJA10 Cx62	---	*Gja10* Cx57	Coupling deficiency in horizontal cells
GJB1 Cx32	X-linked Charcot-Marie-Tooth disease (CMTX)	*Gjb1* Cx32	Late-onset progressive neuropathy, decreased glycogen degradation, increased liver carcinogenesis
GJB2 Cx26	Non-syndromic and syndromic deafness, palmoplantar hyperkeratosis, keratitis-ichthyosis-deafness (KID), Vohwinkel syndrome	*Gjb2* Cx26	Lethality at ED 11
GJB3 Cx31	Non-syndromic and syndromic deafness, Erythrokeratodermia variabilis (EKV)	*Gjb3* Cx31	Transient placental dysmorphogenesis
GJB4 Cx30.3	Erythrokeratodermia variabilis (EKV)	*Gjb4* Cx30.3	reduced behavioral response to a vanilla scent, no hearing anomalies
GJB5 Cx31.1	---	*Gjb5* Cx31.1	Impaired placental development
GJB6 Cx30	Non-syndromic deafness, hydrotic ectodermal dysplasia (Clouston syndrome)	*Gjb6* Cx30	Hearing insufficiency, no skin phenotype
GJB7 Cx25	---	--- ---	---
GJC1 Cx45	---	*Gjc1* Cx45	Lethality at ED 10.5
GJC2 Cx47	Pelizaeus-Merzbacher-like disease-1	Gjc2 Cx47	Vacuoliation of nerve fibers
GJC3 Cx30.2	---	*Gjc3* Cx29	Development of hearing (?)
GJD2 Cx36	Predisposition to juvenile myoclonic epilepsy	*Gjd2* Cx36	Night blindness
GJD3 Cx31.9	---	*Gjd3* Cx30.2	Increased atrio-ventricular conduction velocity
GJD4 Cx40.1	---	*Gjd4* Cx39	---
GJE1 Cx23	---	*Gje1* Cx23	---

Table 1.1: Human and mouse connexin genes, corresponding human disease and phenotypic alterations in null mutated mice.

1.3.1 Connexin43 mutations lead to Oculodentodigital dysplasia (ODDD)

Oculodentodigital dysplasia (ODDD) is an autosomal dominantly inherited disorder characterized by anomalies of face, eyes, limbs and teeth with a high manifestation and variable expression (Judisch et al.,1979). The most common symptoms are syndactyly, enamel hypoplasia, microdontia, microcornea and craniofacial, skeletal and skin alterations (Gillepsie, 1964; Weintraub et al., 1975; Fara et al., 1977; Nivelon-Chevallier et al., 1981; van Steensel et al., 2005). Furthermore, some neurological and cardiac symptoms were described, such as spastic paraparesis, ataxia, progressive leukodystrophy (Loddenkemper et al., 2002) and arrhythmias, which were discussed as the reason for the sudden cardiac death in an affected family (Paznekas et al., 2003). ODDD is caused by mutations in the GJA1 gene, coding for connexin43 (Cx43) protein (Paznekas et al., 2003) (Fig.1.4), which is expressed in many cell types and has essential functions during embryonic development.

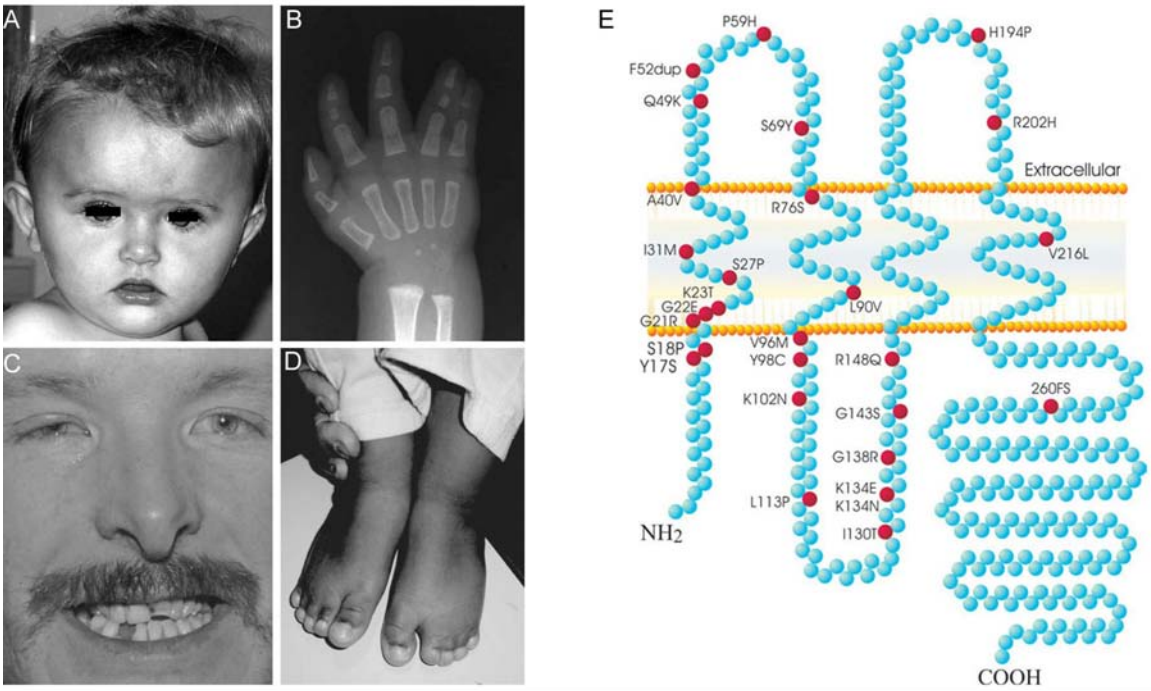

Figure 1.4: Clinical symptoms of ODDD and Cx43 mutations found in affected patients. (A) Child suffering from ODDD showing craniofacial malformations. (B and D) Soft tissue syndactyly of an affected person. (C) Microcornea, long nasal bridge and dental malformations in an ODDD patient. (E) Mutations of Cx43 causing ODDD. (Paznekaz et al., 2003; Farsson et al., 2004; Debeer et al., 2005 ; Laird, 2006)

Currently, over 30 mutations in the *GJA1* gene are known to cause ODDD, but only one frameshift mutation in the carboxy terminal part of Cx43 has been described leading to a premature stop and a truncation of the protein. Patients carrying this mutation develop palmoplantar keratoderma (van Steensel et al., 2005). Morphological alterations of the skin and a defect of the epidermal water barrier have been observed in Cx43K258stop mouse mutants lacking the last 125 aminoacid residues of the carboxy terminal region of Cx43 (Maass et al., 2004). Although, striking differences like the recessivity of the Cx43K258stop mutation or the dissimilarity of the skin phenotypes are obvious between the two species, both mutations in human and mice confirm the transspecies importance of the carboxy terminal Cx43 region. Many phosphorylation and protein binding sites are located in this region. Their loss in mice results frequently in lethality shortly after birth (Maass et al., 2004).

Most ODDD associated mutations are point mutations leading to amino acid exchanges within the first half of the protein. Some of the mutations like Y17S, G21R, I31M, A40V, F52dup, L90V, I130T, K134E, G138R, G143S, R202H (Seki et al., 2004; Roscoe et al., 2005; Shibayama et al., 2005; Lai et al., 2006; Dobrowolski et al., 2007) have been functionally analyzed regarding GJIC and hemichannel activity in cultured cells. All tested mutations disturbed dominantly Cx43 mediated coupling but differently affected the hemichannel activity. Thus, loss-of-function (Y17S, G21R, A40V, F52dup, L90V and I130T) (Lai et al., 2007) and gain-of-function (I31M, G138R and G143S) (Dobrowolski et al., 2007) mutations have been identified. Some of the mutations associated with neurological abnormalities lead to hemichannel dysfunction (Y17S, L90V and I130T) or increase in their activity (G138R). However, the physiological functions of hemichannels or even their identity are still under debate (Spray et al., 2006). It is not clear, whether the disturbed hemichannel activity is responsible for these symptoms. Cx43 null mutated mice are lethal shortly after birth and thus cannot be used as mouse models for ODDD. Thus, mice carrying point mutations in the *GJA1* gene have been developed. Three mouse models were generated, showing ODDD like phenotypes, the Cx43G61S (Flenniken et al., 2005), Cx43G138R (Dobrowolski et al., 2008) and Cx43I130T (Kalcheva et al., 2007) expressing mice.

The generation and characterization of the Cx43G138R expressing mice are the major part of this PhD work.

1.4 The mammalian heart

The mammalian heart consists of four chambers: two atria and two ventricles that are arranged in a parallel manner (Fig. 1.5A). The right half of the heart pumps the blood from the body to the lungs (pulmonary circulation) where it is oxygenated and flows back to the left half of the heart from where it is driven into the body (systemic circulation) (Fig. 1.5B).

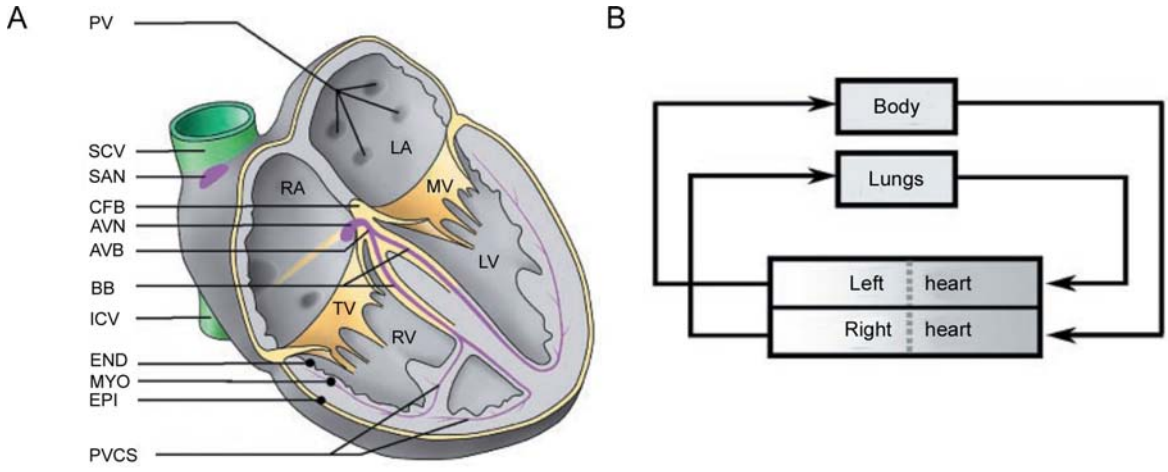

Figure 1.5: Anatomy of mammalian heart and the cardiovascular arrangement. (A) The mammalian heart is composed of the right and left atria (RA, LA) and right and left ventricles (RV, LV). The conduction system is composed of the sinoatrial node (SAN), the atrioventricular node (AVN) and the atrioventricular bundle (AVB), the bundle branches (BB), and the peripheral ventricular conduction system (PVSC). PV, pulmonary veins; S/I CV, superior/inferior caval vein; CFB, central fibrous body; MV, mitral valve; TV, tricuspid valve; END, endocardium; MYO, myocardium.(B) The cardiovascular arrangement. The right half of the heart drives the pulmonary circulation which ends in the left half of the heart. From there the blood is pumped into the body driving the systemic circulation. (Moorman and Christoffels, 2003, modified)

The coordinated contraction of the heart is garanteed by electrical stimulation of each portion of the muscle via its conduction system. The cardiac conduction system is composed of the pacemaking tissues of the sinoatrial node (SAN) and the atrioventricular

node (AVN) as well as the so called fast-conducting components (atrioventricular bundle (AVB), the bundle branches and the peripheral ventricular conduction system (PVSC)). The cardiac impulse is initiated in the pacemaker cells of the SAN, propagated to the crista terminalis through the right and left atria. The stimulus reaches the AVN where its velocity of propagation decreases (in the human heart) from 0.5-1 m/s to 0.05 m/s. This delay is discussed to be necessary for the sequential contraction of atria and ventricles (Mazgalev and Tchou, 2000) and the filtering of high atrial frequencies such as observed during atrial fibrillation protecting the ventricle against tachyarrhythmias (Dobrzynski et al., 2003). Entering the His bundle the velocity of the excitation rapidly increases up to 2 m/s and is transmitted with this velocity to the Purkinje fibers resulting in a contraction of the ventricles.

1.4.1 Gap junctions in the heart: expression and function

Gap junctions in the mammalian heart mediate metabolic and electrical communication between myocytes and isolating cells in working and conductive myocardium allowing proper cardiac contraction and impulse propagation. Today, four connexin genes are known to be expressed in the mouse heart: Cx30.2, Cx40, Cx43 and Cx45 (Fig. 1.6). Cx43 is the major connexin protein of the heart, expressed in the working myocardium of the atria and the ventricle and a part of the conduction system, the Purkinje fibers (Beyer et al., 1989; Gourdie et al., 1993; Coppen et al., 1999a). Cx40, the connexin with the highest single channel conductance (180 pS), is coexpressed with Cx43 in the atria, but also in the entire conduction system except the SA-node, i.e. the His bundle, bundle branches and Purkinje fibers (Kirchhoff et al.,1998; Coppen et al., 1999b). Cx45 and Cx30.2, connexins with the lowest single channel conductance (32 pS or 9 pS, respectively), are coexpressed in all cardiac tissues, i.e. the SA node, AV node, AV bundle and the bundle branches (Coppen et al., 1999a, b; Kreuzberg et al., 2005).
The expression of Cx40, Cx43 and Cx45 has been confirmed in the human heart (Severs et al., 2004), whereas the human Cx30.2 homolog Cx31.9 could not be found neither in the adult nor the embryonic heart (Sara Segschneider, unpublished data) underlining the differences in the cardiac morphology between the two species.

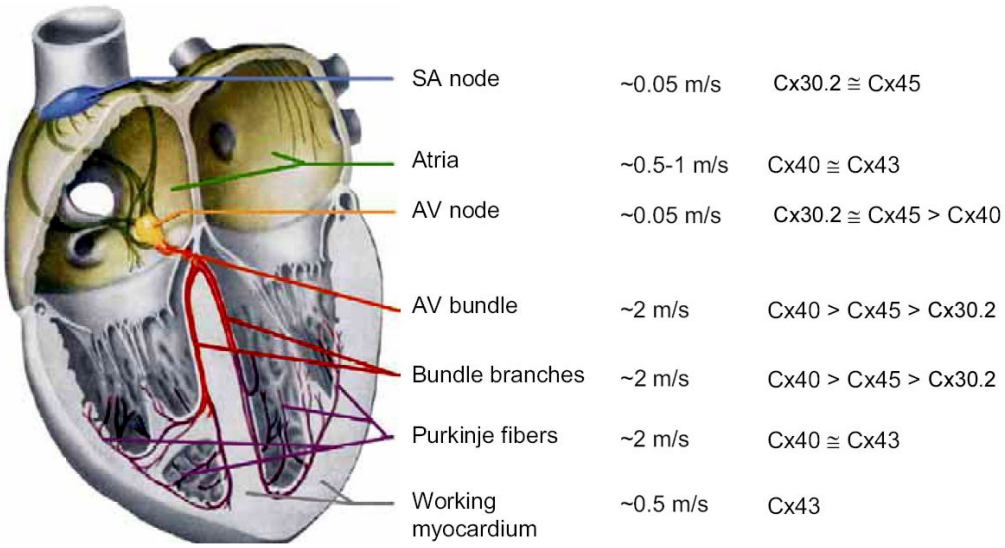

Figure 1.6: Connexin expression pattern and the spread of excitation illustrated in a schematic human heart. (Netter, 1993, modified)

1.4.2 Disturbed cardiac conduction in connexin deficient mice

The deletion of every cardiac connexin leads to a disturbance of cardiac physiology. The ubiquitous deletion of Cx43 resulted in postnatal death due to a failure in pulmonary gas exchange as a result of morphologically altered right ventricular outflow tract in the mutated heart (Reaume et al., 1995). A specific deletion of Cx43 in cardiomyocytes or the tamoxifen induced systemic deletion in adult mice lead to an obvious disturbance of impulse propagation in the ventricle and severe tachyarrhythmias (Gutstein et al., 2001; van Rijen et al., 2004; Eckardt et al., 2006).

Kirchhoff et al. (1998; 2000) had demonstrated the importance of Cx40 and Cx43 mediated intercellular communication in normal heart physiology. Cx40 deficiency in the mouse led to a disturbance of intercellular communication in atrium and conduction system as shown in a prolongation of the atrial and ventricular ECG parameters and atrial arrhythmia (Kirchhoff et al., 1998). Furthermore, $Cx40^{+/-}/Cx43^{+/-}$ mice also exhibited alterations in ventricular conduction (Kirchhoff et al., 2000). Thus, the results obtained from these mouse mutants widely seem to reflect the situation in human patients. Both, the human Cx40 mutations or the Cx40 deficiency in mouse, disturb the proper impulse propagation in the heart generating an arrhythmic substrate due to loss of gap junctional

coupling.

An ubiquitous deletion of Cx45 or the cardiac-actin Cre mediated deletion of this connexin gene resulted in early embryonic lethality due to defective vascular angiogenesis (Krüger et al., 2000) or cardiac cushion defects (Nishii et al., 2003). The observed vascularization defects are most probably a secondary effect of a cardiac insufficiency as observed in Cx45floxKICx36:alphaMyHC-Cre mice in which Cx45 is exchanged by Cx36 specifically in cardiomyocytes (Marina Frank, Diploma thesis, 2008).

Cx30.2 decelerates the impulse propagation in the cardiac conduction system (Kreuzberg et al., 2006). The loss of Cx30.2 in the AV node lead to a significantly shorter PQ interval than in wild-type littermates. Cx30.2 exhibits the lowest unitary conductance of all gap junction channels (Kreuzberg et al., 2005) and shows additionally a high hemichannel activity (Bukauskas et al., 2006) which together may slow down the signal propagation in the AV node of mice.

1.4.3 Gap junction alterations in human heart failure

Altered gap junctional communication can cause certain human heart diseases. Alterations have been described for Cx40, Cx43 and Cx45 in human heart failure (Severs et al., 2004; Kalcheva et al., 2007; Bruce et al., 2008). In the diseased ventricular myocardium two principal gap junction-related alterations have been reported: disturbances in the distribution of gap junctions and reduced levels of their major component, Cx43. The myocardial zone, bordering infarct scar tissue in ventricles of patients with ischaemic heart disease shows such an alteration of Cx43 distribution (Smith et al., 1991). A reduction in the expression of Cx43 has also been described in the diseased ventricles (Peters et al., 1993; Kaprielian et al., 1998). These observed reductions in expression in most cases less than 50%, which in the mouse heart does not seem to affect its proper function (van Rijen et al., 2004). Besides Cx43 remodeling and phosphorylation as shown in ischaemic rat hearts (Beardslee et al., 2000) a changed intermolecular interaction of Cx43 to its partner ZO-1 seems to play an important role in arrhythmogenesis by decreasing the size of Cx43 gap junctions (Bruce et al., 2008). In addition, upregulation of Cx45 was observed in the failing human heart, which is

discussed as a compensatory attempt of the diseased tissue to maintain the gap juctional function (Yamada et al., 2003).

Recently, mutations in the *GJA5* gene, coding for Cx40, have been described in patients suffering from idiopathic atrial fibrillation (Gollob et al., 2006). Lymphocytic blood and cardiac tissue samples were analyzed by PCR amplification and sequencing of the GJA5 gene. Besides one obvious polymorphism (M163S), three mutations (P88S, G38D and A96S) in Cx40 were detected in 4 out of 15 patients with idiopathic atrial fibrillation. Notably, two of the ascertained mutations were somatic, i.e. they were originated and expressed only in the heart, but could not be found in lymphocytic DNA. The Cx40 A96S mutation was genetically inherited. The same publication (Gollob et al., 2006) described functional disturbances of these mutations regarding trafficking, gap junctional coupling in Xenopus oocytes and their influence on wild-type Cx40 and Cx43 function. The mutations (P88S and G38D) which cause defective intracellular protein trafficking as well as the plaque forming mutation (A96S) clearly showed a reduction in intercellular communication, dominance on wild-type Cx40 and trans-dominance on wild-type Cx43 mediated electrical coupling. These findings suggest that the strong reduction of gap junction mediated cellular communication in the heart can cause the observed atrial fibrillation. Others described the predisposition to atrial arrhythmia in patients carrying specific polymorphisms in the promoter region of Cx40 (Groenewegen et al., 2003) which led to attenuated activity of this regulatory element and decreased Cx40 expression (Juang et al., 2007).

In the last years antiarrhythmic peptides targeting Cx43 gap junction channels were discovered (Eloff et al., 2006). Rotigaptide is one of these peptides which increase gap junctional coupling (Axelsen et al., 2007). However, the detailed molecular mechanisms behind the action of antiarrhythmic peptides remain unclear. Recently, effects on the phosphorylation of Cx43 in rat hearts have been described suggesting a more frequent opening of the gap junction channels (Wang et al., 2007).

1.5 General developmental processes in limb and bone

Morphogenesis is a fundamental aspect of developmental biology which consists of cell proliferation, cellular differentiation and tissue patterning.
Several classes of molecules are particularly important during morphogenesis. The first one comprises the morphogens which are diffusible molecules acting through binding to their specific receptors and carrying signals that control cell differentiation in a concentration dependent manner. Morphogen gradients induce different cell types in distinct spatial order. Distinct concentration thresholds induce or maintain the expression of diverse target genes. The second important class of molecules involved in morphogenesis are transcription factors which are capable to determine cell fate by modulation of gene expression and regulation of downstream cascades. Another class of molecules involved in morphogenesis are cell adhesion molecules acting during fundamental developmental processes like gastrulation.
The combinations of target gene expression lead to the development of distinct cell types in developing tissues. The key molecules in the development of limb and bone are sonic hedgehog (Shh), fibroblast growth factors (FGFs) and bone morphogenic proteins (Bmps). Their effects and interactions are described in detail in the following chapters.

1.5.1 Development of the limb bud

The limb develops out of a so called limb field, a morphogenetic area dependent on the homeobox c6 (*Hoxc6*) gene expression and retinoid acid signalling. The limb formation from the limb field occurs out of an interaction between the mesenchymal cells and the overlying ectodermal cells. Directed from the lateral mesoderm and the myotome, cells migrate to the limb field and proliferate to form the limb bud (Fig. 1.7A). Here, the lateral cells produce the skeletal portions of the limb, while the myotome cells produce the muscle components.

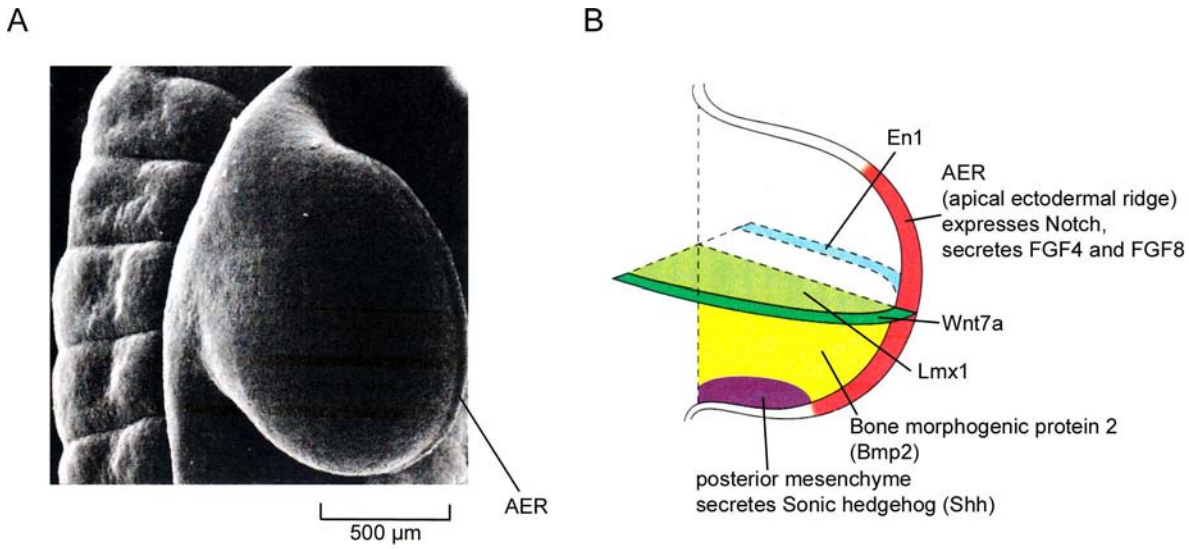

Figure 1.7: Patterning of vertebrate limb bud. (A) Scanning electron micrograph of a chicken limb bud at 4th day of incubation. The line points at a thickened edge of the limb, the apical ectodermal ridge (AER). (B) Schematic expression pattern of the key morphogens of limb development. Ectodermal cells express Notch, fibroblast growth factor 4 (FGF4), FGF8 and Wnt7a, whereas LIM homeobox transcripition factor 1 (Lmx1), bone morphogenic protein 2 (Bmp2) or sonic hedgehog (Shh) are expressed by mesenchymal cells. Posterior mesenchyme secreting Shh has pattern-organizing activity is also called zone of polarizing activity (ZPA). (Alberts et al., 2002, modified)

The lateral mesodermal cells express fibroblast growth factor 10 (FGF10) and induce the cells from the apical ectodermal ridge (AER) to express FGF8 and FGF4 which maintain the FGF10 signal and proliferation in the mesoderm (Fig 1.8 bottom) (Sun et al., 2002).
The position of FGF10 expression is regulated by Wnt8c in the hindlimb and Wnt2b in the forelimb, belonging to the major class of secreted morphogenic ligands. The forelimb and the hindlimb are specified by their position along the anterior/posterior axis and by two T-box containing transcription factors, the Tbx5 and Tbx4, respectively (Li et al., 1997).
The Zone of Polarizing Activity (ZPA) in the limb bud exhibit a pattern-organizing activity via action of a morphogen gradient of Sonic hedgehog (Shh) (Fig. 1.7B). Shh is necessary to create ZPA and specify the anterior/posterior pattern in the distal limb (Riddle et al., 1993). Shh is maintained in the posterior through a feedback loop between the ZPA and the AER (Fig. 1.8). Shh induces the AER to produce FGF4 and FGF8 which

maintain the expression of Shh. Digits 3, 4 and 5 are specified by a temporal gradient of Shh. Digit 2 is specified by a long-range diffusible form of Shh, however, Digit 1, the thumb, does not require Shh (Chiang et al., 2001).

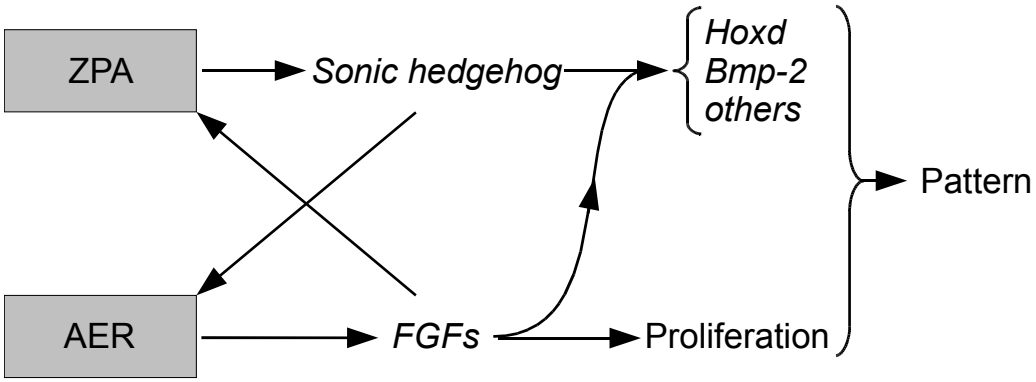

Figure 1.8: Proposed model for coordinated growth and patterning of the limb. Sonic hedgehog (Shh) signalling from the zone of polarizing activity (ZPA) induce the expression of Hoxd and Bmp2 genes in the mesoderm. However, the induction itself needs the signals from the apical ectodermal ridge (AER), i.e. the FGFs. In turn, the expression of FGFs can be induced by Shh and vice versa generating a positive feedback loop of the ZPA and AER. Additionally, FGFs promote mesodermal proliferation. Thus, the patterning and proliferation is dependent on the same signals, the limb patterning and outgrowth are inseperably connected with each other. (Laufer et al., 1994, modified)

In order to separate the digits, programmed cell death is needed which removes the tissue between the digits and joints. The signaling of bone morphogenic proteins induces cell death while Noggin blocks cell death in this tissue (Capdevila et al., 1998). In summary, signals directed from the ZPA and AER are highly regulated and dependent on each other, connecting proliferation and morphogenic patterning (Fig. 1.8).

1.5.2 Contribution of bone morphogenic proteins (Bmp) to limb bud development and skeletogenesis

Bone morphogenic proteins (Bmps) play an important role in a variety of developmental processes, for example in early limb patterning as well as in skeletogenesis. They are secreted signalling molecules which belong to the transforming growth factor ß (TGFß)

superfamily (Reddi et al., 1972; Urist et al., 1965; Wozney et al., 1988).

Bmp2, Bmp4 and Bmp7 are expressed in the early limb bud mesenchyme (Francis et al., 1994; Yang et al., 1997) whereas only Bmp2 and Bmp7 are active downstream of Shh signalling (Bandyopadhyay et al., 2006) (see Fig. 1.8). Bmp4 appears not to be induced by Shh expression as seen in Shh deficient limb buds (Pizette et al., 2001). In contrast, the expression of Bmp2 and Bmp7 is diminished in the absence of Shh activity (Chiang et al., 1996).

All three Bmps induce apoptosis of the interdigital spaces (Ganan et al., 1996; Yokouchi et al., 1999; Zou and Niswander, 1996). The involvement of Bmps in fundamental developmental processes in underlined by the early lethality of Bmp1 and Bmp4 deficient mice (Winnier et al., 1995; Zhang and Bradley, 1996). Using a conditional approach the role of these two molecules in the limb patterning could be determined (Bandyopadhyay et al., 2006). Bmp2 deficient limbs developed striking syndactylies with dramatically reduced apoptosis between the digits, whereas the digits themselves developed normally (Bandyopadhyay et al., 2006). Application of Bmp antagonists leads to a block of apoptosis (Yokouchi et al., 1999; Zou and Niswander, 1996) suggesting that a threshold level of the Bmp signalling is necessary to efficiently induce programmed interdigital death. The impact of Bmp expression on skeletogenesis is well described. For instance, osteoblastic differentiation is diminished in Bmp2 and Bmp7 double deficient limbs whereas Bmp2, Bmp4 or Bmp7 alone did not show any skeletal or chondrogenic anomalies (Bandyopadhyay et al., 2006). A blockade of Bmp2 signalling by its antagonist Noggin in chick embryos resulted in defective formation of a proposed ectodermal signaling center that regulates craniofacial patterning (Foppiano et al., 2007). Similar anomalies in craniofacial development could be seen when Shh signalling was diminished *in vivo*. The inhibition of Shh pathway was achieved by an alkaloid called cyclopamine in a cultured mouse (Nagase et al., 2005) or chick embryo (Cordero et al., 2004) or other teratogens such as alcohol or retinoids (Cohen an Shiota, 2002) where also a reduction of Bmp signalling is expected. However, an involvement of Bmp signalling in holoprosencephaly (HPE), a craniofacial malformation in human associated with a disturbed Shh signalling, was recently described (Fernandes et al., 2007). In summary, the threshold of Bmp signalling is important in many developmental processes, especially the limb formation and skeletogenesis.

1.5.3 The impact of Cx43 containing gap junction channels on morphogen expression

During chick limb development Cx43 is expressed in restricted domains in the apical ectodermal ridge (AER) and mesenchyme of the zone of polarising activity (ZPA) (Makarenkova et al., 1999). Application of gel beads soaked with Cx43 antisense oligonucleotides at stages before limb outgrew resulted in obvious limb phenotypes such as truncation or fragmentation of the limb bud, or a complete splitting into two or three branches (Makarenkova et al., 1999). This knock down of Cx43 expression led to a drastic reduction of Shh and Bmp2 mRNA *in situ*. Others described a knock down of Cx43 in chick which resulted in limb patterning defects including deletion of the anterior digits (Law et al., 2002). Here both, Shh and Bmp2 were also clearly downregulated in treated limbs while expression of FGF8, Bmp4 or Muscle segment homeobox-like gene (Msx-1) remained unchanged. Thus, Cx43 mediated gap junctional signalling or expression is required for chick limb development. Also a modulation of chondrogenic differentiation *in vitro* by Bmp2 involves gap junctional coupling. The inhibition of gap junction mediated intercellular communication by 18 alpha glycerrhetinic acid decreased chondrogenic differentation by 50% 96 h after plating while the inhibition during the first 24-48 h, a critical initial phase of condensation, did not have any effects (Zhang et al., 2002). This suggests that gap junctional coupling is not critical for the initiation but plays important roles in the continuation of chondrogenesis, a process in which Bmp signalling is crucial. In contrast, gap junctional communication has also been described to be modified by Bmp2 and Bmp4 in P19 cells, an embryonic carcinoma cell line (Bani-Yaghoub et al., 2000). Cells treated with Bmp2 or Bmp4 lose their capacity to differentiate into neurons and maintain extensively coupled by gap junctions. Recently, an endogenous blockade of Shh signalling in the developing midbrain has been proposed to be mediated by gap junctions preventing radial columns of cells from differentiation (Bayly et al., 2007). This inhibition is discussed to be achieved by an intercellular propagation via gap junctions of pro-vitamin D3 and subsequent secretion (Bijlsma et al., 2006). The release of these small inhibitory molecules is dependent on Patched and takes place after Shh binding to its receptor. Thus, Cx43 function seems to modify and to be modified by Shh and Bmp2 cascades in diverse tissues and developmental stages.

1.6 Mouse as model for human disease

Transgenic are suitable models for genetic human diseases, primarily because their genes show a high degree of homology with man.
The function of genes in general can be determined in two approaches: the gain of function and the loss of function concept. The targeted insertion of gene mutations like deletions, resulting in so called knock-out mice, or in replacements, so called knock-in mice, are two major approaches in molecular genetics. Using reporter genes like green fluorescent protein (GFP) or ß-galactosidase driven by the promoter of the corresponding gene the expression of this gene can be localized to certain cells.
Transgenic mice can be used to answer many central questions in biology like molecular reasons of human diseases giving the opportunity to develop new therapeutic agents and procedures.

1.6.1 Targeted insertion of a conditional gene mutation

The insertion of a targeted gene mutation can be achieved by homologous recombination of the vector construct into the genome of mouse embryonic stem cells (Nagy et al., 2003). These vectors include homologous sequences to the targeted gene which flank the sequence to be inserted. Once the vector is located in the nucleus of the cell the homologous sequences in the vector can allign to the ones in the genome and recombine. These so called crossing-over events are highly infrequent with 10^{-6} to 10^{-7} depending on the targeted locus. After this *in vitro* manipulation ES cells are injected into the blastocyst allowing the generation of chimaeras and after matings with mice of homogenous genetic background, the generation of transgenic mice.
For conditional deletion or activation of genes the Cre/loxP- and Flp/frt-systemes can be used (Kühn et al., 1995). Cre is a recombinase derived from the P1 bacteriophage with a molecular mass of 38 kDa (Sternberg et al., 1986). Flp is the other common recombinase in molecular genetics which has a similar size but was derived from the yeast *Saccharomyces cerevisae* (Buchholz et al., 1998). Both enzymes consist of two different subunits and are not dependent on any cofactor (Lewandoski et al., 2001). Cre and Flp recombinases recognize and bind to their specific sites: loxP sites in the case of Cre and

frt sites in the case of Flp. The core sequences in both recognition sites determine their orientation (Fig. 1.9A). If both sites are orientated in the same direction, the flanked sequence will be deleted and one loxP site remains (Fig. 1.9B). If the sites point in different directions, the flanked sequenced will be inverted.

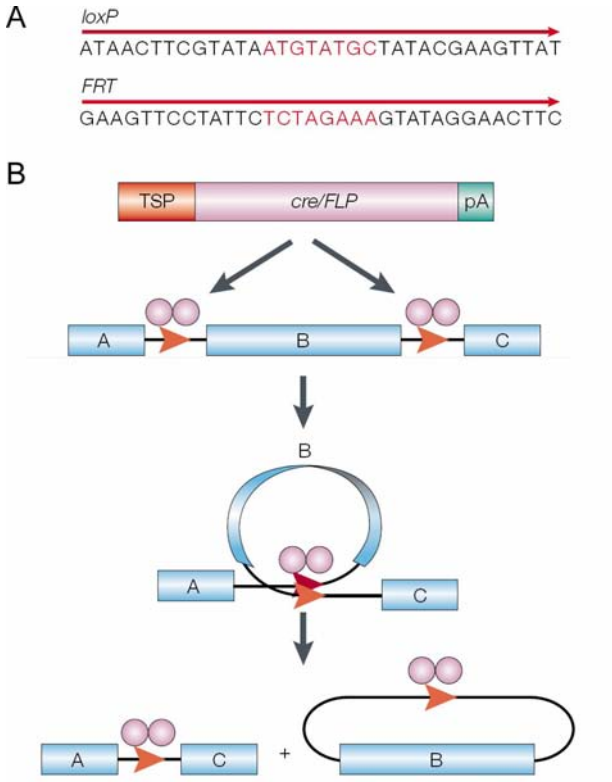

Figure 1.9: Schematic illustration of the cre/loxP and FLP/frt recombination system. (A) The 34 bp loxP and frt sites consist both of two inverted 13 bp repeats and an asymmetric 8 bp core sequence determining its orientation. (B) Cre or Flp recombinase dimers bind to their recognition sites and mediate the excision of the target DNA sequence in between the loxP or frt sites, if both sites have the same orientation. (Lewandoski, 2001)

1.6.2 The Cx43G138R targeting vector for conditional replacement of Cx43 in mice

The targeting vector mCx43ODDD-KI vector was generated and used during my diploma thesis (2004) for the targeted replacement of the endogenous Cx43 wild-type gene in mouse embryonic stem (ES) cells (Fig. 1.10). The vector contains 5' (4.9kb) and 3' (1kb) homologous regions which are needed for the targeted recombination in ES cells, the floxed region (black arrows in Fig. 1.10) that consists of the Cx43 wild-type coding DNA as well as the PGK-neomycin selection cassette (phoshoglycerate kinase promoter with neomycin resistance gene) which in turn is flanked by frt sites (green arrows in Fig. 1.10). After Flp mediated recombination the PGK-neomycin cassettes can be deleted. Both loxP sites were positioned within intron sequences to avoid any reduction in transcription of the wild-type gene. In addition, the flirted PGK-neo box was integrated in inverse orientation to the Cx43 coding region which minimizes disturbances of the Cx43 promoter by the strong PGK promoter driving neomycin resistance. Additionally, an ectopic reporter gene expression by a read through of the selection gene could be avoided.

After a Cre mediated recombination the vector effects the transcription of the mutated Cx43G138R gene, the internal rebosomal entry site (IRES, Attal et al., 1999) and enhanced green fluorescent protein (eGFP). This combination of gene cassettes allows the expression of the mutated Cx43 protein and the reporter eGFP without affecting the properties of the mutated protein as described for some GFP fusion proteins. The expression of an *in vivo* reporter gene such as GFP allows the detection of Cx43G138R localization in living and fixated mouse tissues. This is important because the point-mutated and the wild-type genes cannot be distinguished from each other in antibody-based assays.

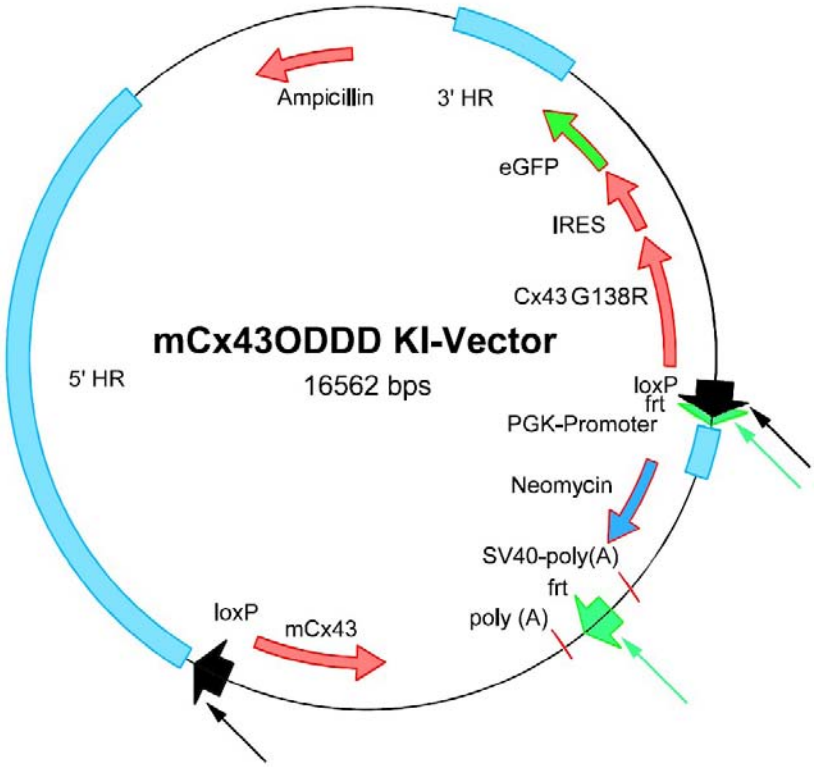

Figure 1.10: The conditional mouse Cx43G138R vector. The 5' and 3' homologous regions flank the entire region to recombine into the genomic locus of Cx43 in mouse ES cells. The floxed region which can be removed after a cre mediated recombination contains the wild-type Cx43 gene and the PGK-neomycin resistance cassettes which again were flanked by frt sites. Downstream of the last loxP site Cx43G138R gene followed by the internal ribosomal entry site (IRES) and enhanced green fluorescent protein (eGFP) are coded. This order of gene cassettes allows the translation of the mutated Cx43 protein and eGFP from one long, bicistronic messenger RNA connecting the expression of the two genes and avoiding possible disturbances of the mutated protein as known for some GFP fusion proteins (R. Dobrowolski, Diploma thesis, 2004).

1.7 Aims of the study

The *GJA1* gene encodes the human Connexin 43 (Cx43) protein, the best described member of the connexin gene family. Mutations in Cx43 cause oculodentodigital dysplasia (ODDD), a rare pleiotropic human disorder (Paznekas et al., 2003).

The main goal of this study was to explore the molecular mechanisms underlying ODDD and the impact on gap junction channel and hemichannel function in the Cx43G138R mutation causing this disorder. In order to investigate this mutation *in vivo* a mouse targeting vector was cloned during my diploma thesis and used for transfection of mouse embryonic stem (ES) cells. ES cell clones which had undergone homologous recombination had to be identified and used for generation of mice conditionally expressing the Cx43G138R mutation. Furthermore, recombinant ES cells after cre transduction as well as HeLa and primary cells had to be used for the characterization of molecular consequences of Cx43G138R expression. As reporter gene in this study eGFP allows to detect Cx43G138R expressing cells *in vivo* and *in vitro* making it possible to assess primary cell cultures and prove the expression pattern of the mutated gene.

The impact of the Cx43G138R mutation in mice had to be investigated after activation of the mutant gene using different cre expressing mice. Conditional expression in the heart or the brain would offer the opportunity to determine the effect of the mutation in certain tissue at a certain developmental stage. Furthermore, the occurrence of possible morphological anomalies and cardiac function described to be altered in one ODDD affected family should be characterized in the conditional Cx43G138R mouse mutant. Thus, the impact of this Cx43 mutation on regulation, phosphorylation and channel function *in vivo* and *in vitro*, as well as embryonic development and cardiac physiology had to be determined.

2. Material

If not specially mentioned in the methods chapter, solutions and materials were prepared in general as described previously in detail (Dobrowolski, 2004, diploma thesis; Degen, 2003, PhD thesis). Plasmids, bacterial strains, eukaryotic cell lines, mouse strains, primers and antibodies utilized during this PhD thesis are listed below.

2.1 Plasmids

Plasmid	Reference	Properties
mCx43ODDD_KI	Dobrowolski et al., 2008	Conditional Cx43floxG138R targeting vector, ampicillin and neomycin resistance
pGEM-T Easy Vector	Promega, A1360	Ampicillin resistance
pMJ-green	Maxeiner et al., 2005	Eukaryotic expression vector, ampicillin resistance
HeLaCx43G138R	Dobrowolski et al., 2007	Eukaryotic expression vector, carrying the Cx43G138R point mutation ampicillin and zeocin resistance
HeLaCx43I31M	Dobrowolski et al., 2007	Eukaryotic expression vector, carrying the Cx43I31M point mutation ampicillin and zeocin resistance
HeLaCx43I143S	Dobrowolski et al., 2007	Eukaryotic expression vector, carrying the Cx43I143S point mutation ampicillin and zeocin resistance
HeLaCx43H194P	Dobrowolski et al., 2007	Eukaryotic expression vector, carrying the Cx43H194P point mutation ampicillin and zeocin resistance

2.2 Bacterial strains

Bacterial strain	Reference	Properties
XL-1 blue	Bullock et al., 1987	tetracycline resistance, plasmid ampli-fication, α-complementation
Top10	Invitrogen	plasmid amplification, α-comple-mentation

2.3 Eukaryotic cell lines

Eukaryotic cell line	Reference	Annotations
HM1 mouse ES-cells	Magin et al., 1992	mouse embyonic stem cells, SV129/ola
HeLa wild-type	Jones et al., 1971	Zervix-carcinoma derived cell line
HeLaCx43	Welcker, 2004, diploma thesis	stable Cx43 wild-type expression
HeLaCx43-eGFP	Welcker, 2004, diploma thesis	stable Cx43-eGFP fusion protein expression
HeLaCx43G138R	Dobrowolski et al., 2007	stable Cx43G138R expression
HeLaCx43I31M	Dobrowolski et al., 2007	stable Cx43I31M expression
HeLaCx43I143S	Dobrowolski et al., 2007	stable Cx43I143S expression
HeLaCx43H194P	Dobrowolski et al., 2007	stable Cx43H194P expression

2.4 Transgenic mouse strains

Transgenic mouse strain	Reference	Application
PGK-Cre	Lallemand et al., 1998	ubiquitous Cre-mediated deletion of loxP -sites flanked genes in mice
αMyHC-Cre	Agah et al., 1997	cardiomyocyte specific Cre-mediated deletion of loxP -sites flanked genes in mice
Nestin-Cre	Tronche et al., 1999	early neuron specific Cre-mediated deletion of loxP -sites flanked genes in mice
Cx43KILacZ	Theis et al., 2001	replacement of Cx43 coding region by LacZ reporter coding DNA
Cx43KICFP	Degen et al., not yet published	replacement of Cx43 coding region by CFP reporter coding DNA

2.5 Primers

2.5.1 Primers for mice genotyping

Primer	Sequence (in 5'-3' direction)
Vor_poly A	GGGGGTGAAGGAGTTTTCAGCAGTGC
In_kod_Reg.Cx43	GCTTCCCCAAGGCGCTCCAGTCACCC
Vor_LoxP	GCACTTGGTAGGTAGAGCCTGTCAGGTC
UP-IntCre	TTTGCCTGCATTACCGGTCGATGC
IntCre-rev	TCCATGAGTGAACGAACCTGGTCG
43del_for	GGCATACAGACCCTTGGACTCC
43del_rev	TGCGGGCCTCTTCGCTATTACG
PGK1	GCTGTTCTCCTCTTCCTCATCTCC
Nestin	TCCCTTCTCTAGTGCTCCACGTCC
MHC5P	ATGACAGACAGATCCCTCCTATCTCC
Cre3	CTCATCACTCGTTGCATCGAC

2.5.2 Primers for real-time RT-PCR analyses

Primer	Sequence (in 5'-3' direction)
ß-actin_for	ACGGCCAGGTCATCACTATTG
ß-actin_rev	ATGGATGCCACAGGATTCCAT
GAPDH_for	TCAACGACCCCTTCATTGAC
GAPDH_rev	ATGCAGGGATGATGTTCTGG
Gli1_for	TGGATATGATGGTTGGCAAGTG
Gli1_rev	ACAGACTCAGGCTCAGGCTTCT
Gli2_for	CACAGGGCGGGCACAAGAT
Gli2_rev	GGAGGGCAGTGTCAAGGAA
Shh_for	CGGCAGATATGAAGGGAAGA
Shh_rev	GGTCCAGGAAGGTGAGGAAGT
β-catenin_for	TCTACGCCATCACGACAC
β-catenin_rev	CAGACAGACAGCACCTTC
MmBmp2_for	TGCGCAGCTTCCATCACGAA
MmBmp2_rev	GTGAGAAACTCGTCACTGGG

2.6 Antibodies

2.6.1 Primary antibodies

Primary antibody	Reference/Company	Species/Order No.	Dilution
anti-Cx30	Zymed	Rabbit/71-2200	1:500
anti-Cx40	Alpha Diagnostics	rabbit/Cx40-A	1:150
anti-Cx43	Traub et al., 1994	rabbit	1:500
anti-Cx43	Zymed	mouse/35-5000	1:300
anti-Cx43	Sigma	rabbit/C6129	1:1000
anti-Cx45	Dedek et al., 2006	rabbit	1:750
anti-NeuN	Chemicon	mouse/MAB377	1:1000
anti-Nestin	Chemicon	Mouse/MAB353	1:1000
anti-GFAP	Sigma	mouse/G-3893	1:1000
anti-EGFP	Abcam	rabbit/Ab290	1:1000
anti-EGFP	Abcam	chicken/Ab13970	1:500
anti-ß-galactosidase	Sigma	mouse/G-8021	1:1000
anti-ß-actin	Sigma	mouse/A4700	1:500
anti-Bmp2	Abcam	rabbit/Ab14933	1:300
anti-Bmp2	SantaCruz	goat/sc-6895	1:100
anti-Bmp4	Abcam	rabbit/Ab18865	1:300
anti-Noggin	RnD Systems	goat/AF719	1:500
anti-FGF8	RnD Systems	mouse/MAB323	1:500
anti-Shh	RnD Systems	goat/AF464	1:500
anti-Shh	SantaCruz	goat/sc-1194	1:150
anti-Oct3/4	SantaCruz	mouse/sc-5279	1:1000
anti-Vimentin	Progen Biotechnik	guinea pig/GP53	1:100
anti-MECA-32	PharMingen	rat/09921D	1:200

2.6.2 Secondary antibodies

Secondary antibody	Reference/Company	Order No.	Dilution
Alexa(594)-goat anti-rabbit	Molecular Probes	A-11037	1:1000
Alexa(488)-goat anti-mouse	Molecular Probes	A-11029	1:1000
Alexa(488)-goat anti-rabbit	Molecular Probes	A-11008	1:1000
Cy2-goat anti-chicken	Dianova	103-225-155	1:1000
Cy3-donkey anti-mouse	Dianova	715-165-151	1:1000
Cy3-donkey anti-rabbit	Dianova	711-165-152	1:1000
Cy5-donkey anti-mouse	Dianova	115-175-166	1:1000
Cy3-goat anti-guinea pig	Jackson ImmunoResearch	106-165-003	1:1000
HRP-goat anti-mouse	Dianova	111-035-144	1:15000
HRP-goat anti-rabbit	Dianova	115-035-146	1:15000
Alkaline phosphatase-goat anti-rabbit	Pierce	31340	1:15000
Biotin-goat anti-rabbit	Zymed	81-6140	1:5000

3. Methods

If not specially mentioned, all standard laboratory methods were performed in general as previously described (Dobrowolski, 2004, diploma thesis; Degen, 2003, PhD thesis).

3.1 Generation and analysis of Cx43G138R conditionally expressing mice

3.1.1 Generation, genotyping and Northern blot analysis of Cx43G138R transgenic mice

The Cx43G138R mutation from a human patient (Paznekas et al., 2003) was inserted by PCR mutagenesis in the corresponding mouse gene, cloned into the pBluescript vector and sequenced in both directions by AGOWA (Berlin, Germany) as already described in my diploma thesis. For the screening of ES cell clones for homologous recombination the targeting vector DNA (150 mg) was linearized by *Not*I digestion and transfected by electroporation (800 V and 3 mF) into murine ES cells (HM1) (Magin et al., 1992). Selection of vector containing cells was performed using 350 µg/ml G418 (Invitrogen, Karlsruhe, Germany). In order to test for homologous recombination, genomic DNA from the ES cell clones was processed for PCR analysis using a 5' upstream primer, binding to the eGFP sequence in the targeting vector (eGFP_rev), and an external 3' downstream primer specific for the 30 region of Cx43 (Cx43_30HR). To exclude clones in which recombination occurred partially, a second PCR analysis was performed with cells positive in the first one. Here, we used primers annealing upstream of the 5' loxP site (Cx43/31for) and downstream behind it (Cx43/31rev). Clones found to be positive in both PCR analyses were tested by Southern blot hybridization. For this purpose, DNA from the PCR-positive clones was digested with *Hin*cII or *Bam*HI (both for the hybridization with the internal probe) or *Hin*dIII (external probe). After electrophoretic separation on agarose gels, blotting onto Hybond N^+ membranes (Amersham Biosciences, Buck, UK) and ultraviolet crosslinking for fixation, hybridization was performed under stringent conditions using the Quick Hyb solution (Stratagene, La Jolla, CA, USA) at 68°C for 1.5 h. A 550 bp *Hin*cII fragment from the coding region of Cx43

was used as the internal probe and a 550 bp *Ava*I fragment of the 3' homology region served as the external probe.

The homologously recombined ES cell clone was injected into C57BL/6 blastocysts, as described previously (Theis et al., 2000). Blastocyst injections of ES cells resulted in mice, showing a high-degree fur-color chimerism, were afterwards mated with C57BL/6 mice. Germline transmission of the recombinant allele was checked in agouti offspring by PCR analyses of isolated tail DNA. The heterozygous Cx43+/floxG138R mice were backcrossed with C57BL/6 mice to increase the C57BL/6 genetic background and mated to PGK-Cre (Lallemand et al., 1998), alphaMyHC-Cre (Agah et al., 1997) or Nestin-Cre (Tronche et al., 1999) expressing mice for deletion of the floxed Cx43WT coding DNA and activation of the Cx43G138R allele ubiquitously, in cardiomyocytes or in early neurons, respectively.
To check for recombination after exposure to Cre-recombinase activity, *Bam*HI digestion and hybridization with the internal probe were performed as described for screening of ES cell clones.
Genotyping was performed by the PCR analysis using primers flanking the 5' upstream loxP site (primer1_loxP and primer2_Cx43). All experiments were carried out with littermates of 87.5 % C57BL/6 genetic background.

For Northern blot hybridization hearts and brains from transgenic and control mice were collected in liquid nitrogen. Total RNA was extracted using TRIZOL (Invitrogen, Carlsbad, USA), following the instructions of the manufacturer. Twenty micrograms were electrophoretically separated, blotted and hybridized as described (Hannemann et al., 1992). The same 550 bp *Hin*cII fragment of the Cx43 coding region that was used for Southern blot hybridizations was also applied for Northern blot hybridization.

3.1.2 Morphologic abnormalities in Cx43G138R heterozygous mice equal those in ODDD patients

For recording of syndactylies, malformations of teeth and fur mutant and control mice were anesthetized and photographed using a Kodak 5 Megapixel camera.
Comparative analyses of skull bones were performed using skulls from mutant and control mice of 3 weeks and 6 months of age. The skin, the brain and most of the flesh were removed. Then, the skulls were incubated with maggots cultures over night. The remaining tissue was removed carefully, and the skull bones were cleared in a 13 % H_2O_2 solution for 5–10 min.

3.1.3 Bone and cardiac morphology of Cx43 +/G138R mice

Hearts investigated in the electrophysiological studies were fixed in 4 % paraformaldehyde for 24 h at 48 °C, dehydrated and embedded in paraffin. The 3 mm thick sections were dried, deparaffinized with xylene, hydrated in a dilution series of ethanol, stained with hematoxylin/eosin, treated with xylene and mounted in Entellan (Merck, Hohenbrunn, Germany). For bone analyses, tibiae were dissected and fixed in 10 % formalin, decalcified in 14 % EDTA for 14 days and embedded in paraffin. Sections were stained with hematoxylin/eosin. Quantitative histomorphometry was performed in an area 175–875 mm distal to the growth plate using the OsteoMeasure software program (Osteometrix, Atlanta, GA, USA) in an epifluorescence microscopic system, as detailed (Castro et al., 2004) elsewhere. The following parameters of bone remodeling were estimated: trabecular bone volume as a percentage of total tissue volume (BV/TV), trabecular separation (Trabec.Sp. in micrometers) and osteoblast perimeter per bone surface (Ob.Pm/BS. in percent).

3.1.3.1 Tissue preparation, fixation and sectioning

Hearts or brains were frozen in liquid nitrogen and embedded in Tissue Tec (Miles Inc., OH, USA) for cryostat sectioning. The sections (9 mm) were dried on air, fixed with absolute ethanol for 5 min, washed three times with PBS^-, blocked in 4 % bovine serum

albumin (Sigma Aldrich, Steinheim, Germany) for 30 min and incubated with rabbit anti-Cx43 serum (Wilgenbus et al., 1992) in blocking solution for 1 h. After washing with blocking solution, the specimen were incubated for 50 min with goat anti-rabbit antibodies conjugated with Alexa 594 (1:2000 in blocking solution; MoBiTec, Göttingen, Germany) followed. After an additional washing step, the sections were embedded in Permaflour and analyzed with a Laser Scanning Microscope (LSM Axioplan 2; Zeiss, Germany).

3.1.4 Immunoblot analysis and immunoprecipitation

Hearts, brains or HeLa cells were solubilized in RIPA buffer and 1x Complete (Roche, Mannheim, Germany) and sonicated three times for 10 s during incubation on ice. For immunoprecipitation, rabbit Cx43 serum (1:1000 in blocking solution) (Wilgenbus et al., 1992) was incubated with 10 ml protein A–Sepharose beads (Amersham Bioscience) for 30 min at 4°C. Three hundred and fifty microgram protein were incubated with the antibodies–bead complexes for 1.5 h at 4°C and washed three times with RIPA washing buffer for 10 min. For immunoblotting, the total protein was separated in SDS–PAGE and blotted onto Hybond ECL membrane (Amersham Bioscience). After blocking with 5 % milk powder in washing buffer (8.5 mM Tris– HCl, 1.7 mM Tris-base, 50 mM NaCl, 0.1 % Tween-20) for 1 h at room temperature, a 1 h incubation was performed with rabbit Cx43 antibodies (1:2000 in blocking solution) and a 45 min incubation with goat anti-rabbit horseradish peroxidase (HRP)-conjugated antibodies (1:25000 Dianova, Hamburg, Germany), with three wash steps in-between and afterwards. The membranes were incubated with enhanced chemiluminescence reagents (Amersham Bioscience) and developed on X-ray films.

3.1.5 The Cx43G138R mutation frequently results in premature death because of cardiac expression

Genotype statistics for progeny from heterozygous Cx43floxG138R mice after mating with PGK-, alphaMyHC- or Nestin-Cre mice were calculated using Microsoft Excel. In the case of PGK-Cre mice mating n = 32 litters were genotyped and counted out. For the

conditional activation of the Cx43G138R mutation in the heart (alpha-MyHC-Cre mating) n = 29 matings and for the activation of the mutation in early neurons n = 15 matings were used for the statistical evaluation.

3.1.6 Cardiac function in cardiac specific Cx43G138R mutants

All cardiological analyses were performed in cooperation with Dr. Philipp Sasse and Prof. Dr. Bernd Fleischmann from the Institute of Physiology I, University of Bonn, Dr. Jan W. Schrickel and Prof. Dr. Thorsten Lewalter, Dr. Alexander Ghanem, Dr. Clemens Troatz and PD Dr. Klaus Tiemann for the Medical Clinic and Polyclinic, University of Bonn.

3.1.6.1 Electrophysiological examination and Langendorff measurements

All electrophysiological in vivo measurements were carried out as previously described (van Rijen et al., 2004). For evaluation of *ex vivo* myocardial conduction velocities and characteristics, hearts were Langendorff-perfused, and epicardial activation mapping (EAM) was performed using a 128-electrode array. Hearts were excorporated, dissected from surrounding tissue in ice-cold Krebs–Henseleit buffer and retrogradely perfused in a Langendorff apparatus (Radnoti Technologies Inc., Monrovia, CA, USA) at constant pressure (80 mmHg). The perfusate composition was (in millimolar): NaCl 110, KCl 4.6, $MgSO_4$ 1.2, $CaCl_2$, NaH_2PO_4 2, $NaHCO_3$ 25, glucose 8.3, Na-pyruvate 2 and gassed with carbogen (O_2 95 %, CO_2 5 %), pH, 7.3–7.45 at constant 37 °C.

Under normal perfusion conditions, all hearts started beating spontaneously. Hundred twenty-eight unipolar extracellular electrograms were recorded from the epicardial surface of the left ventricle using a custommade electrode array. Interelectrode distance was 300+7 mm. Unipolar electrograms were recorded using a 128 channel computer-assisted recording system (Multi Channel Systems, Reutlingen, Germany), with a sampling rate of up to 25 kHz. Data were bandpass-filtered (50 Hz), digitized with 12 bit and a range of 20 mV.

Activation maps were calculated from these data using custom-made software (Labview 7.1, National Instruments, Austin, TX, USA). The first derivative of each unipolar

electrogram was evaluated, and the maximal negative dV/dt activation was defined as time point of local activation in these mappings, as described before (van Rijen et al., 2004; Lammers et al., 1990; Li et al., 1999). Color-coded mapping indicated in red earliest activated and in blue the latest activated areas during heart beat.

3.1.6.2 *In vivo* recordings of electrocardiograms and hypoxic stimulation

For *in vivo* ECG recordings, each animal was placed in a small apparatus (ECG tube, QRS Phenotyping Inc., Calgary, Canada), where the feet had contact to gel electrode pads (Hesse et al., 2007). ECG waves and intervals were measured with a PowerLab 26T device (ADInstruments, Colorado Springs) and tabulated using a pattern recognition program (Chart 5 Pro ADInstruments). For hypoxic stimulation *in vivo*, the animals were placed into the ECG tube, anesthetized with 0.5 % isoflurane and exposed to hypoxic (hypoxia = gas mixture of 5–10 % O_2 with 95–90 % argon) for 2 min or normoxic conditions.

3.1.6.3 Echocardiography

High-resolution echocardiography was performed using an ultrasound system equipped with a linear array transducer operating at an emission frequency of 15 MHz (harmonic-mode) with frame rates up to 280 Hz (HDI-5000, Philips Medical Systems). Axial resolution was about 100 μm.
Because ubiquitous and cardiac-specific mutants showed in contrast to wild-type mice a high lethality during isoflurane or sevoflurane anesthesia following standard protocols were administered for sedation at a constant body temperature (37°C): ketamine (10 mg/ kg weight) with disoprivan (0.05 mg/kg weight). Data sets were obtained as previously described (Tiemann et al., 2003; Ghanem et al., 2006).

Heart frequency, left ventricular muscle mass, left ventricular end-diastolic volume and left ventricular ejection fraction were measured. Parasternal short-axis views were visually divided into six segments. Imaging was considered adequate when the endocardial and epicardial borders could be properly visualized in at least five segments.

End-diastolic measurements were obtained at the peak of the R-wave, whereas end-systolic measurements were obtained at the time of minimum internal chamber dimensions.

3.2 Analysis of Cx43-/G138R hemizygously mutated mice

3.2.1 Simultaneous detection GFP and LacZ in mice tissues

The simulataneous detection of *eGFP* (reporter gene in the Cx43G138R mutant) and *LacZ* (reporter gene in the Cx43LacZ mutant) gene products was performed in immunofluorescence analyses of brain and heart thick slices. The animals were anesthetized with Rompun (0.2 %) and Ketavet (0.5 %) (10 ml/kg), thereafter 1 ml Heparin (Roche, Manncheim) was injected into the left ventricle of the mouse to avoid blood clots. Using the same condition 10 ml PBS^- were applied, whereas the right atrium was transsected to wash out the blood from the tissues. Subsequently the mice were transcardially perfused with 50 ml 4 % PFA/PBS^-. The brains and hearts were isolated and postfixed at 4 °C overnight with 4 % PFA/PBS^- and sectioned with a Leica microtome in 60 µm slices. For ß-galactosidase, GFP, GFAP and NeuN immunofluorescence analyses floating slices were washed three times for 10 min in PBS^-/0.1 % Triton X-100, blocked for 2 h at room temperature in washing solution containing 2 % normal goat serum and incubated overnight at 4 °C with a mixture of primary antibodies diluted in blocking solution. The slices were washed three times and were incubated for 2 h at room temperature with the appropriate secondary antibodies diluted in blocking solution and washed again. The appropriate antibodies are listed in the Material chapter (2.6). Cover slips were mounted with Permafluor aqueous mounting solution (Immunotech, Marseille, France). Immunofluorescence signals were visualized using a confocal Zeiss LSM510 microscope.

3.2.2 Analyses of apoptosis in interdigital spaces

TUNEL assays (Roche, Mannheim, Germany) were performed on 12 µm thick cryo-slices for detection of apoptotic cells between the developing digits in paws from ED 12.5 and 13.5 old embryos following the instructions of manufacturer.

3.2.3 Expression of diverse morphogens during development of limb bud

Diverse morphogens were detected in situ by immunohistochemistry staining of whole mount embryos following the adapted protocol from Dent et al. (1989) and LeMotte et al. (1989).

Cx43 +/del female mice were mated with Cx43 del/G138R males. Pregnant females were prepared, embryos were collected in PBS^- and yolk sacs were used for DNA isolation and genotyping. Embryos were fixed in freshly prepared methanol/DMSO (4:1) at 4°C overnight. For blocking endogenous peroxidase activities the embryos were transferred into methanol/DMSO/H_2O_2 (4:1:1) solution for 5-10 hours at room temperature. At this point the supplements can be stored in 100 % methanol at -20 °C for several months. All following steps were carried out in siliconized microtubes. The preparations need to be rehydrated in 50% methanol, PBS^- and twice PBS^- with 2 % nonfat instant milk and 0.5 % Triton X-100 (PBSMT) for 30 min with rocking, respectively. The primary and secondary antibodies are applied in PBSMT at 4 °C overnight consecutively and washed five times with PBSMT after their incubation as follows: once with 1 ml for 1 hour at 4 °C, one with 10 ml for 1 hour at 4 °C , three times in 10 ml for 1 hour at room temperature. The supplements are rinsed in PBS^- with 0.2 % BSA and 0.5 % Triton X-100 (PBT) two times (once with 5 ml and once with 1 ml) for 20 min, respectively. The staining is achieved with DAB/$NiCl_2$ or Histogreen reagent (Linaris, Wertheim-Bettingen, Germany) and H_2O_2 to a 0.03 % final concentration for 2-10 min. The supplements were photographed directly after staining

3.2.4 Real-time RT-PCR analyses

RNA was obtained from ED 11.5, 12.5, 13.5 and 14.5 old mutant and control embryonic limb buds after dissection using the RNeasy kit (Quiagen, Hilden, Germany). Reverse transcription of RNA was performed according to Söhl et al. (1998). One twentieth of the transcribed cDNA was amplified by PCR. The reaction was performed using 20 µl of total reaction mixture volume, containing 1 µl of cDNA reaction products and 0.2 µl of SYBR Green I as follows: one cycle at 95 °C for 10 min, followed by 40 amplification cycles, each cycle consisting of denaturation at 95 °C for 30 s, primer annealing at 59 °C for 30 s and extension at 72 °C for 30 s. Alterations were determined based on average cycle threshold values for duplicates.

3.2.5 Limb bud cultures

For assessment of limb bud cultures ED 11.5 and ED14.5 embryos were dissected from pregnant female mice, the limb buds were removed, fragmentated and digested with a collagenase/trypsin (3:1) solution for 20 min at 37 °C. The enzyme solution was discarded and tissue fragments collected at the bottom of the tube. The primary cells were separated by pipetting of 300 µl primary cell culture medium as described for cardiomyocyte cultures (Herr et al., 2001). After an incubation for 30 min at room temperature with rocking the cells were seeded onto cover slips for immunofluorescence analyses, standard cell culture dishes for Western blot lysates or ibidi µ-dishes® (ibidi, Martinsried, Germany) for calcium imaging.

3.2.6 Immunofluorescence analyses of limb bud cultures

Limb bud cells from wild-type, Cx43 LacZ/G138R and Cx43 LacZ/LacZ embryos grown on glass cover slips to a confluence of 70 %-100 % were fixed in 4 % PFA, washed in PBS^- and preincubated for 1 h in blocking reagent (PBS^- containing 5 % NGS). All slides were incubated overnight at 4 °C with polyclonal anti-Cx43 (1:500, Traub et al., 1994), anti-Oct3/4 (Santa Cruz, CA), Vimentin (Progen Biotechnik), Shh (RnD Systems) or Bmp2 (RnD Systems) antibodies. The localization of the proteins was visualized using

the following secondary antibodies: Alexa(488)-goat anti-rabbit (Molecular Probes), Cy5-donkey anti-mouse (Dianova) or Cy3-goat anti-guinea pig (Jackson ImmunoResearch).
Cover slips were washed in PBS^- and mounted with the aqueous mounting medium Permaflour (Immunotech, Marseille, France). Fluorescent signals were recorded using Zeiss LSM510 confocal microscope.

3.2.7 Calcium imaging

The imaging of calcium concentrations in living cells was performed in cooperation with Dr. Hartmann Harz (Bioimaging Zentrum, University of Munich).

The calcium imaging technique allows to detect changes in intracellular calcium concentration with high temporal and spatial resolution. Here, fluorescence microscopy with a CCD-camera and image processing were combined. In order to measure free intracellular calcium ions fluorescent, polycyclic chelate molecules were used which change their fluorescence properties in Ca^{2+} bonded or Ca^{2+} unbonded state. These Ca^{2+} indicators can be divided into such shifting their excitation and emission spectra (for example Fura-2 or Indo-1) or such increasing their fluorescence ability after binding to Ca^{2+} (for example Fluo-4, Calcium Orange, Calcium Crimson). The diverse Ca^{2+} indicators show different Ca^{2+} binding affinities. Indicators with a high affinitiy are: Fura-2, Fluo-4, Indo-1, whereas Fluo-4FF, Fluo-5N, Calcium Crimson show relative low affinities for Ca^{2+} ions. The dissociation constant (K_D) of each indicator assigns the concentration range in which it should be used.
For Ca^{2+} visualization during this PhD work the indicator Fura-2AM was used to determine high Ca^{2+} concentrations. The acetoxymethyl(AM)-ester group coupled to the Fura molecule is hydrophobic and uncharged, thus, could pass through the plasma membrane. In the cytosolic compartment of the cell the AM group can be cleaved by unspecific esterases. After cleavage the indicator is negatively charged and cannot penetrate through the plasma membrane and therefore stays in the cytosol.
The changes of intracellular Ca^{2+} concentration can be recorded as changes in fluorescence intensities which were converted into false color images by the associated

computer software. Low Ca^{2+} concentrations were indicated in dark blue, whereas high concentrations were displayed in bright red colors. A pile of images can be recorded during one experiment and can be processed and calculated with the associated imaging software. Thus, images from one experiment can be arranged into a movie showing the temporal change of Ca^{2+} concentration in cultured cells. Also kinetics of regions of interest, i.e. cells can be assessed.

3.3 *In vitro* analyses of the Cx43G138R and other ODDD associated Cx43 mutations

HeLa cells were stably transfected with a vector containing the Cx43G138R-IRES-eGFP cassettes or the Cx43-coding DNA driven by a CMV promoter for overexpression. Double transfectants were generated by stable transfection of Cx43 expressing cells (Traub et al., 1994) with the Cx43G138R vector. The recombinant ES cells were generated by homologous recombination, as described earlier. To express the Cx43G138R protein, the ES cells were transduced with Cre protein and subcloned, as previously described (Nolden et al., 2006). The cardiomyocytes were derived from Cx43+/floxG138R:alphaMyHC-Cre and for controls from Cx43+/floxG138R ventricles of embryonic hearts on ED 12.5 and ED 16.5, as described previously (Herr et al., 2001). Each heart was dissociated and plated separately; its genotype was identified by green fluorescent protein and proven by PCR of the remaining embryonic tissue.

3.3.1 Tracer coupling of Cx43G138R expressing cells and electrophysiological measurements of Cx43G138R channels

All tested cells were microinjected by iontophoresis with neurobiotin at confluency. In the case of embryonic cardiomyocytes, the peripheral cells of beating cell clusters were injected. The cultures were fixed in a fresh 1 % glutaraldehyde in PBS^- for 5 min, washed twice with PBS^- and permeabilized with 2 % Triton X-100 for 2 h at room temperature. After washing with PBS^-, the cells were incubated with HRP-conjugated avidinD (Vector Laboratories, Burlingame, CA, USA) solution for 90 min, washed again and stained with

the HistoGreen POD substrate kit (Linaris, Wertheim- Bettingen, Germany), following manufacturer's instructions. To study whether heterotypic Cx43G138R-Cx43WT channels are functional, Cx43G138R expressing HeLa cells and HeLa cells expressing Cx43WT-eGFP as a fusion protein were co-cultured. Cell pairs showing visible eGFP fluorescent plaques were identified and measured. Patch clamp protocols were used, as described previously (Kreuzberg et al., 2005).

3.3.2 ATP release and dye uptake studies

To measure the activity of ATP-releasing channels, cells were incubated in 500 ml modified Hank's balanced salt solution (HBSS; Sigma Aldrich) with or without Ca^{2+}, Mg^{2+} and additional 1 mM EGTA for 20 min at 37 °C. For hypoxic stimulation, the cells were incubated for 2 h in a hypoxic incubator (Herolab, Wiesloch, Germany). For ATP release experiments, 100 ml of the supernatant was collected and incubated with 100 ml nucleotide releasing reagent (ViaLight HS kit, Cambrex, Rockland, ME, USA) for 20 min. The luciferase activity indicating ATP concentration was measured for 10 s with a Berthold Microplate LB96V luminometer after addition of 20 ml ATP monitoring reagent. The luminometric results were normalized to whole protein amount. In studies with HeLa transfected cells, the expression level of the mutant and the wild-type Cx43 protein were determined by the immunoblot analysis. Expression of Cx43G138R was normalized by GFP fluorescence and protein amount.

Hypoxic stimulation of hemichannels was also performed by chemical induction (chemical induced hypoxia, CIH) using KCN and NaI-acetate as recently described for gap junction full channels by Li et al. (2005). Because KCN also oxidizes luciferase, the assay could only be carried out with a saturated $FeCl_2$ solution. By binding of the iron ions to the cyanide$^-$ generating the highly stable $K_4[Fe(CN)_6]$ complex preventing the inactivation of luciferase (Fig. 3.1).

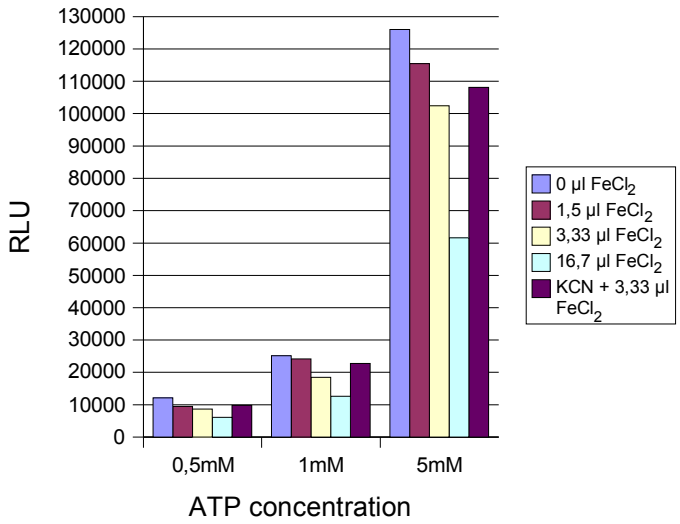

Figure 3.1: $FeCl_2$ prevents the inactivation of luciferase by cyanide. Different amounts of the saturated $FeCl_2$ solution were added to wells containing 0.5, 1 or 5 mM ATP for luciferase assay. $FeCl_2$ inhibits the reaction (see the 16,7 µl $FeCl_2$ bars). However, using 3.33 µl of the saturated $FeCl_2$ solution the inhibition is negligible and the cyanide can efficiently be complexed preventing the inactivation of luciferase (see the KCN + 3.33 µl $FeCl_2$ columns). (RLU=relative luciferase units)

For dye uptake studies, ED 16.5 cardiomyocytes were incubated for 20 min in HBSS solutions with 10 mM propidium iodide, washed twice after bathing, fixed in 4% paraformaldehyde and mounted in Permaflour mounting medium (Immunotech, Marseille, France). The propidium iodide fluorescence was detected with a Zeiss microscope. To exclude all dead cells showing a weak fluorescence, only the number of pixels above a fixed threshold was used for further evaluation.

3.3.3 Contractions of cultured embryonic cardiomyocytes

The beating frequency of cultured embryonic cardiomyocytes was measured after application of different drugs. Cells were exposed to FFA (50 mM, Sigma Aldrich) or the mimetic peptide Gap26 (300 mM, Genscript, USA) for 30 min at 37 °C. Movies of beating cardiomyocytes were recorded with a Sony XCD-X710 (Koeln, Germany) camera at 30 frames/s, and beating areas were analyzed off-line with a custom written software (Labview 7.1 and IMAQ, National Instruments). The number of pixels, which

change their intensity above a defined threshold in consecutive frames, increased with each beat. This was used to calculate interspike intervals that were averaged over at least 20 s to obtain the average frequency.

3.3.4 Determination of the half-life of mutated and wild-type Cx43 proteins by pulse chase analyses

All proteins expressed by HeLa cells were radioactively labelled using ^{35}S-methionine as described by Hertlein et al., 1998. After 4 h of incubation the medium was replaced by one containing non-radioactively labelled methionine. The cells were harvested in RIPA buffer directly or 2, 4, 6 or 8 h after labelling. The expressed connexin proteins were immunoprecipitated using anti-Cx43 antibodies coupled to protein A-Sepharose beads (Amersham Bioscience, Buck, U.K.) overnight. In order to avoid purification of proteins unspecifically binding to the Sepharose, the protein lysates were prehybridized with pure Sepharose beads before immunoprecipitation. On the next day the protein sepharose complexes were denaturated at 60 °C for 5 min and separated by SDS-PAGE. The gels were fixed in a solution containing 50 % methanol, 10 % acetic acid and 40 % water, incubated for 20 min in Amplify (Amersham, Bioscience, U.K.), dried and exposed for 24 h 1 to 14 days. The resulting bands were quantified using the Herolab software (Herolab, Wiesloch, Germany). For dosimetric evaluation the band intensities obtained without chase were defined as 100 %. The half life time of each mutated Cx43 protein was determined as the mean of at last 3 independent measurements using the GraphPad Prism software version 4.02.

3.3.5 ^{32}P labeling of HeLa cells expressing Cx43G138R or wild-type Cx43

HeLa cells cultured on 35 mM dishes were incubated in 500 ml deficiency medium (Dulbecco's modified Eagle's medium without L-glutamine and L-methionine or phosphate, c.c.pro, Neustadt, Germany) for 1 h at 37 °C and afterwards with 50 mCi ^{32}P ATP or 10 mCi ^{35}S methionine per 10^5 cells in same medium for 4 h at 37 °C. The labeled cells were washed three times with PBS$^-$ and harvested in cold RIPA buffer (Degen et al., 2004).

4. Results

4.1 Generation and analysis of Cx43G138R conditionally expressing mice

In order to investigate the influence of Cx43G138R mutation in different tissues, mice were generated in which the cell type-specific activation of this mutated gene could be accomplished by Cre-recombinase-mediated deletion of the loxP flanked Cx43WT region (Fig. 4.1A and B). The Cre-recombinase activity led to the expression of the Cx43G138R-internal ribosomal entry site (IRES)-eGFP cassettes (Fig. 4.1C) under the control of the endogenous Cx43 regulatory elements.

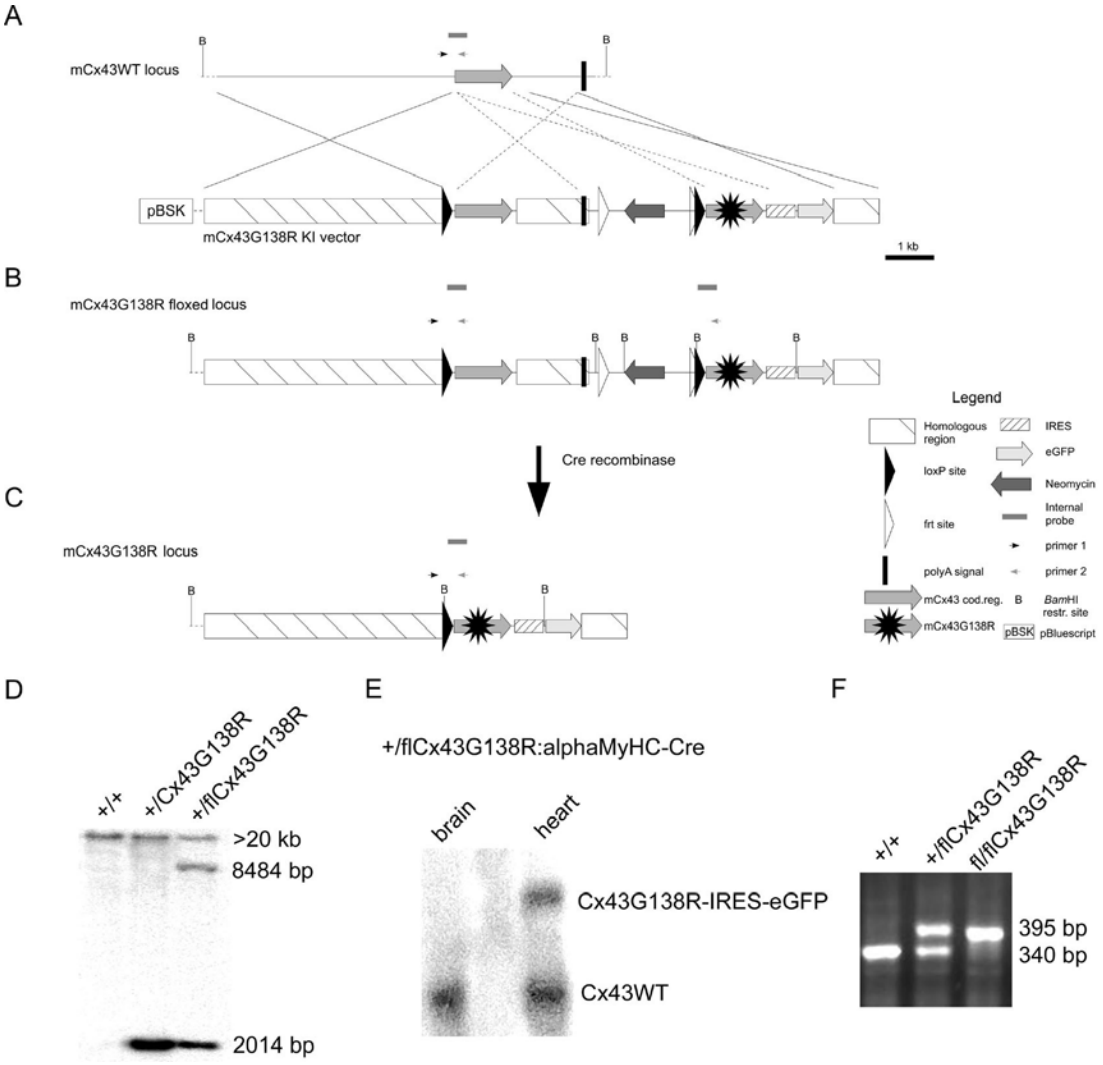

Figure 4.1: Generation of the conditionally Cx43G138R mutated mice by homologous recombination (see next page).

(A) Homologous recombination of the targeting vector into the genomic locus of Cx43. (B) The resulting recombinant chromosome corresponds to the floxed state. (C) After Cre-mediated recombination, sequences between both loxP sites were excised resulting in the Cx43G138R gene expression. (D) Southern blot analysis indicating homologous recombination in mice. The 8484 bp band is missing in the middle lane, demonstrating the deletion of loxP-flanked regions on the DNA. (E) Northern blot analysis indicates the conditional transcription of the mutated Cx43 construct in the heart, but not in the brain after mating with alphaMyHC-Cre mice. (F) PCR genotyping using the primers as shown in A–C.

For the selection of vector containing HM1 embryonic stem (ES) cells, the neomycin resistance gene, flanked by frt sites, was cloned directly after the polyA signal of Cx43WT.

One of 251 ES cell clones (= 0.4 %; clone no. 234) had undergone correct homologous recombination into the Cx43 locus, showed normal caryotype and was used for blastocyst injections. The integration into the Cx43 locus was demonstrated in the different genotypes of the Cx43floxG138R mouse line before and after Cre-mediated recombination (Fig. 4.1D). The Cx43+/floxG138R mice were mated with PGK-, alphaMyHC- or Nestin-Cre-expressing mice for ubiquitous, cardiac myocyte- or early neuron-specific activation of the mutated gene. Furthermore, the cell type-specific transcription of the Cx43G138R-IRES-eGFP cassette, as a long 4.4 kb mRNA, was found in heart but not in brain after the alphaMyHC-Cre activity (Fig. 4.1E). The mice were genotyped by polymerase chain reaction (PCR), as shown in figure 4.1F, using primers (primer 1 and 2 in Fig. 4.1) flanking the first loxP site but binding to endogenous sequence.

4.1.1 Morphologic abnormalities in Cx43G138R heterozygous mice equal those in ODDD patients

The ubiquitous and heterozygous expression of the Cx43G138R mutation resulted in mice exhibiting different ODDD characteristics with variable penetrance and appearance. The observed phenotypic manifestations were syndactyly in 70% (Fig. 4.2A–E), enamel hypoplasia in 80% (Fig. 4.2F and G), craniofacial abnormalities in 70% (Fig. 4.2H) and sparse hair in 30% (Fig. 4.2I) of all mutants. Syndactyly affected only the soft tissue

(type III syndactyly) (Fig. 4.2E) and was observed between the second, third and fourth digits on all limbs. The reduction of dental enamel was obvious as translucent teeth and their faster abrasion with age. Furthermore, the craniofacial anomalies described in ODDD patients, i.e. the prominent and depressed nasal bridge and microcephaly (Paznekas et al., 2003), could largely be observed in the Cx43+/G138R mice. The morphologic skull analysis of 3–9-week-old mutants (Fig. 4.2H) revealed an obvious compactness of the facial region and differences in the angle of the nasal bone, the zygomatic arch, the eye pits and the size of the mandible, similar as reported in ODDD patients (Paznekas et al., 2003). Sparse hair, an infrequent symptom of ODDD, was rarely observed and became more pronounced in adult mice (Fig. 4.2I).

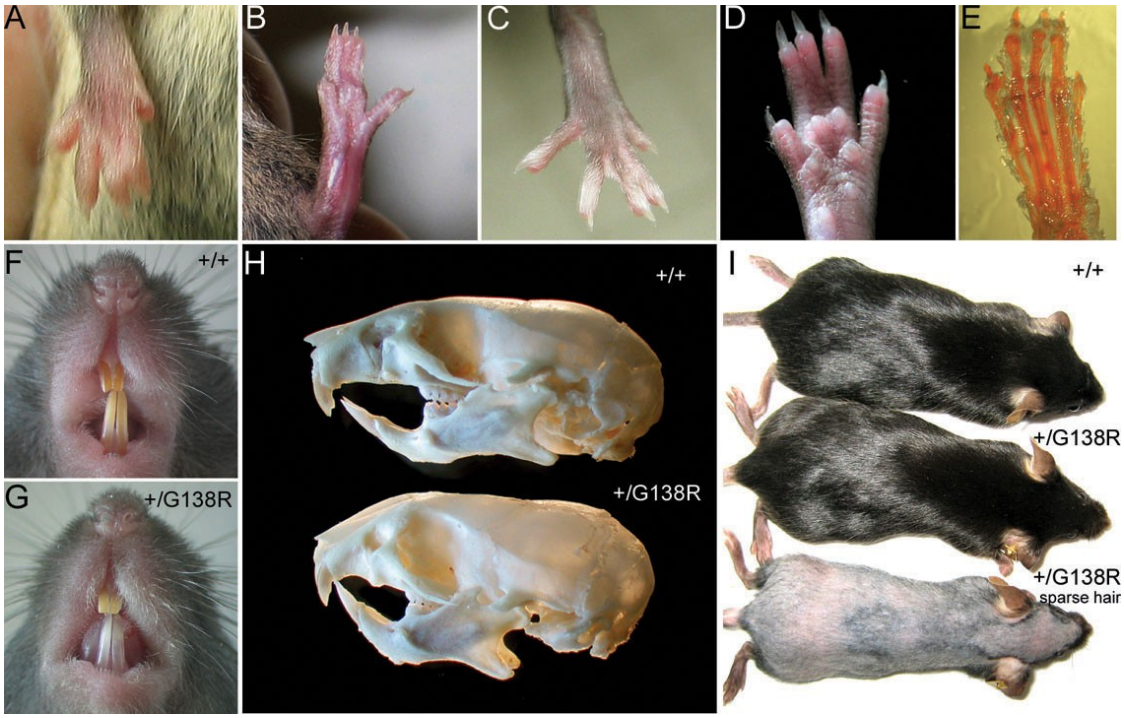

Figure 4.2: Morphological anomalies of the Cx43+/G138R ubiquitously expressing mice. (A–D) Syndactyly of all types. (E) Alcian blue and alizarin red staining for bones and cartilage indicates that bones are not affected by syndactyly. (F and G) Comparison of teeth reveals enamel hypoplasia in mutants (G). (H) Skull bones in mutant mice show significant changes in the craniofacial regions (bottom). (I) Sparse hair could be observed in a small number of mutants but never in wild-type littermates.

4.1.2 Bone morphology of Cx43+/G138R mice is similar to the one observed in ODDD patients

Hypoplasias of the phalages, broad tubular bones and hyperostosis of the skull have also been reported in patients with ODDD (Paznekas et al., 2003). In Cx43+/G138R mice, a significant osteopenia was observed. Seven males per genotype group were used for analysis. The results show significantly lower trabecular bone volume in ODDD relative to wild-type littermates, indicating a reduction in trabecular bone mass. Accordingly, trabecular spacing was increased and the number of osteoblasts was not significantly decreased in the mutant mice (Fig. 4.3), even though trabecular thickness was not different. In all mutants investigated, a high variability of this phenotype was observed.

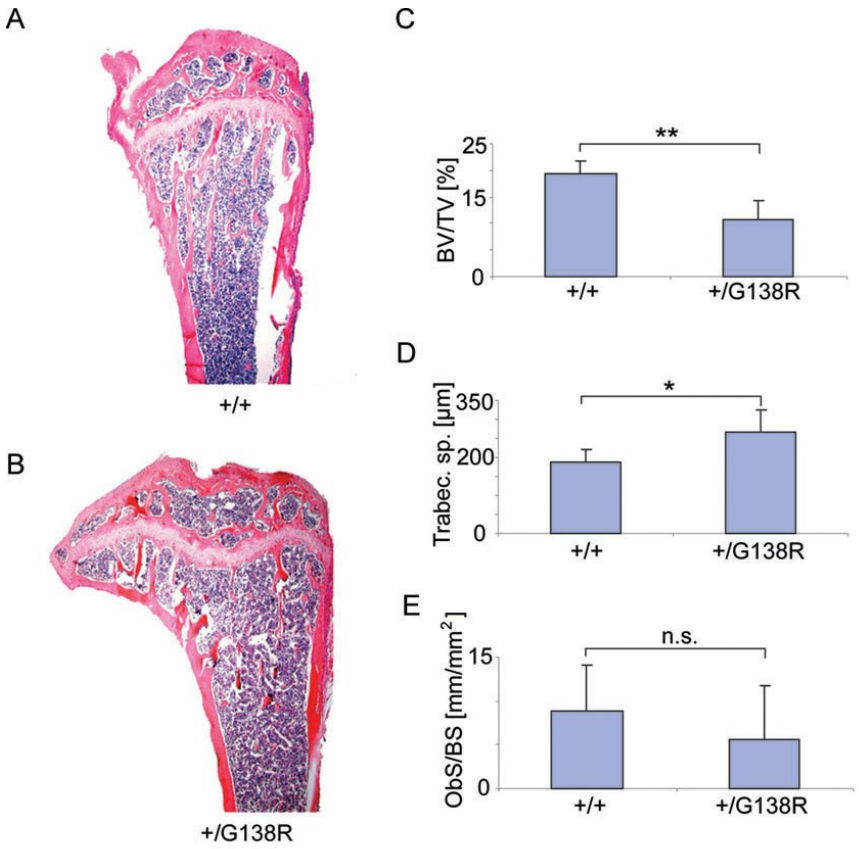

Figure 4.3: Skeletal phenotype of the ODDD-mutated mice. Comparison of wild-type (A) and Cx43+/G138R (B) tibial epiphysis and metaphysis shows more rarefied trabecular structure in the ODDD mutant relative to a wild-type littermate. Histomorphometric analysis reveals lower bone volume/total volume (P=0.001) (C), an increase in trabecular space (P=0.01) (D) and a non-significant (n.s.) decrease in osteoblast number (E) in mutants.

4.1.3 The Cx43G138R mutation frequently results in premature death because of cardiac expression

The matings of Cx43+/floxG138R male mice with PGK-Cre female mice (n = 32) yielded a reduction in the Mendelian ratio from 50 % to 23 % of mutants in a litter (Fig. 4.4). The mutants were Cx43+/G138R:PGK-Cre (5%) and Cx43+/G138R (18%) because of the activity of active Cre protein on the oocyte level (Lallemand et al., 1998). The observed embryonic lethality of 54% in mutants could be narrowed to a period between ED 14.5 and ED 16.5 (data not shown). In order to ascertain the tissue responsible for the lethality, the Cx43+/floxG138R female mice were mated with alphaMyHC-Cre or Nestin-Cre male mice to specifically activate the mutation in heart or early neurons.

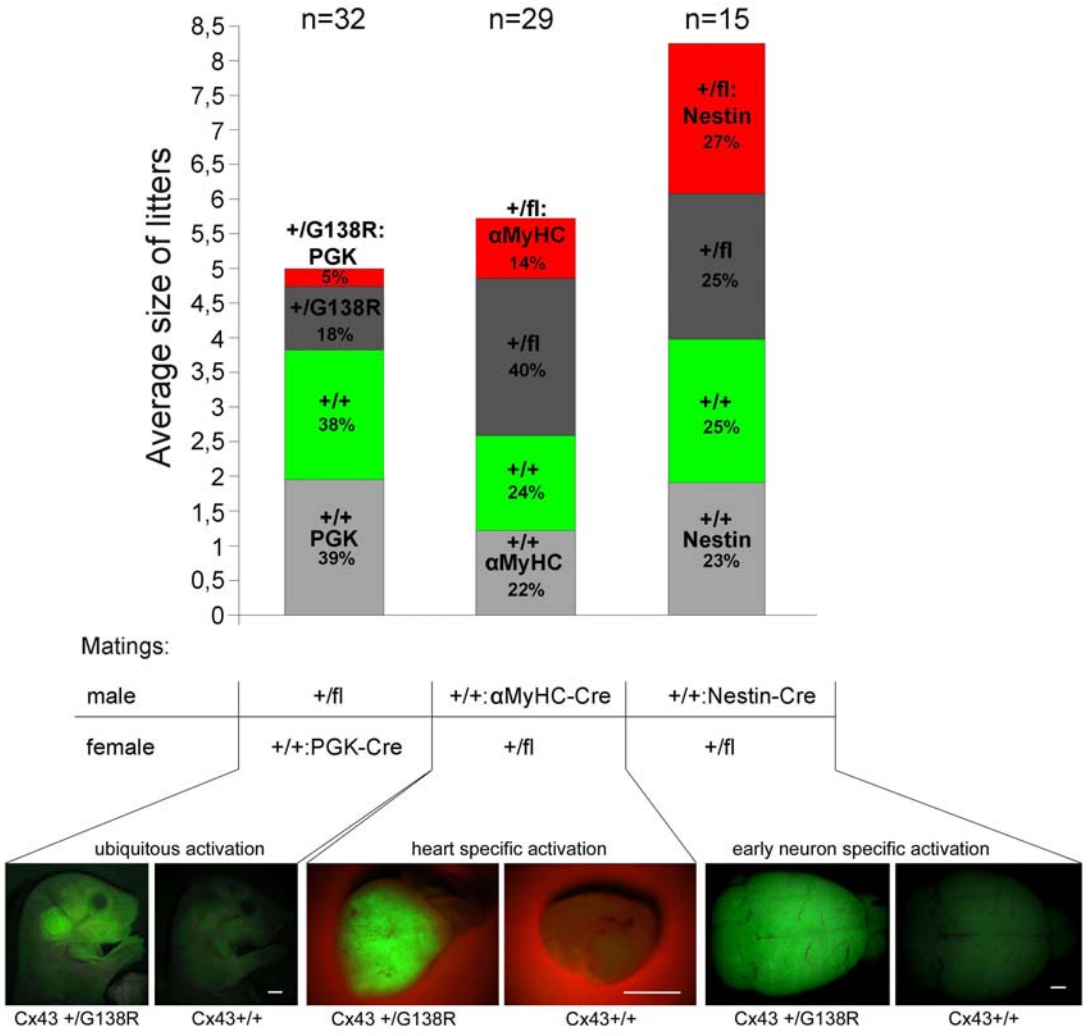

Figure 4.4: Genotype statistics for progeny from heterozygous Cx43floxG138R mice after mating with PGK-, alphaMyHC- or Nestin-Cre mice (see next page).

The ubiquitous expression of the mutated gene after matings with PGK-Cre mice results in the reduction of the number of littermates from the expected 50% to 23% of mutants in a litter. The conditional activation of the Cx43G138R mutation in the heart (alpha-MyHC-Cre mating) led to a smaller reduction in the expected number of mutants per litter from the expected 25% to 14% born. The activation of the mutation in early neurons does not influence the survival of the mutants (Nestin-Cre mating); (n =number of litters). (Scale bars = 1 mm)

Conditional activation of the Cx43G138R mutation in the heart (29 matings) revealed a reduction in the expected number of mutants in a litter (mutants were Cx43+/flox:alphaMyHC-Cre; expected frequency of mutants: 25%, born: 14% and reduction: 44%). Thus, the lethality of mice with cardiac-specific mutation was similar to that observed with the ubiquitous mutants (44% to 54%; P = 0.1, n.s.) and occurred at the same embryonic stage. In contrast, the activation of the point-mutated gene in early neurons, using the Nestin-Cre mice (n = 15 matings), did not influence the survival of the heterozygous mutants (mutants were Cx43+/flox:Nestin-Cre).
The surviving cardiac-specific mutants died during the first 6.5 months after birth (Fig. 4.5). Thus, these data imply that the mutant mice die because of cardiac alterations.

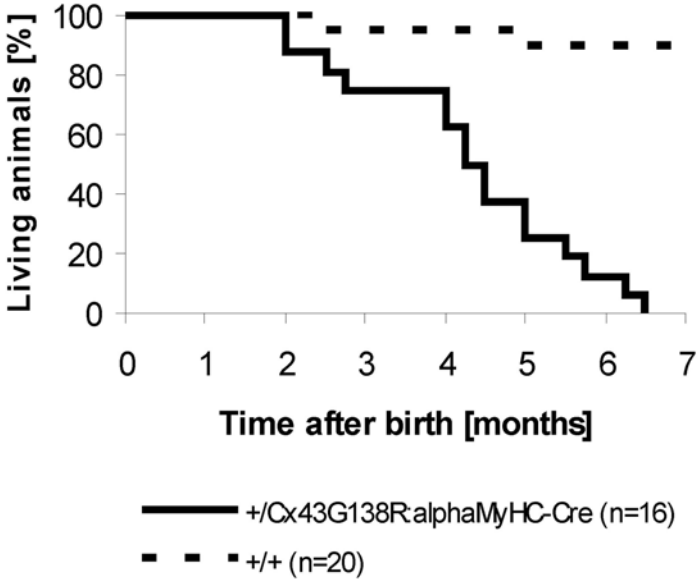

Figure 4.5: Premature death in adult cardiac-specific mutants. The Kaplan–Meier survival curve of Cx43+/floxG138R: alphaMyHC-Cre mice (n =16) in comparison to wild-type mice (n =20) shows premature death of cardiac-specific mutants between 2 and 6.5 months after birth.

These findings reveal the heart as the responsible tissue for the observed lethality and demand further examinations.

4.1.4 Morphologic development of the heart and connexin expression in ODDD mutated hearts

As Cx43-deficient mice died at birth due to a failure in pulmonary gas exchange as a result of an altered right ventricular outflow tract (Reaume et al., 1995), it was important to check the heart morphology in adult mutants (Fig. 4.6 A-D). Nine Cx43+/floxG138R: alphaMyHC-Cre hearts, two Cx43+/+:alphaMyHC-Cre hearts and three Cx43+/+ hearts were morphologically investigated. Two of the nine Cx43+/floxG138R:alphaMyHC-Cre hearts were smaller than that of the control groups. Microscopically, no structural defects were detected. Both atrial septation and ventricular septation were normal. The pulmonary outlet was open, in contrast to subpulmonary obstruction with abnormal pouch formation in Cx43-deficient mice. Coronary arteries originated from the aorta normally, and their arrangement appeared the same as in wild-type mice.

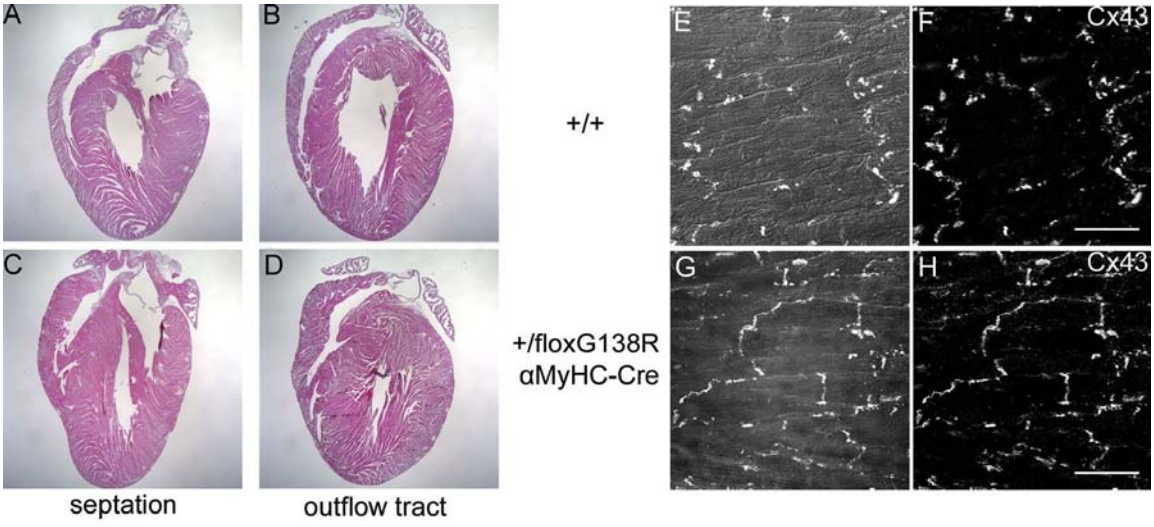

Figure 4.6: Conditional expression of Cx43G138R in the heart reveals normal cardiac morphology. Morphological analyses reveal no obvious change in the right ventricular outflow tract or the septation of mutant hearts (C and D) in comparison to wild type controls (A and B). (E-H) Immunofluorescence analyses indicate localization of Cx43 in controls (E and F) and in heterozygous Cx43G138R mice (G and H), suggesting an unhindered trafficking of the mutated proteins *in vivo*. Some dyslocalization of Cx43 protein from intercalated discs to lateral contact membranes is apparent [phase contrast and Cx43 staining merged in (E) and (G); Cx43 staining in (F) and (H); scale bar = 20 μm].

Immunofluorescence analyses of connexin isoforms in the ventricle revealed a slightly altered localization of these proteins in mutated hearts. Cx43-specific signals were detected in intercalated discs and in lateral contact membranes of ventricular cardiomyocytes (Fig. 4.6G–H), indicating an unhindered trafficking but a slightly changed localization of the Cx43G138R channels. Additional analyses to determine the expression of Cx40 in the atria and Cx45 in the ventricle, where Cx43 and Cx43G138R are co-expressed, revealed no changes in mutated relative to wild-type hearts (Fig. 4.7). This suggests no trans-dominant effects of the mutated protein onto Cx40 and Cx45 in the heart. Thus, this Cx43 mutation is solely responsible for the effects onto cardiac physiology described in chapter 4.1.5.

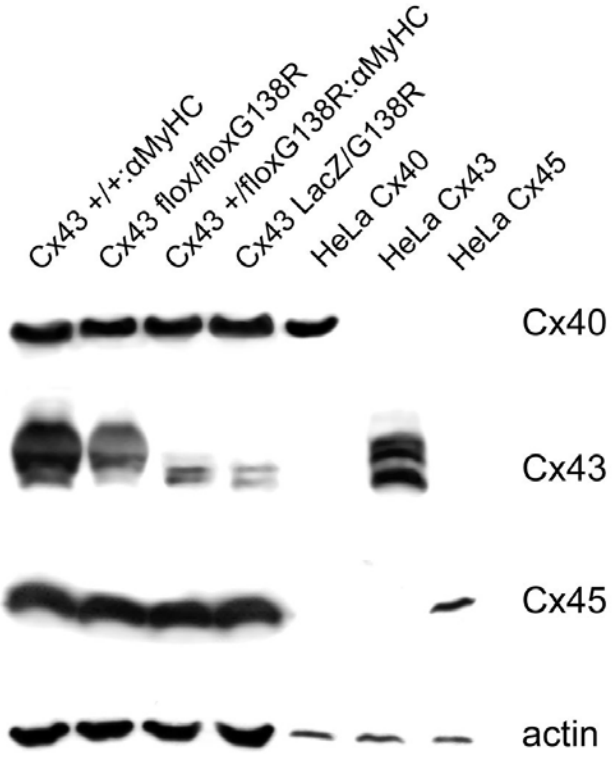

Figure 4.7: Expression of connexin proteins in the ODDD mutated heart. For estimation of Cx40, Cx43 and Cx45 expression in mutated hearts immunoblot analyses were performed. Besides reduced Cx43 levels in heterozygous heart specific mutants (Cx43+/floxG138R: alphaMyHC-Cre) and Cx43LacZ/G138R (see chapter 4.2 for detailed analysis) no alterations of Cx40 or Cx45 expression could be detected.

The Cx43 immunoblots suggest a partial non-phosphorylation of these proteins in mutants. This aspect has been investigated in detail and described in chapter 4.3.6.

4.1.5 Cardiac function in heart specific Cx43G138R mutants (Cx43+/floxG138R: alphaMyHC-Cre)

In two ODDD families, severe cardiac abnormalities have been described resulting in sudden cardiac death probably due to arrhythmia (Paznekas et al., 2003). All Cx43+/floxG138R:alphaMyHC-Cre mice died during the first 6.5 months postnatally (n = 16, Fig. 4.5). Thus, analyses of cardiac function followed to ascertain the impact of the Cx43G138R mutation in the heart and the cause of death in the heart specific mutants.

4.1.5.1 No alteration in echocardiography

Anesthetized mice were also functionally analyzed using echocardiography. This analysis yielded no significant changes to wild-type mice in regard to the heart frequency, left ventricular muscle mass, left ventricular end-diastolic volume or left ventricular ejection fraction (Fig. 4.8).

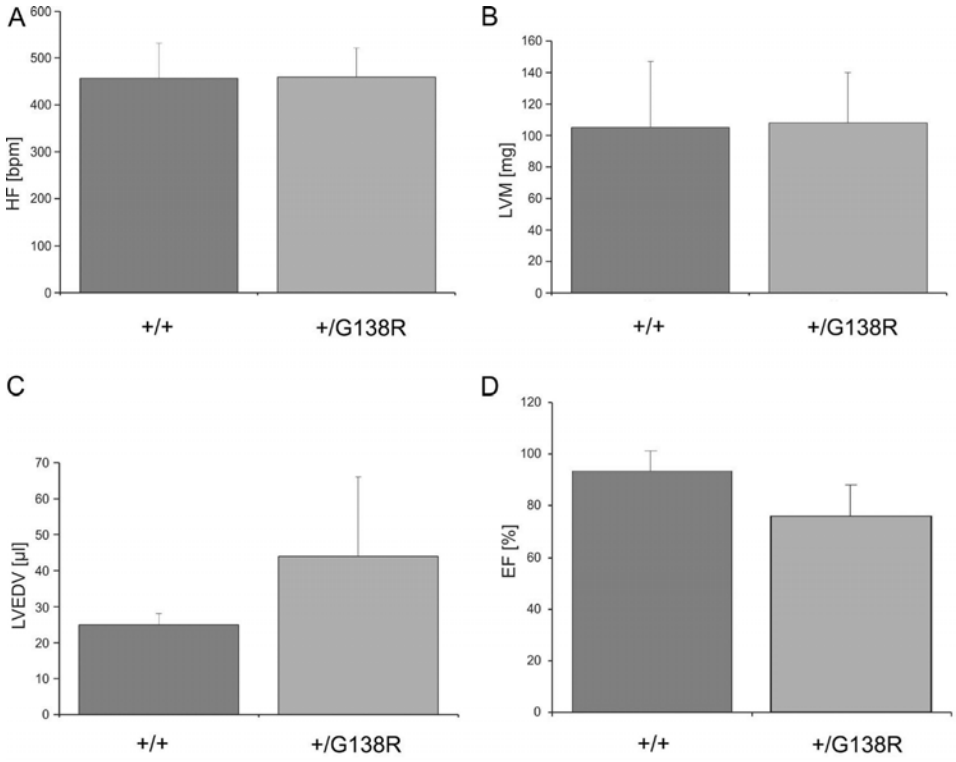

Figure 4.8: Echocardiographic results yield no significant changes in mutant hearts. The mice were analyzed for heart frequency (A), left ventricular muscle mass (LVM) (B), left ventricular enddiastolic volume (LVEDV) (C), and left ventricular ejection fraction (EF) (D) but no significant changes compared to wild type could be observed in the investigated mutants.

4.1.5.2 Disturbed impulse propagation in surface electrocardiograms

The surface and intercardiac ECG studies showed significant changes in P, PQ, QRS and QTc intervals and R and RS amplitudes. The most prominent change was the broadening of the QRS complex and decrease in the R wave, indicating disturbed impulse propagation in the ventricle accompanied by low voltage ECG (Fig. 4.9 and Table 4.1).

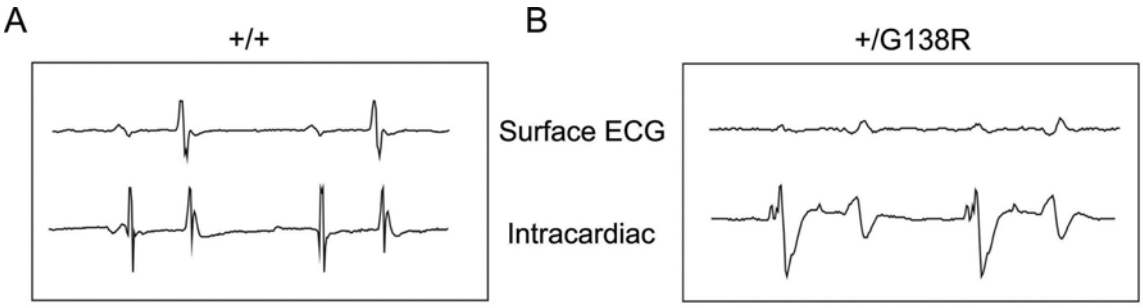

Figure 4.9: Disturbed impulse propagation in mutated hearts. In comparison to wild-type hearts (A) the mutated ones clearly show a disturbed impulse propagation in the ventricle as seen in the striking broadening of the QRS complex in the surface ECG of the mutated hearts (B).

	Cx43 +/+	Cx43 +/G138R	P
P (ms)	14.8±1.3	23.0±3.4	0.013
PQ (ms)	42.8±6.3	53.0±2.0	0.043
QRS (ms)	14.0±0.8	23.8±4.4	0.02
Qtc (ms)	30.1±1.6	36.7±3.4	0.023
R (mV)	0.55±0.07	0.12±0.02	0.001
RS (mV)	1.17±0.25	0.28±0.06	0.005

Table 4.1: Results of surface ECG analyses, including low voltage ECG in Cx43G138R mice. R, R-wave amplitude measured from the isoelectrical line to the maximum of R-wave; RS, maximal amplitude from the maximum of the R-wave to the most negative spike of the S-wave.

4.1.5.3 Spontaneous arrhythmias *ex vivo* in Langendorff analyses

The functional cardiac *ex vivo* analyses in the Langendorff setup revealed spontaneous and sustained ventricular tachycardias or other types of cardiac arrhythmias starting directly after excorporation and continuing during perfusion in all mutants investigated (n=8), but in none of the wild-type animals (n=6; Fisher's test: P=0.0003) (Fig. 4.10B–I). This prevented analysis of sinus rhythm and application of stimulation protocols to Cx43+/floxG138R:alphaMyHC-Cre hearts. Therefore, no systematic evaluation of conductive properties could be carried out, and the mechanism(s) responsible for the induction of these arrhythmias could not be further explored. Epicardial activation maps revealed a heterogeneous distribution of activity in the ventricles during these episodes.

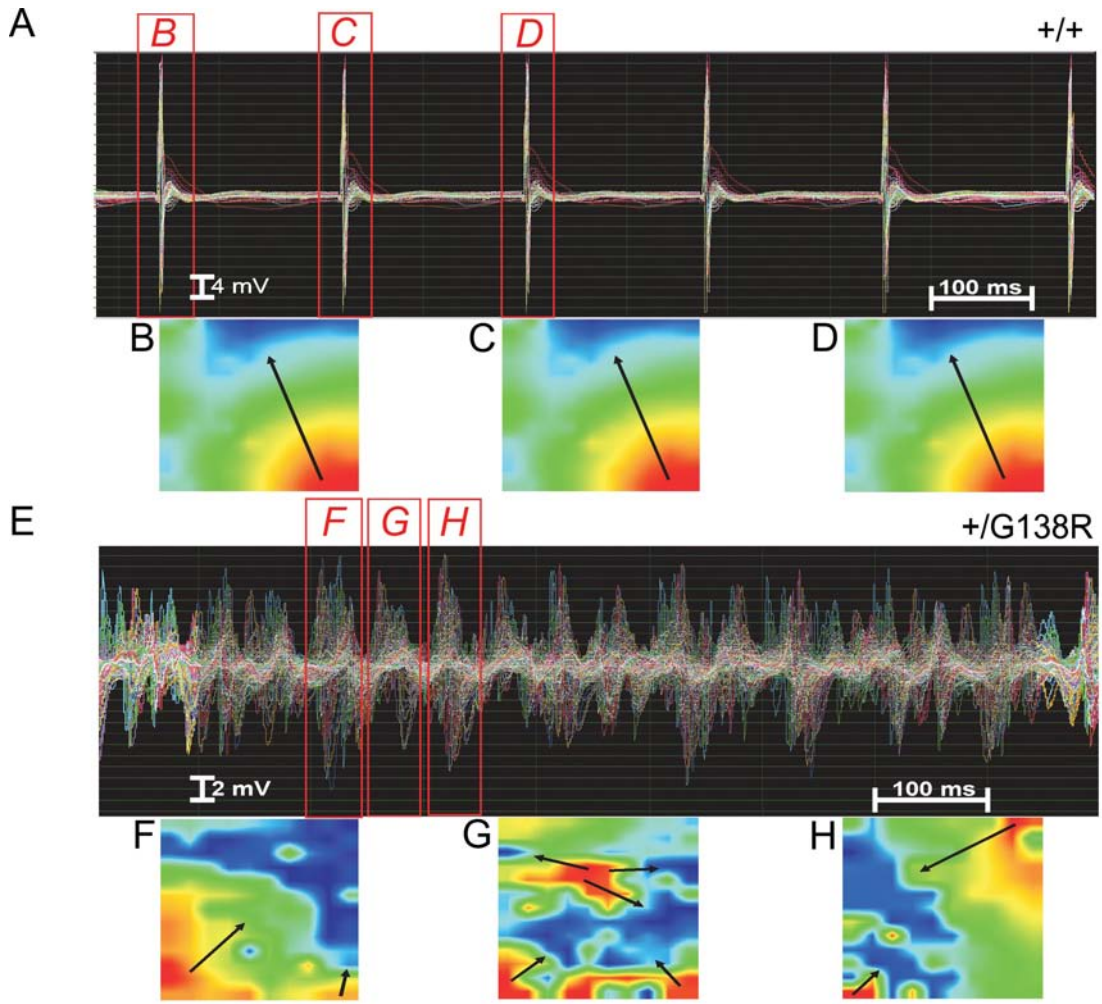

Figure 4.10: Spontaneous cardiac arrhythmias developed in mutated hearts (see next page).

(A) Normal impulse propagation and activation pattern in wild-type (n = 6) but ventricular tachycardias (VT) of all mutated (n = 8) hearts in Langendorff measurements. The cumulative Langendorff recordings of 128 epicardial electrograms clearly show repetitively directed and homologous conduction without signs of conduction disturbances or shifts of conduction speed and direction in wild-type hearts during sinus rhythm (A–D) but a chaotic appearance of field potentials in the mutated ventricles during a polymorphic, high-frequency VT (E–H). Such polymorphic, incessant VTs were spontaneously present in all mutant hearts directly after the initiation of Langendorff extracorporal perfusion. EAMs of the left ventricular epicardium at three different time points during sinus beats in wild-type or polymorphic VTs in mutant hearts are shown in (B-D) or (F-H), respectively. The false color-coded reconstruction with red representing earliest and blue representing latest epicardial activation shows a heterogenic distribution of field potentials with inconsistent direction and speed of ventricular conduction in the Cx43G138R mutated mouse heart (arrows) during VT. This indicates different conduction pathways during different VT beats as typically present in polymorphic VT.

4.1.5.4 Application of inhalation anesthetics induces ventricular arrhythmias in cardiac-specific ODDD mutants

Ubiquitous and cardiac-specific mutants showed in contrast to wild-type mice a high lethality during isoflurane or sevoflurane anesthesia following standard protocols. In order to investigate the reason for the obvious incompatibility towards inhalation anesthetics, ketamine (10 mg/kg weight) with disoprivan (0.05 mg/kg weight) were administered for sedation and isoflurane (0.3 % till exitus) was increasingly applied during echocardiographic recording. Between 2 % and 5 % isoflurane, all investigated cardiac-specific Cx43+/floxG138R:alphaMyHC-Cre mutant mice developed tachycardias and ventricular fibrillation, whereas wild-type mice tolerated these concentrations. Moreover, mutated mice developed apnea at normal sinus-rhythm electrocardiograms, indicating possible hemodynamical complications because of electromechanical uncoupling. This suggests severe electrical and electromechanical disturbances as the cause of death.

However, ECGs could be successfully recorded with several mice before these alterations occurred. These data are already presented in Figure 4.8.

4.1.5.5 Spontaneous arrhythmias *in vivo*

Using surface ECG recordings *in vivo* under normal normoxic conditions, spontaneous arrhythmic events such as ventricular extra systoles (VES) were observed in the Cx43+/floxG138R:alphaMyHC-Cre mice (Fig. 4.11). The frequency and severity of arrhythmic events were strongly increased by hypoxic stimulation (Fig. 4.11 and Fig.4.12). In fact, VES developed with 5.1-fold higher probability during application of hypoxia in mutants, whereas no VES could be seen in wild-type littermates. Even VTs (defined as four or more consecutive VES events) could rarely be observed in mutated mice (Fig. 4.11, middle panel); none of the tested mice died during the hypoxic stimulations.

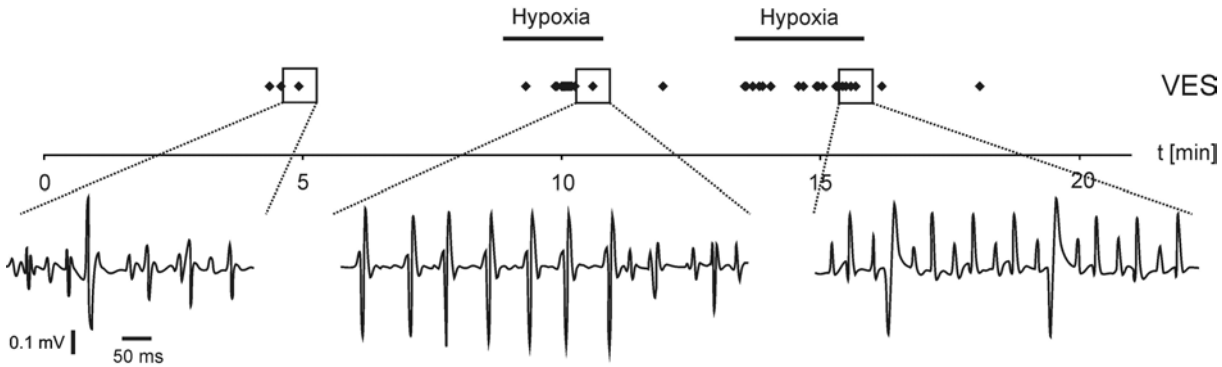

Figure 4.11: Cardiac arrhythmias recorded *in vivo* in cardiac-specific mutants. The frequency of the arrhythmias could be increased by hypoxia (hypoxia bars). Adjustment of O_2 to normoxia largely abolished the arrhythmias. Arrhythmic events (VES) are displayed as individual points (VES during normoxia and under hypoxia). Even VT (1 VT = 4 consecutive VES) could be recorded as a rare arrhythmic event during hypoxia (middle panel).

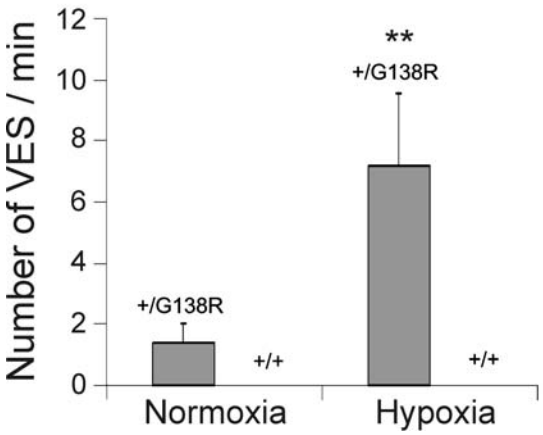

Figure 4.12:

The occurrence of arrhythmic events (ventricular extrasystoles = VESs) increases only in cardiac specific mutants during hypoxic phases. Under normoxic conditions mutant mice developed VES (1.4 event per minute) whose frequency increased while applying 5-10 % O_2 to 7.2 events per minute ($P < 0.005$, $n = 4$).

4.2. Analysis of Cx43G138R/LacZ hemizygously mutated mice

Lethal homozygous connexin mutants which were viable in the hemizygous state were described for Cx43K258stop (Maas et al., 2004) and Cx31F137L (Schnichels et al., 2007) expressing mice. Also in case of the Cx43G138R mice this question remained open. The Cx43G138R hemizygous mutants (Cx43LacZ/G138R) which arose from the matings of Cx43LacZ (Theis et al., 2001) with Cx43G138R mice, were viable. These hemizygous ODDD mutants will be described in the following chapters.

4.2.1 Expression of reporter genes in the two Cx43 mutant mice

The Cx43LacZ/G138R mutants express two reporter genes driven by the Cx43 promoter. It was important to know whether the eGFP reporter protein indicating expression of the point-mutated form of Cx43 is co-localized with ß-galactosidase, indicating Cx43 deficiency. This would demonstrate that the mutation is properly expressed in the mouse tissue. As already mentioned, both reporter genes are driven by the same (Cx43) promoter but the constructs used for the generation of the two mutants differ in their untranslated regions (UTRs). By insertion of the LacZ gene into the genomic locus of Cx43, the 3' regulatory region of the gene was modified but remained unaffected in the Cx43G138R mice. The co-immunfluorescence analyses using anti-eGFP, anti-LacZ and anti-GFAP antibodies revealed a very high co-localization of the two reporter proteins in astrocytes in the brain (Fig. 4.13) and in working cardiomyocytes in the heart (Fig. 4.14). Rarely only LacZ positive cells (5-8 cells in one field of sight) could be detected in the brain.

These data confirm the proper localization of the G138R mutated form of Cx43 in the two tissues (the brain and the heart) and show a negligible percentage (<1%) of not co-localized signals. Cells only expressing LacZ but not GFP might posttranscriptionally down-regulate expression of Cx43. Such regulation of this connexin by microRNA was reported during skeletal muscle development for MIR-2006 (Kim et al., 2006) and the cardiac arrhythmogenesis for miR-1 (Yang et al., 2007). The function of this very small cell population in the brain remains unclear.

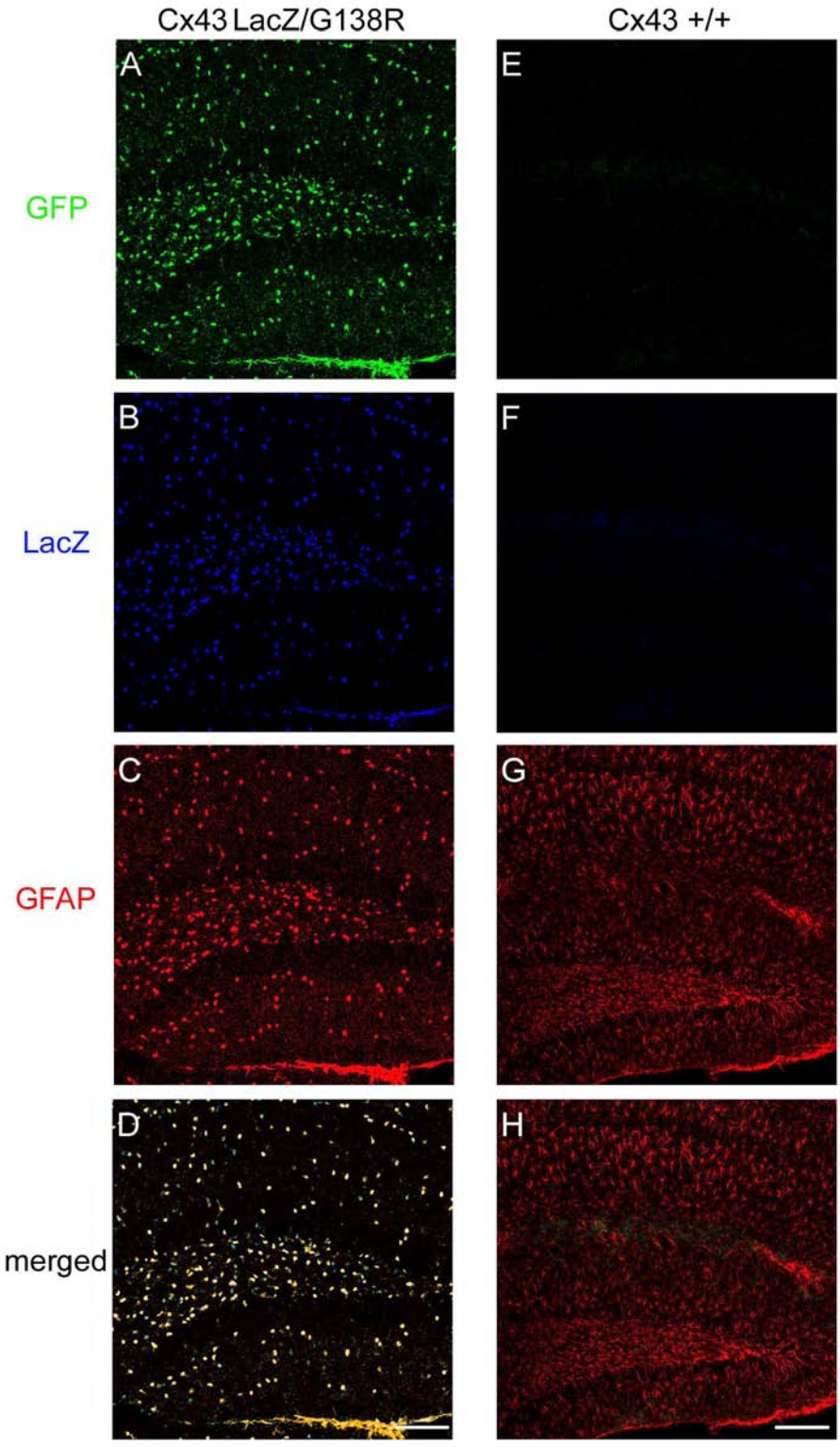

Figure 4.13: Expression of the reporter genes eGFP and LacZ in hemizygous Cx43G138R/LacZ hypocampi. (A+B) Both reporter genes are driven by the Cx43 promoter and are expressed in the hemizygously mutated ODDD mice at the same time in the astrocytes (C). (D) The merged picture shows a high coexpression of the two genes, whereas no GFP or LacZ staining could be detected in wild-type GFAP positive cells (E-H). (Scale bars = 100µm)

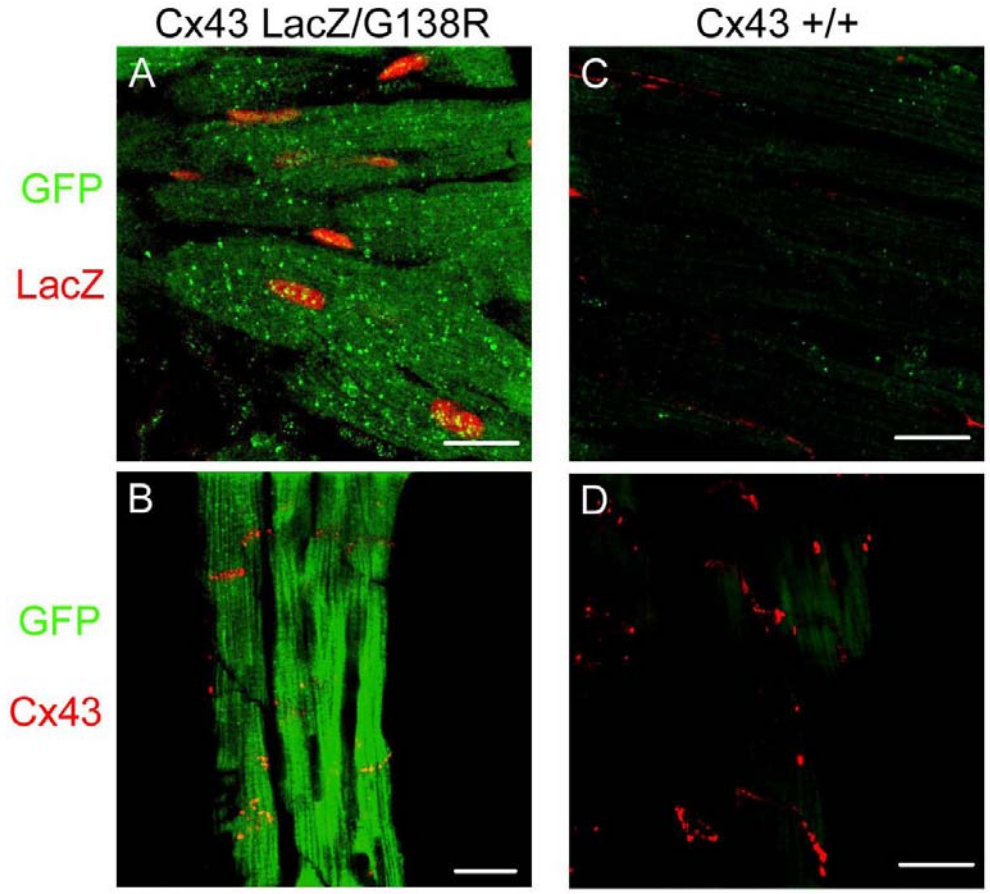

Figure 4.14: Expression of GFP, LacZ and Cx43 in ventricular cardiomyocytes. (A) Cardiomyocytes of Cx43LacZ/G138R express cytosolic GFP and ß-galactosidase in the nuclei, (C) no expression of the reporter genes in wild-type animals. (B) Cx43 containing gap junction plaques are visibly smaller than those found in control mice (D). (Scale bars=20µm in A and C, scale bars = 100µm in B and D)

Furthermore the localization and expression of Cx43 of the hemizygously mutated mice especially in the heart was analyzed (Fig 4.14B). In comparison to wild-type controls (Fig 4.14D) the size of Cx43 immunosignals which may represent gap junction plaques was apparently diminished but still localized in the intercalated discs.

4.2.2 Cx43G138R hemizygousity is not compensated by Cx30 over-expression in the brain

Both, Cx43 and Cx30 are expressed by astrocytes in the mature central nervous system (Nagy et al., 1999). Astrocytes play a neurosupportive role in the brain by secreting cytokines and neurotrophic factors. However, the function of astrocytic connexins remains largely unknown. The gap junction channels, especially consisting of Cx43, seem to play an important role in the brain by decelerating of spreading depression or locomotory activity (Theis et al., 2003). The same authors report a partial compensation of the astrocytic Cx43 deletion by Cx30 up-regulation. The coordinated expression of both connexins was also seen in Cx43flox/flox:Nestin-Cre mice, the only living homozygous ODDD mutant. Here, an 2.5 fold up-regulation of Cx30 was detected relative to wild-type mice or other mutants (Fig. 4.15).

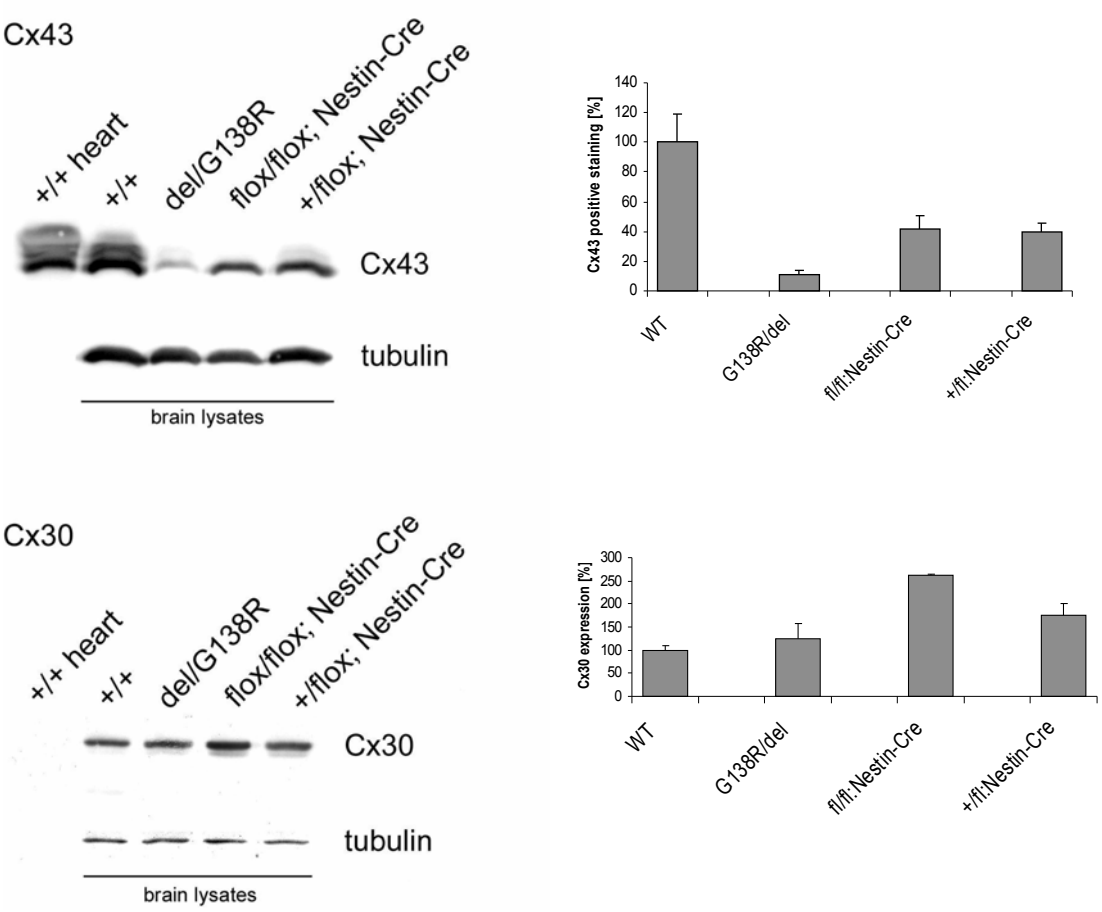

Figure 4.15: Quantified expression of Cx43 and Cx30 in Cx43G138R mice (see next page).

The anti-Cx43 immunoblot (upper left) shows a normal phosphorylation of Cx43 in wild-type heart and brain but an obvious phosphorylation deficit of these proteins in all mice expressing the Cx43G138R mutation. Quantitative evaluation (upper right) revealed a strong down-regulation of Cx43 expression in Cx43del/G138R mice to approx. 15% and in Cx43+/flox:Nestin-Cre and Cx43flox/flox:Nestin to 40%. Quantification of anti-Cx30 immunoblots (bottom left and right) showed no significant up-regulation of Cx30 expression in Cx43del/G138R or Cx43+/flox:Nestin-Cre mice but hints to a possible compensation by Cx30 in the homozygous brain specific mutants (Cx43flox/flox:Nestin-Cre). (n=3, respectively)

The hemizygous mice showed a strongly diminished expression of Cx43 to approx. 15% and no alteration of Cx30 expression. Thus, the hemizygous ODDD mice with strongly reduced Cx43 expression and lack of Cx30 compensation are an interesting model to explore connexin function in the brain.

4.2.3 Nearly all Cx43G138R hemizygous mutants develop similar morphological abnormalities characteristic as ODDD patients

The most noticeable feature of the hemizygously mutated mice was the clear increase of penetrance of the ODDD specific phenotypes. Thus, the appearance of syndactylies in these mice shifted from 70% in heterozygous mutants to 95%, whereas enamel hypoplasia and craniofacial alterations could be observed in over 90% of all born Cx43Lacz/G138R mutants. The high penetrance in these mice was utilized to analyze the underlying molecular mechanisms for the morphologic anomalies in ODDD mutants and were used in all following analyses of this chapter.

4.2.4 Syndactylies are caused by decreased apoptosis in ODDD mutated mice

The programmed cell death occurs in the development of the limb for separating the digits by removing the tissue in between.
To test for apoptosis in the mutated limbs embryonic paws at ED12.5 were prepared from Cx43LacZ/G138R mutated and control mice, sectioned and used for TUNEL assays (Fig.

4.16C and D). Apoptotic cells were admittedly present in mutant limbs but located far in the interdigital tissue (arrows in Fig 4.16D) in comparison to controls (arrow in Fig 4.16C). The limitation of apoptosis in embryonic limbs could be correlated with the appearance of syndactylies in the adult (Fig. 4.16B). Here, the adhesion of the digits was prominent, the separation occurred initially but was strongly limited. Hence, syndactylies in ODDD mutated mice are likely caused by impaired apoptosis of the interdigital tissue.

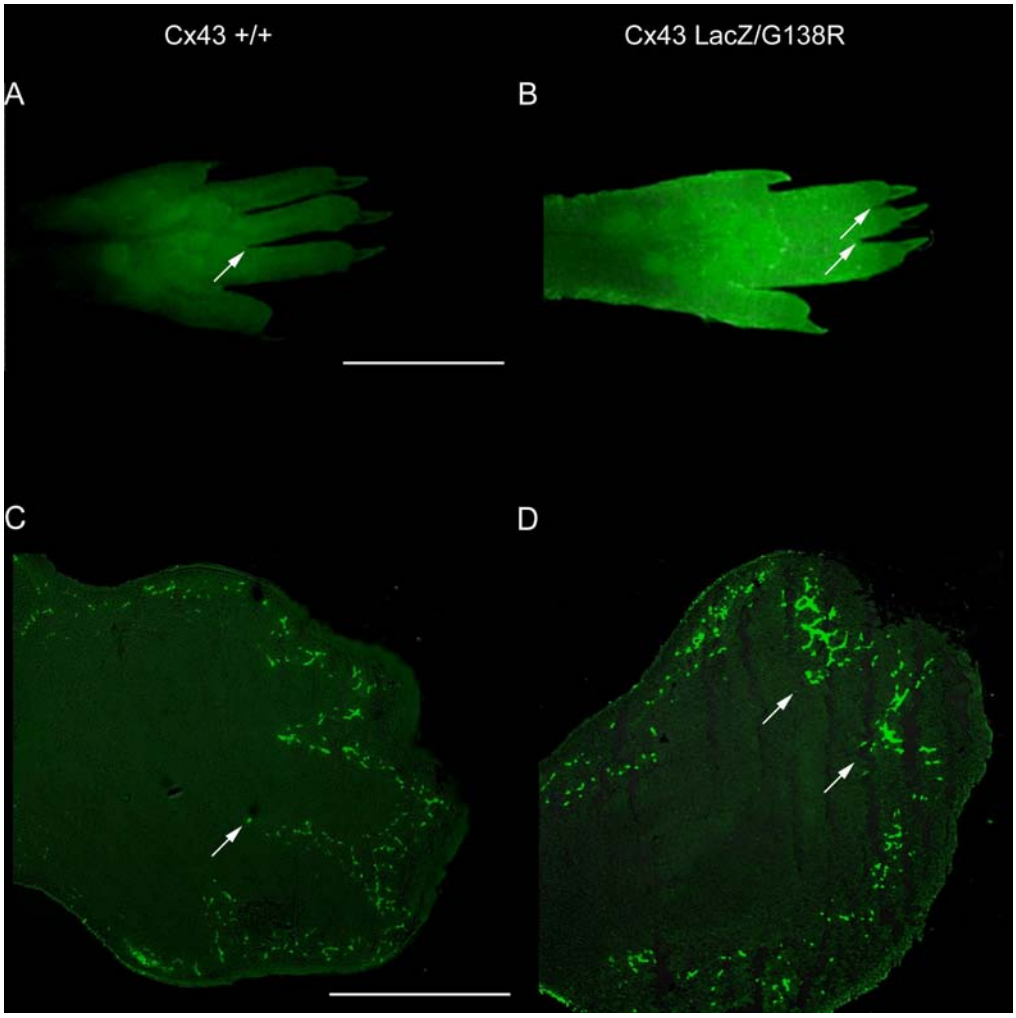

Figure 4.16: Syndactylies are caused by disturbed apoptosis in ODDD mutated mouse limbs. (A and B) GFP fluorescence could be detected in hemizygously mutated mice paws (B) indicating the expression of the Cx43G138R mutation, whereas wild-type paws (A) showed no GFP-fluorescence. (C) Normal apoptosis in wild-type embryonic limbs (ED12.5) and disturbed apoptosis in mutants (D). Arrows point at the apoptotic progression clearly showing the impairment of apoptosis in mutants (D). (Scale bars in A and B = 5 mm, in C and D = 500 µm)

4.2.5 Expression of diverse morphogens in Cx43 mutated mice

The morphologic phenotypes of the Cx43G138R expressing mice like syndactylies, craniofacial or dental anomalies as well as osteopenia are developmental disorders or disturbances in bone homeostasis. Important for these processes are morphogens, i.e. proteins acting mainly during differentiation and patterning. Thus, the expression of some of these proteins in mutated and control animals was analyzed and will be presented in this chapter.

4.2.5.1 Detection of morphogens in mutated and control whole mount embryos

The expression and localization of crucial developmental markers like bone morphogenic protein 2 (Bmp2), sonic hedgehog (Shh) and Noggin were analyzed in whole mount embryos using appropriate antibodies.

The expression of the key protein (Bmp2) regulating osteoblast differentiation and induction of apoptosis between the digits was strongly diminished in mutants in comparison to wild-type controls (Fig. 4.17A and B). Most prominent was the reduction in the craniofacial region (Fig. 4.17C and E) as well as in fused neural tube (arrows in Fig 4.17D and F) in mutant embryos. The expression of the processed N-terminal peptide of Shh was also altered. The diffuse localization of Shh in the zone of polarizing activity in limb buds expanded more in control animals (Fig 4.17G and H) than in the ODDD mutated ones (Fig 4.17I and J). To distinguish whether an excessive blockade of apoptosis between the digits led to syndactylies in mutants, the expression of Noggin was analyzed. Noggin is an antagonist of apoptosis preventing the tissues from death. However, no difference in the expression of this protein could be detected between the two genotypes.

Thus, it can be excluded that a partial blockade of cell death between the digits is responsible for the development of syndactylies in ODDD mutated mice. However, the induction of apoptosis by Bmp2 could be affected leading to the interdigital fusion. This suggests a reduction of Bmp2 expression in mutated embryos.

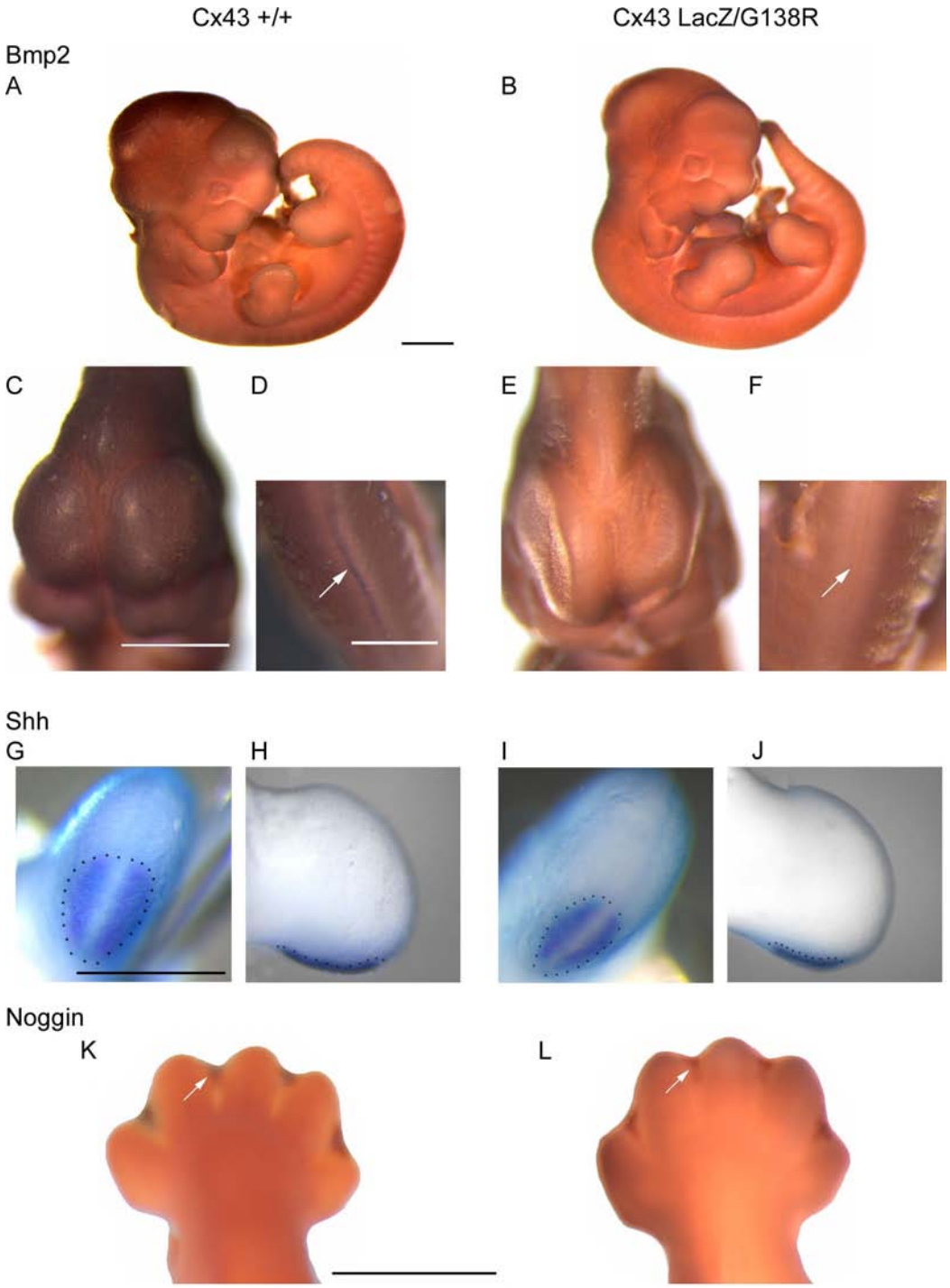

Figure 4.17: Expression of morphogens in ODDD mice. (A-F) Expression of Bmp2 proteins is reduced in Cx43LacZ/G138R mutant embryos (B) in comparison to wild-type mice (A) (ED11.5). Bmp2 could be detected in craniofacial region (C) and the fused neural tube (arrow in D) in control mice but showed a clear reduction in mutants (E or F). Sonic hedgehog (Shh) expression was also reduced in the zone of polarizing activity in mutated limb buds (I and J) compared to wild-type ones (G and H) (ED11.5). The Bmp2 antagonist Noggin showed no clear alterations in its expression (K and L) between the genotypes (ED13.5). (Scale bars = 1 mm)

4.2.5.2 Limb bud cultures express morphogens *in vitro*

Establishment of limb bud cultures can facilitate the examination of the Cx43 influence on morphogen expression. Such cultures avoid the laborious mice matings and preparations of embryos and allow analyses, like visualization of intercellular calcium concentrations, which are not possible in multilayered, three-dimensional tissues.

Here, limb bud cultures were assessed and analyzed for their expression of Cx43, Shh and Bmp2. Furthermore, their molecular characteristics were ascertained using anti-vimentin and anti-Oct3/4 antibodies.

In all cultures cells were found showing highly fluorescent signals after labeling with antibodies to the N-terminal peptide of Shh (Fig. 4.18A-C). Thereby fluorescent signals were also detected on adjacent regions of the Shh expressing cells which may indicate the secretion of the Shh peptide. A slight reduction of Shh positive signals was apparent in Cx43LacZ/G138R as well as Cx43LacZ/LacZ cultures. The combination of Shh and Cx43 immunofluorescence analyses revealed that both the ODDD mutated and wild-type cultures expressed Cx43 protein, the Cx43LacZ/LacZ were negative for Cx43 as expected (Fig 4.18A-F). Shh expressing cells also expressed this connexin protein (Fig 4.18A and B).

The Bmp2 expressing cells showed mesenchymal characteristics by expression of vimentin and, in a small percentage (approx. 1%), also stem cell characteristics by expression of the transcription factor Oct3/4 (red nuclei in Fig. 4.18 G-L). A clear difference between the genotypes regarding the expression of Bmp2, vimentin or Oct3/4 could not be seen in these immunofluorescence analyses.

For quantitative evaluation of Cx43, Bmp2 and Shh expression, cell lysates were separated on SDS gels for immunoblot analyses (Fig. 4.19). As positive control, lysates of embryoid bodies (EBs) were used which were obtained after a differentiation of HM1 cells for 7 days. The hemizygously mutated cultures showed a reduced expression of all detected proteins: Cx43, Bmp2 and Shh. A similar reduction of the two morphogens could be seen in Cx43 deficient cells which did not show any Cx43 specific bands as expected. Hence, the reduction of morphogen expression correlates with the expression of Cx43 and reflects the results from the immunohistochemistral analyses of whole mount embryos (Fig. 4.15).

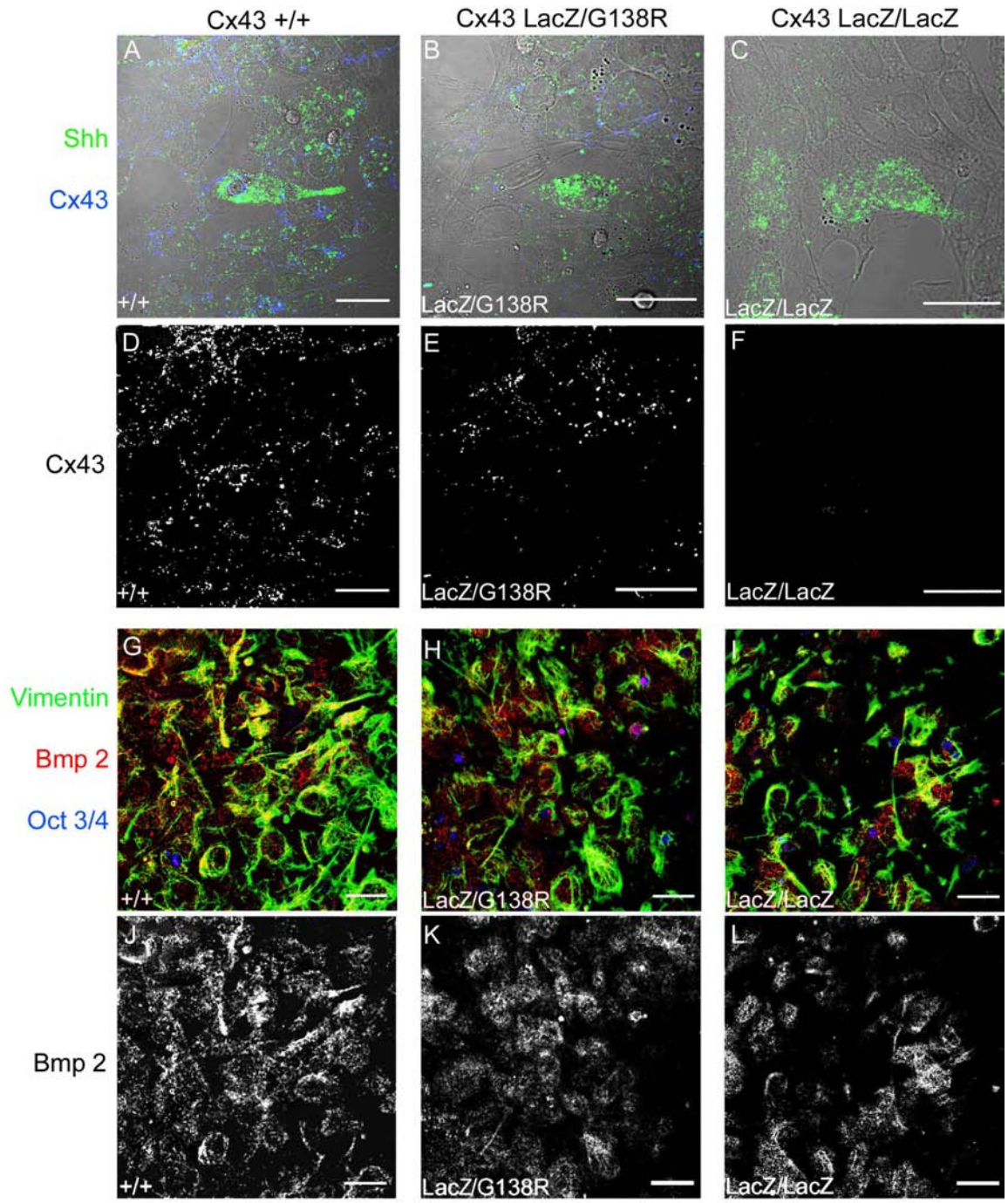

Figure 4.18: The mesenchymal cells in limb bud cultures express sonic hedgehog (Shh), bone morphogenic protein 2 (Bmp2) and Connexin43 (Cx43). (A-F) Shh expressing cells (punctated green staining) could be found in all cultures independent on the genotype, whereas Cx43 expression (in blue) was diminished in Cx43 LacZ/G138R (E) or missing in Cx43 LacZ/LacZ cells (F). (G-L) Most cultured cells had a mesenchymal origin (vimentin expression, green staining), some expressed the stem cell markers Oct3/4 (blue nuclei in G-I) and Bmp2 (punctated red staining in J-L). (Scale bars = 20 µm)

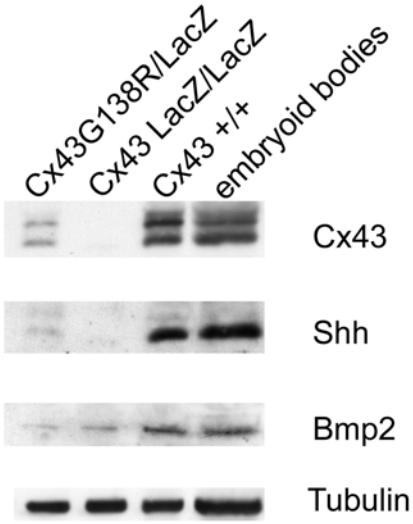

Figure 4.19: Expression of Connexin43 (Cx43), Sonic hedgehog (Shh) and bone morphogenic protein 2 (Bmp2) in limb bud cultures. The expression of Cx43 is reduced in Cx43G138R/LacZ and missing in Cx43Lacz/LacZ cells. These mutated cells also show a clear reduction of Shh and Bmp2 expression in comparison to wild-type Cx43 limb bud cells or embryoid bodies. Embryoid bodies (differentiated for 7 days from HM1 cells) were used as positive controls.

4.2.5.3 Calcium imaging of limb bud cultures

In order to understand the correlation between Cx43 and morphogen expression, as seen in whole mount embryos and limb bud cultures, further cell culture experiments were done. Recently, the intracellular calcium concentration has been described to be elevated by Shh application to differentiating embryonic stem cells and suggested to be a cascade modulator (Heo et al., 2007). On the other hand, it is well known that the two second messengers Ca^{2+} and inositol-1,4,5-trisphosphate (IP_3) are able to pass gap junction channels (Saez et al., 1989). Thus, it was important to investigate the ability of the mutated gap junction channels to mediate the intercellular propagation of Ca^{2+} or IP_3.
Cx43G138R/LacZ, Cx43LacZ/LacZ and control limb bud cultures were loaded with the calcium indicator Fura-2AM (Invitrogen, Karlsruhe, Germany) and were tested for

spreading of the spontaneous calcium oscillations to adjacent cells (Fig. 4.20). Here, cells expressing the point mutated form of Cx43 as well as Cx43 deficient cells (data not shown) were able to oscillate but failed to transfer Ca^{2+} or IP_3 to neighboring cells (Fig. 4.20A-D and E). Figure 4.20E shows three clear increases in calcium concentration of cell 1 without propagation into cells 2 or 3 whereas wild-type cells (Fig. 4.20F and G-J) showed a distribution of the raised calcium into cell 2.

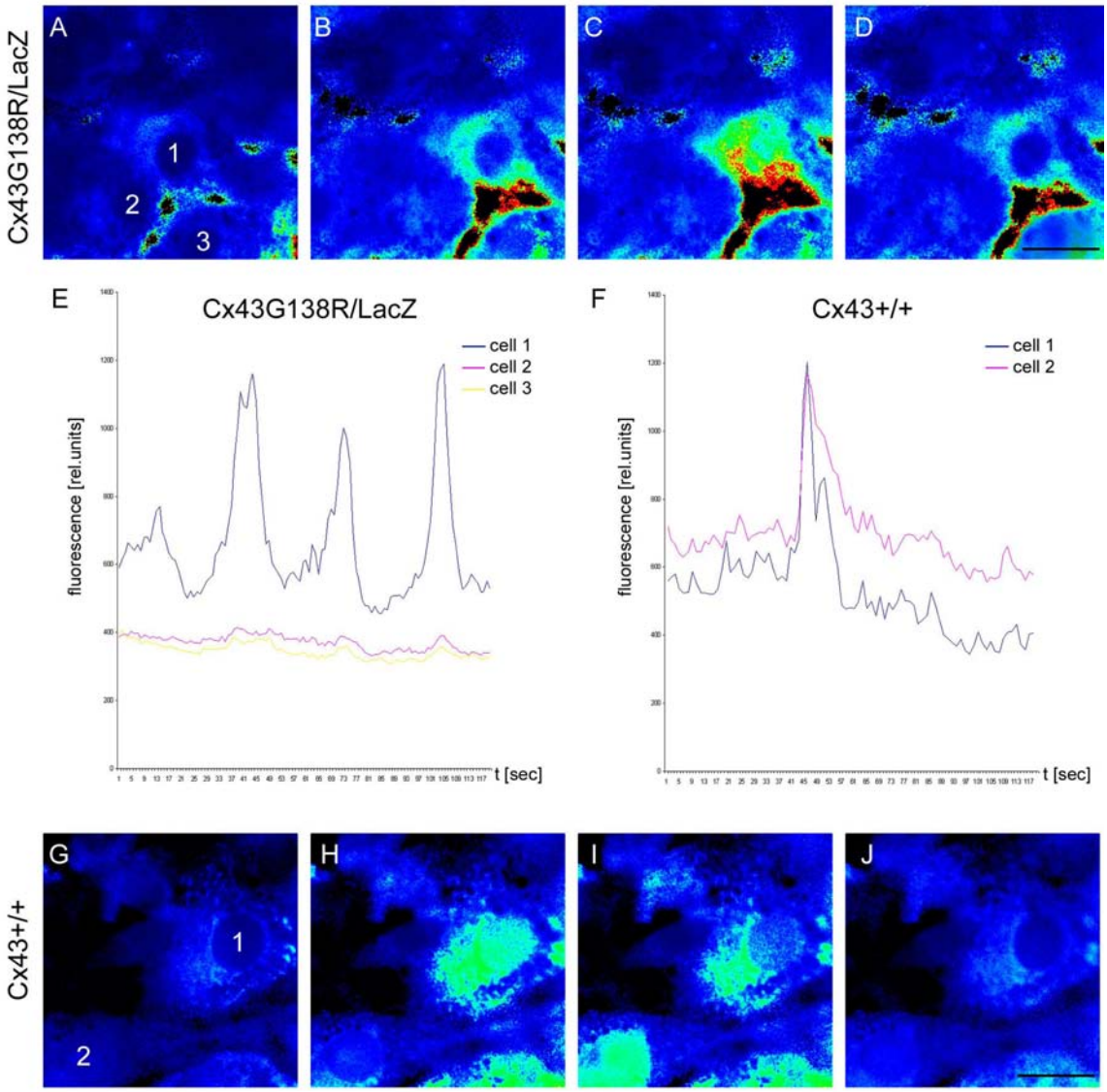

Figure 4.20: Visualization of calcium concentrations in limb bud cultures. Spontaneous calcium oscillations (in cell 1) which cannot be propagated to neighboring cells (cell 2 and 3) in mutated limb bud cultures (A-D time scaled) are illustrated in a diagram (E). Here, the particular oscillations could only be detected in one single cell (E), whereas wild-type cells (cell 1) showed a spreading of calcium or IP_3 to surrounding cells (cell 2) (G to J and evaluation in F). (Scale bars = 20µm)

4.3 *In vitro* analyses of the Cx43G138R and other ODDD associated Cx43 mutations

4.3.1 The Cx43G138R mutation leads to a loss of Cx43 mediated conduction in HeLa cells, mouse embryonic stem cells (HM1) and primary cardiomyocytes

In order to determine the function of the Cx43G138R mutated protein, microinjections of tracers and electrophysiological studies were performed using mouse embryonic cardiomyocytes, ES cells and stably transfected HeLa cells (Fig. 4.21A–H). The micro-injections into cardiomyocytes resulted in a reduction of neurobiotin transfer by 94%, thus indicating that only 6% of connexin-mediated conduction is maintained in Cx43+/G138R cardiomyocytes (Fig. 4.21I).

Furthermore, the neurobiotin transfer in Cx43+/G138R mouse ES cells, which heterozygously expressed the Cx43 mutation, was reduced by 79% (Fig. 4.21I). Because of possible co-expression of additional connexins in cardiomyocytes (Cx45) or ES cells (Cx45 and Cx31), microinjection analyses using cells expressing only Cx43 isoforms were performed.

Thus, HeLa cells stably expressing Cx43G138R alone or in the presence of Cx43WT proteins were investigated. No neurobiotin transfer could be detected in cells expressing only Cx43G138R (n = 15), whereas in cells co-expressing Cx43WT and Cx43G138R, neurobiotin transfer was slightly higher, suggesting a strong reduction or even a loss of Cx43-mediated conductance in Cx43+/G138R mice. Electrophysiological studies using dual whole-cell voltage clamp (Kreuzberg et al., 2005) revealed that all 14 examined HeLa Cx43G138R cell pairs exhibiting eGFP fluorescence (Cx43G138R-IRES-eGFP construct) demonstrated complete absence of coupling.

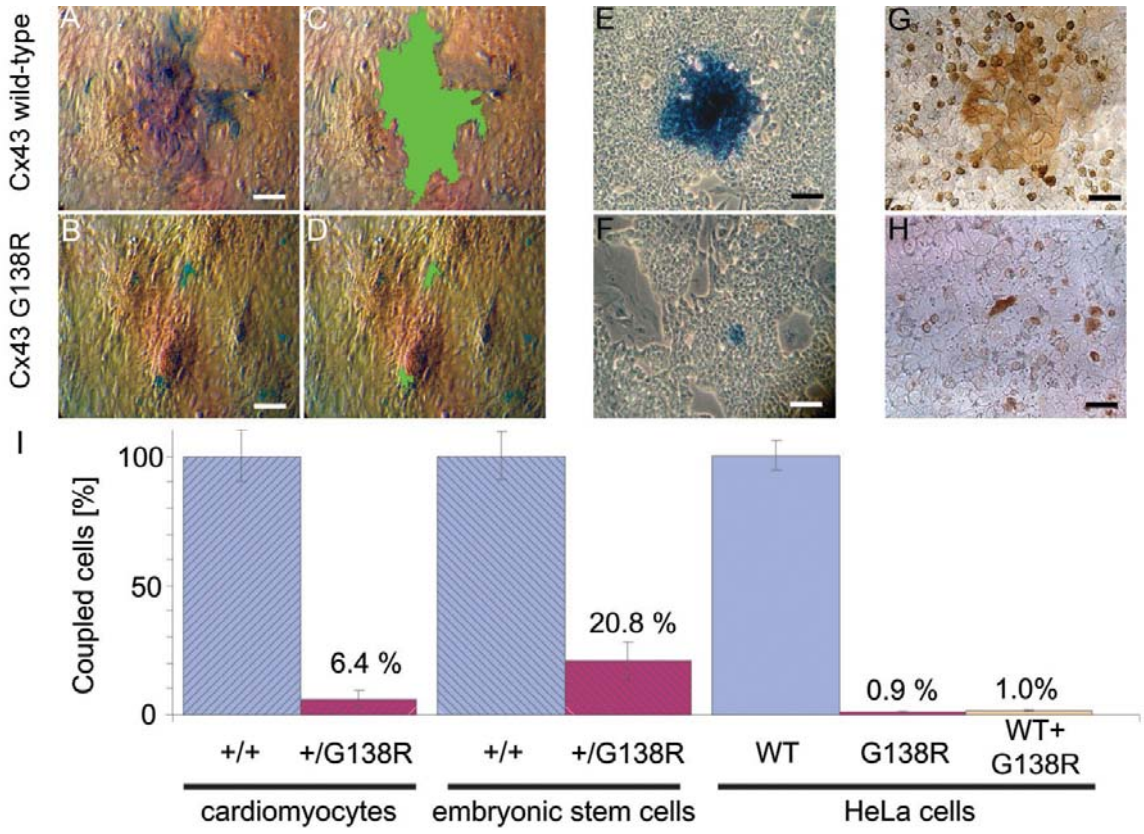

Figure 4.21: Cx43-mediated coupling is disturbed in cells expressing the ODDD-mutated proteins. Intercellular transfer of microinjected neurobiotin in wild-type Cx43-expressing cells [primary mouse cardiomyocytes (A and C), ES cells (E) and HeLa cells (G)] in comparison to Cx43G138R-expressing cells [primary mouse cardiomyocytes (B and D), ES cells (F) and HeLa cells (H)]. In (C) and (D), the coupling area is outlined in pseudo-color. The diagrams shown in (I) compare neurobiotin transfer in wild-type and mutated cardiomyocytes and stem cells as well as in HeLa cells expressing Cx43WT or Cx43G138R alone or co-expressing Cx43WT and Cx43G138R. A residual coupling in approximately 2.5 cardiomyocytes (6.4%) was observed. In stem cells dye transfer was substantially higher (six cells; 20.8%). HeLa cells expressing Cx43G138R alone or in parallel with Cx43WT showed a very low level of dye transfer. (Scale bars = 20 µm)

4.3.2 Cx43 mediated conduction can be maintained in heterozygous animals by Cx43WT homotypic and Cx43G138R/Cx43WT heterotypic channels

In order to determine whether Cx43-mediated coupling in Cx43+/G138R mice is maintained through Cx43G138R/Cx43WT heterotypic channels besides wild-type homotypic channels, cell–cell coupling in co-cultures of HeLa cells expressing Cx43G138R and Cx43-eGFP (fusion construct) was examined. Well distinguishable and, in many cases, multiple junctional plaques were found in the contact regions between cells expressing Cx43G138R and cells expressing Cx43-eGFP (Fig. 4.22). Figure 4.22B shows the averaged dependence of junctional conductance (Gj) on transjunctional voltage (Vj) that was obtained by measuring junctional current (Ij) dynamics over time in response to long (150 s) Vj ramps that change from 0 to +120 mV and from 0 to -120 mV [for more details see Fig. 3 in (Rackauskas et al., 2007)]. In all nine examined cell pairs, Gj2Vj dependence was asymmetric with higher Vj gating sensitivity at positive voltage on the Cx43-eGFP side. GJC gating at the single-channel level (Fig. 4.22C) shows a tendency to open during a negative voltage step and to close during a positive voltage step, applied to the HeLaCx43-eGFP cell. This gating asymmetry at the single-channel level is in accordance with macroscopic Gj2Vj dependence, as shown in Figure 4.22B. Figure 4.22D shows the Ij record of a single channel in a heterotypic junction during application of hyperpolarizing Vj step of 87 mV with a HeLaCx43G138R cell. In the example shown, the single channel conductance at the open state is ~103 pS, and channels mainly gate between the open state and a substrate or the residual state with a conductance of ~25 pS. This kind of gating is ascribed as the fast gating (Bukauskas et al., 2006). Besides the fact that most gating transitions are between open and residual states of ~78 pS in magnitude, more rarely transitions between the open state and the fully closed state could be observed (indicated by arrows), which can be ascribed to the slow gating (Bukauskas et al., 2004). Earlier, it was reported that Cx43-eGFP channels exhibit the slow but not the fast gating mechanism. Therefore, the data shown in Figure 4.22D should be ascribed to the gating of Cx43G138R hemichannels, which presumably retain both fast and slow gating mechanisms such as wild-type Cx43. Gating to the substate can also be seen in Figure 4.22D at the negative Vj step. Both macroscopic and microscopic gating properties shown in Figure 4.22B and D suggest that Cx43G138R

hemichannels exhibit higher Vj gating sensitivity than Cx43-eGFP hemichannels and presumably gate at negativity on the cytoplasmic side of Cx43G138R.

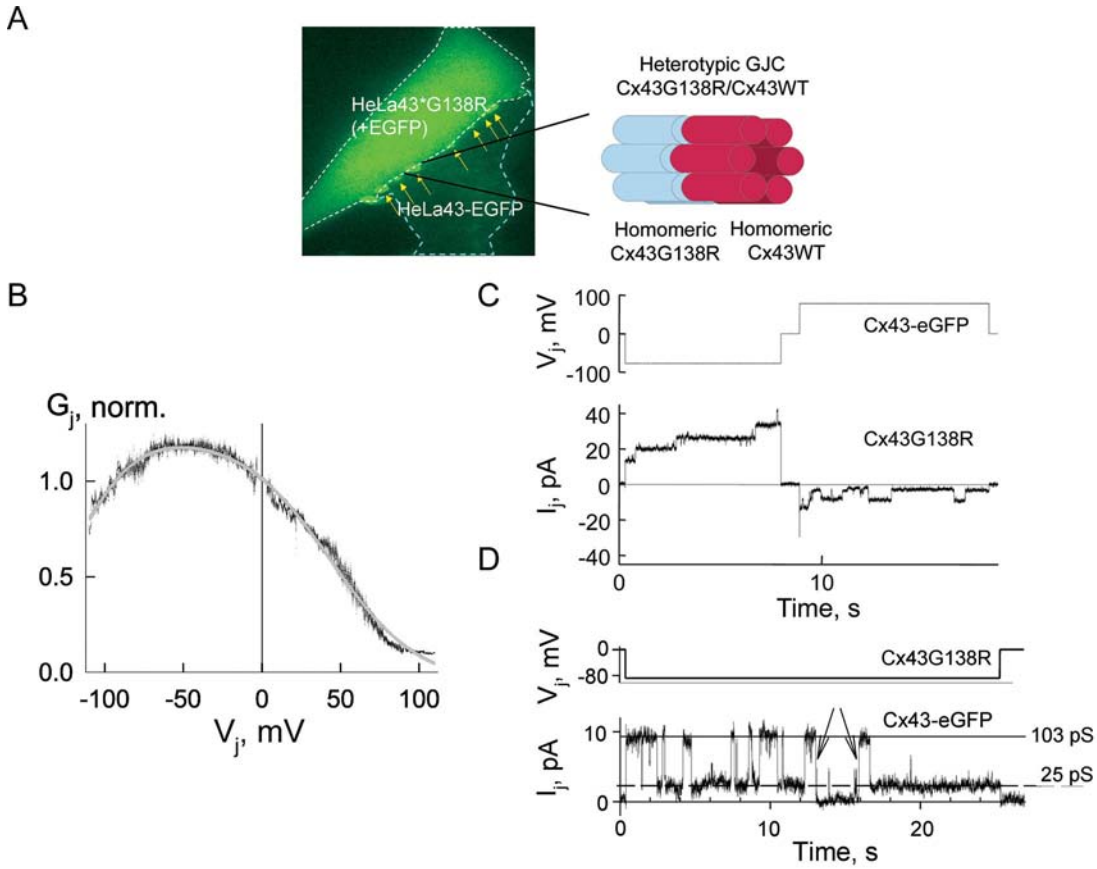

Figure 4.22: Cx43–eGFP/Cx43G138Rheterotypic junctions, shown in (A), form junctional plaques (see arrows) in the junctional region between HeLaCx43G138Rcell (left/top) exhibiting homogenous eGFP in cytoplasm and HeLaCx43-eGFP cell (right/bottom) exhibiting punctate staining of eGFP prominently in contacting membranes. (B) Summarized junctional conductance dependence on transjunctional voltage (Gj2Vj) measured in nine cell pairs forming heterotypic Cx43–eGFP/Cx43G138R junctions. These exhibit an asymmetric Vj gating with higher sensitivity at positive voltages on the HeLaCx43-eGFP side. (C) Unitary opening and closing events at the single-channel level of Cx43–eGFP/Cx43G138R heterotypic GJ channels seen as stepwise junctional current (Ij) transitions in response to consecutive negative and positive voltage steps applied to the HeLaCx43-eGFP cell. Channels show a tendency to open during a negative voltage step and to close during a positive voltage step that is in accordance with macroscopic Gj2Vj dependence shown in (B). (D) Single-channel record demonstrating that both fast and slow gating mechanisms operate in Cx43G138R/Cx43 heterotypic GJC. During application of hyperpolarizing Vj step to HeLa Cx43G138R cell, the channel operates mainly between the open state with a conductance of 103 pS and the residual state with a conductance of 25 pS. Arrows point to transitions between the open state and the fully closed state.

HeLa cells are known to express intrinsically Cx45, but at a very low level (Rackauskas et al., 2007). If one assumes that the cell–cell coupling shown occurs through Cx43-eGFP/Cx45 heterotypic junctions then:

(i) the macroscopic Gj/Vj dependence should be more asymmetric with higher voltage sensitivity at positive Vj (Bukauskas et al., 2002),

(ii) single-channel conductance of the open state should be ~55 pS (Bukauskas et al., 2002) instead of ~100 pS (Fig. 4.22D),

(iii) among 14 examined HeLaCx43G138R cell pairs, at least one or few of them should show coupling with some Cx45 channels instead of full absence of coupling and

(iv) junctional plaques should be much smaller than those shown in Figure 4.22A (Rackauskas et al., 2007). Therefore, the observed coupling is not due to the formation of Cx43/Cx45 instead of Cx43/Cx43G138R channels but it can be suggested that at Vj = 0 mV, only a fraction of Cx43G138R hemichannels are open. At Vj = 0 mV, open probability of the Cx43WT hemichannel is close to 1 and therefore the open probability of Cx43G138R/Cx43WT GJ channels will be limited by the open probability of Cx43G138R hemichannels (pCx43G138R). If, for example, pCx43G138R equals 0.1, then only one of 100 Cx43G138R homotypic channels will be open, which may explain the low functional efficiency of Cx43G138R homotypic junctions.

4.3.3 Cells expressing Cx43G138R show enhanced release of ATP

As recently described, some ODDD mutations can lead to the reduced release of ATP through hemichannels (Lai et al., 2006). To investigate whether the Cx43G138R mutation alters cellular ATP release, extracellular ATP concentration and propidium iodide uptake of cultured cells expressing Cx43G138R were measured upon stimulation

in calcium-free solution or under hypoxic conditions (Fig. 4.23).
All measurements revealed approximately doubled activity of ATP releasing channels in cells expressing the Cx43G138R mutation. The ODDD mutated channels expressed in HeLa cells released in calcium free medium 2.3 fold more ATP than Cx43WT expressing cells. HeLa transfectants expressing the same Cx43WT background but different amounts of Cx43G138R (Cx43WT+Cx43G138R (++) or (+)) showed an ATP release in a Cx43G138R-dependent manner (Fig. 4.23A). The use of HeLa WT cells was important to determine the background ATP concentration of 0.03 μM which was not due to connexin expression. HeLa cells expressing Cx43 release twice as much ATP than the wild type cells indicating the presence of functional hemichannels (Fig. 4.23A).

The heterozygously recombined ES cells expressing the ODDD-mutated Cx43 besides Cx43WT released 2.0-fold more ATP than wild-type ES cells cultured in calcium-free medium (Fig. 4.23B and C). Furthermore, they could be stimulated by chemical induced hypoxia for 6 or 12 minutes. Here, a gradual increase of ATP in the extracellular medium could be detected (Fig. 4.23 C).
Cardiomyocytes derived from embryonic Cx43+/floxG138R: alphaMyHC-Cre or wild-type hearts on ED 12.5 or ED 16.5 were tested in the hypoxic incubator. The activity of ATP-releasing channels in oxygen-dependent cardiomyocytes on ED 16.5, but not in the oxygen-independent ED12.5 cells, could be stimulated by hypoxia (Fig. 4.23D). A 1.8-fold higher ATP concentration in media from mutant cells was measured. The increased activity of ATP-releasing channels was also confirmed by propidium iodide uptake in embryonic cardiomyocytes stimulated in calcium-free medium (Fig. 4.23E). The mutated cells exhibited 2.5-fold higher ATP release than wild-type cells.

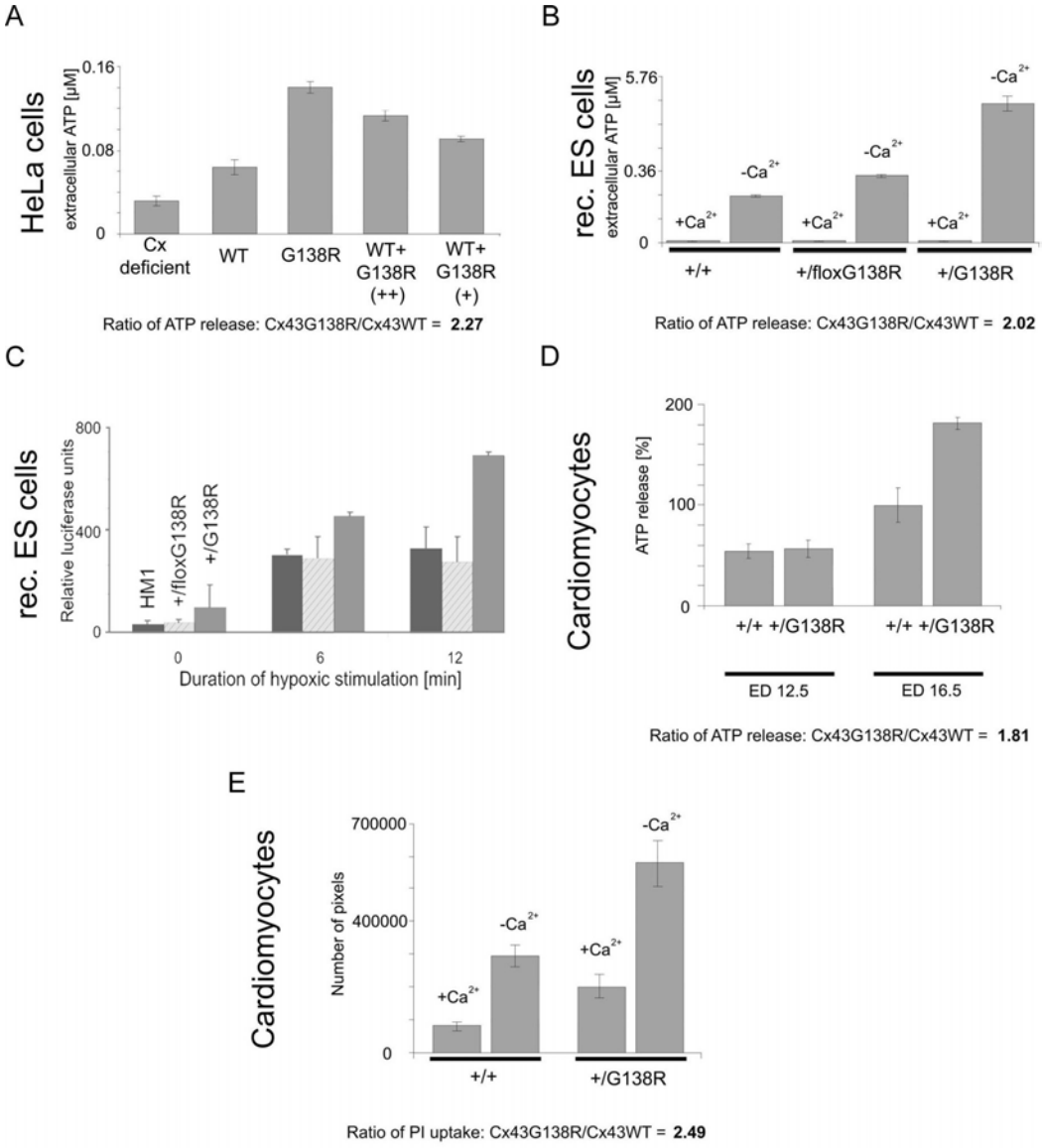

Figure 4.23: Cx43G138R leads to increased activity of ATP-releasing channels. Measurements of ATP concentrations in media of cultured cells expressing Cx43G138R (A - D), and tracer uptake studies (E) showed a doubled activity of ATP-releasing channels. (A) HeLa transfectants expressing different amounts of Cx43G138R protein reveal that the ATP release proportionally increases with the amount of Cx43G138R protein (+ = low expression, ++ = high expression). (B and C) Recombined, heterozygous ES cells expressing the mutation showed an increased activity of the ATP-releasing channels and could be stimulated by zero calcium conditions (B) or chemical induced hypoxia for 6 or 12 min (C). (D) In oxygen-dependent cardiomyocytes (ED 16.5), the activity of ATP-releasing channels could be observed after 1.5 h of stimulation in a hypoxic incubator, but was not detected in oxygen-independent cells derived from younger embryos (ED 12.5). (E) Studies of tracer uptake of Cx43+/floxG138R:alphaMyHC-Cre cardiomyocytes also indicate the doubled activity of these channels before and after stimulation.

4.3.4 The activity of ATP releasing channels influences the beating frequency of embryonic Cx43 +/floxG138R:alphaMyHC-Cre cardiomyocytes

To investigate the potential functional relevance of ATP-releasing channels, the beating rates in mutant and wild-type cardiomyocytes were assessed. Embryonic cardiomyocytes isolated from cardiac-specific mutants exhibited a 1.6-fold higher beating frequency (242 bpm) than wild-type cardiomyocytes (148 bpm; P=0.001) (Fig. 4.24).

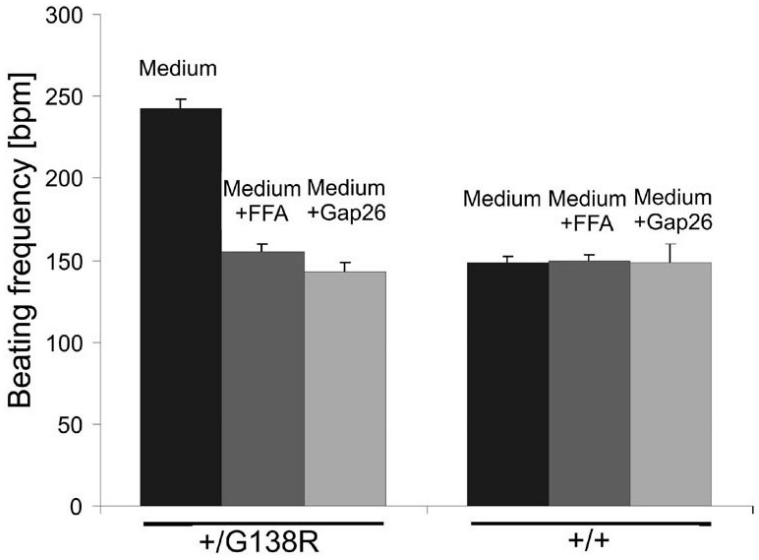

Figure 4.24: Activity of ATP-releasing channels influences the beating frequency of mutated cardiomyocytes. Mutated cardiomyocytes beat faster than the wildtype ones (P=0.001). Application of FFA or the mimetic peptide Gap26 at concentrations blocking the ATP-releasing channel activities decreased the beating frequency of mutant cells to the wild-type level (P=0.001).

This finding in combination with the increased ATP release and dye uptake indicated an ATP release channel-dependent positive chronotropic effect. This was further investigated by using peptides and drugs that have been reported to inhibit the activity of ATP-releasing hemichannels. Flufenaminic acid (FFA) (50 mM) or the mimetic peptide Gap26 (300 mM) blocked the ATP-releasing channels, whereas the activity of GJCs was not affected (Fig. 4.25). Both of these pharmacological agents reduced the beating frequency of mutated cardiomyocytes to the level of wild-type cardiomyocytes (FFA:

155 bpm and Gap26: 143 bpm), supporting a functional impact of ATP-releasing channels.

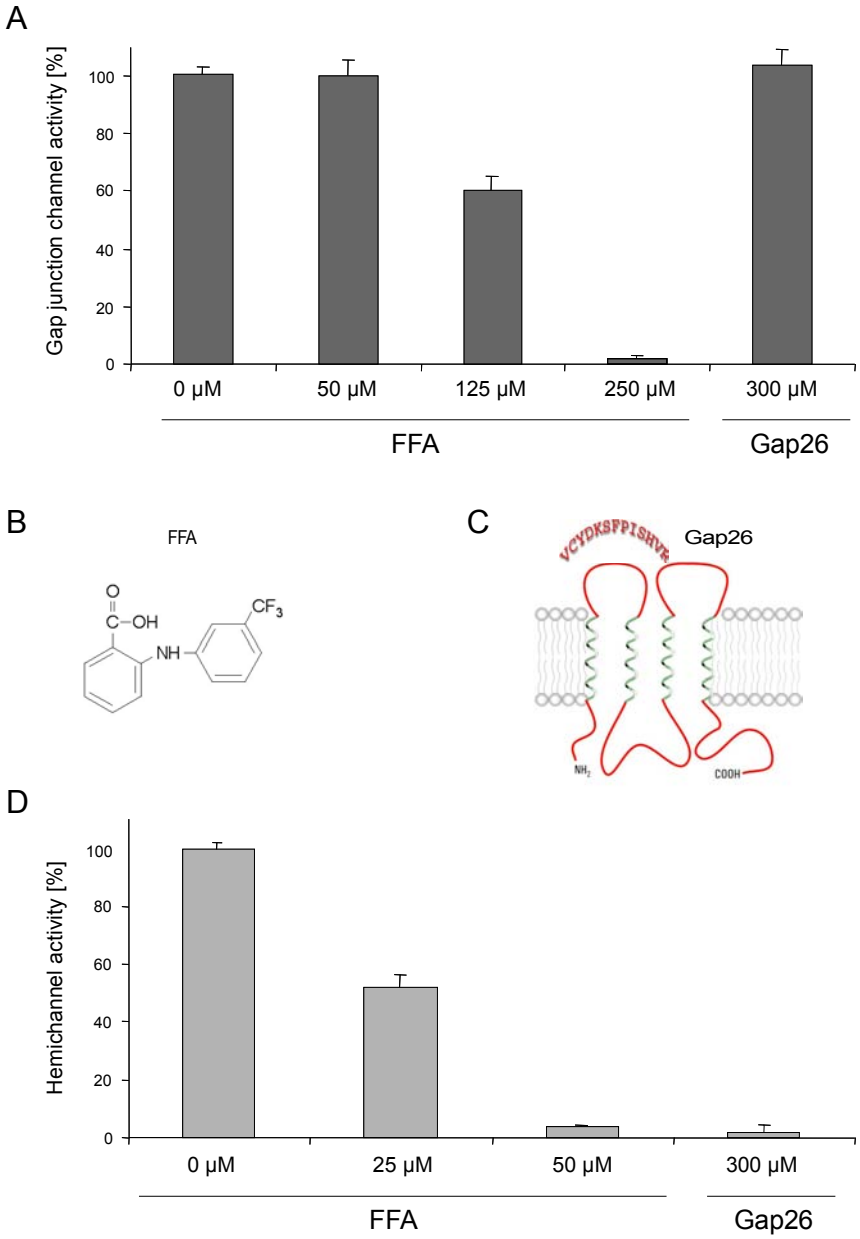

Figure 4.25: Determination of hemichannel blocking concentrations of FFA and Gap26. (A) Gap junction channel activity was not changed neither by 50 µM FFA nor by 300 µM Gap26. However, increasing concentrations of FFA (125 µM and 250 µM) gradually inhibited the spread of injected dye. (B) Chemical structure of FFA. (C) The predicted binding of Gap26 to the first extracellular loop of Cx43 and its aminoacid sequence. (D) Abolishment of hemichannel activity by 50 µM FFA and 300 µM Gap26 after 20 min incubation at 37°C.

4.3.5 Determination of the half-life of mutated and wild-type Cx43 proteins in HeLa cells

A possible explanation for the observed increased ATP releasing channel activity of some Cx43 mutants (Cx43I31M, Cx43G138R, Cx43G143S) could be a disturbed turnover of the proteins resulting in an increased amount of channels in the membrane. Thus, pulse-chase experiments followed by Cx43 immunoprecipitations with lysates from mutant and wild-type Cx43-expressing cells were performed (Fig. 4.26).

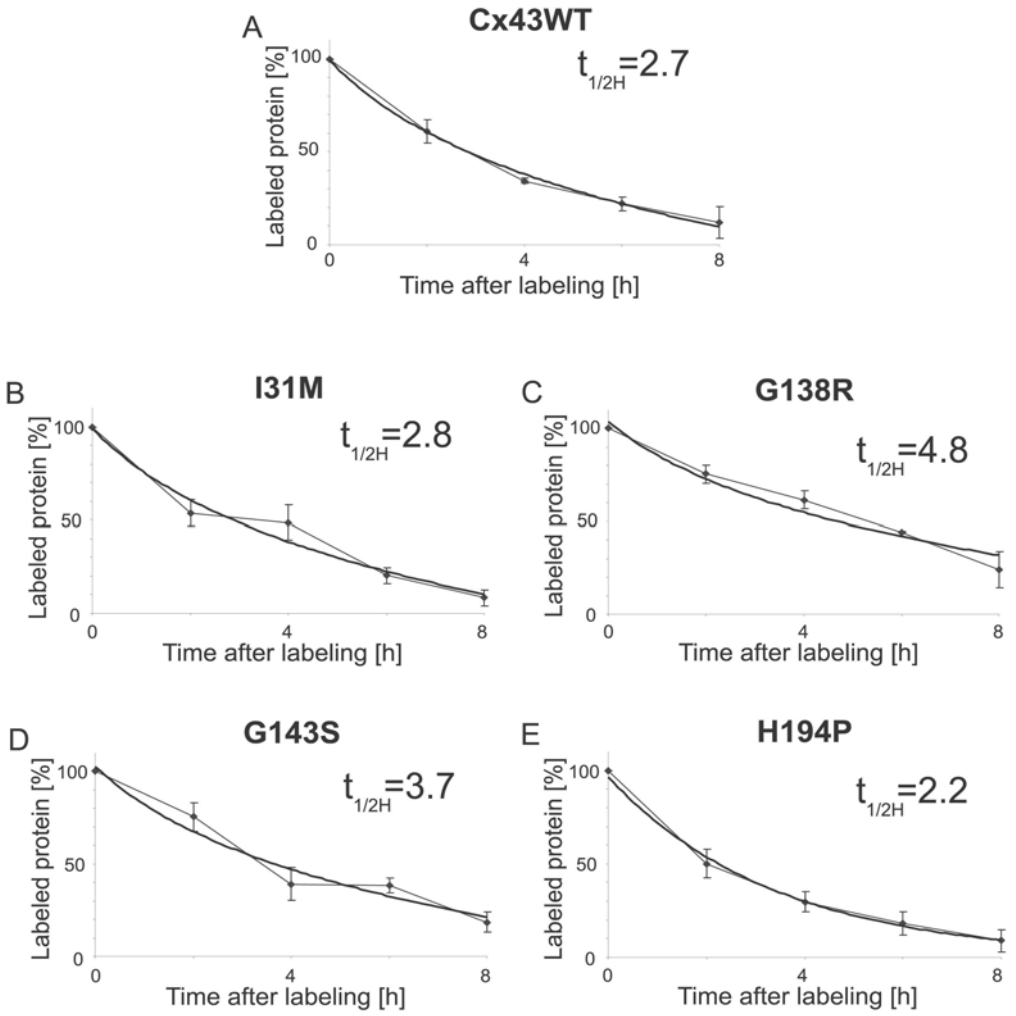

Figure 4.26: Pulse-chase analyses indicate degradation defects in some ODDD mutants. The G138R as well as G143S mutants showed a halflife increase from 2.7 h in Cx43WT (A) to 4.8 h in G138R (C) and 3.7 h in G143S (D) mutants, suggesting a degradation problem of these proteins. The I31M (B) and H194P (E) mutated proteins showed no obvious turnover alterations, as indicated by the similar half-lives (2.8 and 2.2 h, respectively)

The Cx43G138R and G143S mutations showed an increased half-time ($t_{1/2,G138R}$ = 4.8 h, $t_{1/2,G143S}$ = 3.7 h) (Fig. 4.26C and D). However, the I31M mutation, which also exhibited increased hemichannel activity, did not show an obvious turnover defect ($t_{1/2,I31M}$ = 2.8 h) (Fig.4.26B), similar to the H194P mutation without altered hemichannel activity, the Cx43H194P mutation ($t_{1/2,H194P}$ = 2.2 h). The half-life of Cx43 wild-type protein was confirmed to be 2.7 h.

4.3.6 The phosphorylation of Cx43G138R and other ODDD associated Cx43 mutants is largely disturbed

Previously, it has been described that the phosphorylation of Cx43 regulates gap junctional and even the activity of ATP-releasing channels (Evans et al., 2006). Therefore it had to be tested whether the phosphorylation of Cx43G138R-containing channels is affected *in vitro* and *in vivo*. Immunoprecipitations of Cx43 from ^{32}P-labeled HeLa transfectants (Fig. 4.27A) and immunoblot analyses of heart lysates (Fig. 4.27B) clearly showed a partial lack of phosphorylation of the Cx43G138R isoform.

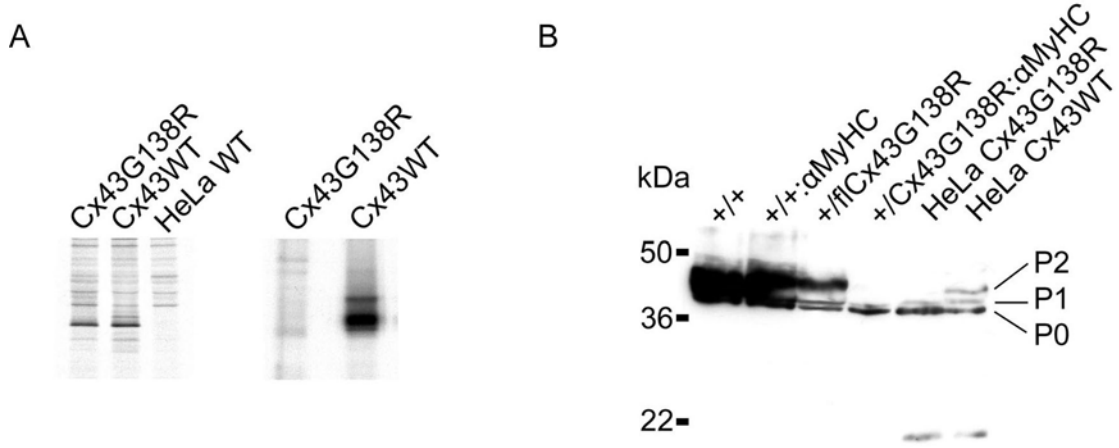

Figure 4.27: Cx43G138R is not phosphorylated at the P2 state *in vitro* as well as *in vivo*. Immunoprecipitation of Cx43 from ^{32}P-labeled HeLa cells and immunoblot analyses of tissue lysates are shown. (A) Equal numbers of Cx43-expressing cells (culture dish tested by ^{35}S methionine labeling, left picture) were labeled with ^{32}P ATP (right picture). Subsequent Cx43 immunoprecipitation reveals a reduced phosphorylation of Cx43G138R protein by 80%. (B) Immunoblot analyses show lack of P2 phosphorylation of Cx43G138R protein in hearts.

Equal amounts of Cx43WT- or Cx43G138R-expressing cells (see ^{35}S methionine labeling) were labeled with [gamma^{32}P]ATP, followed by immunoprecipitation of Cx43.

The results clearly indicate that up to 80% of the Cx43G138R protein is not phosphorylated, in comparison with Cx43WT. Immunoblot analyses also showed in Cx43+/floxG138R:alphaMyHC-Cre hearts that the P2 phosphorylation isoform of Cx43 is absent.

5. Discussion

5.1 Generation of Cx43G138R expressing mice

The Cx43G138R expressing mice were generated by homologous recombination of the conditional construct shown in Fig. 1.10 which has been cloned during my diploma thesis (2004). This construct allows the targeted exchange of the endogenous Cx43 wild-type coding region by a loxP sites flanked wild-type gene followed by neomycin resistance and Cx43G138R-IRES-eGFP cassettes. The region flanked by loxP sites (Cx43 wild-type and neomycin genes) could be conditionally removed after Cre mediated recombination. The remaining Cx43G138R-IRES-eGFP cassettes were expressed driven by the endogenous Cx43 promoter. The combination of these cassettes allows the labeling of cells expressing the G138R mutated protein, the only way to detect this expression since no antibodies were available to distinguish between wild-type and mutated Cx43 isoform.

After transfection of the embryonic stem (ES) cells only one of 251 clones had undergone correct homologous recombination which corresponds to a recombination rate of 0.4 %. The most PCR positive ES cell clones showed a lack of 8484 bp band in Southern blot analyses using *Bam*HI and Cx43-internal probe (data not shown but resembles the difference between +/Cx43G138R and +/flox alleles in Fig. 4.1D). This implies the absence of the Cx43 wild-type gene and a partial integration of the construct into the locus. It is probable that the unusually big internal homology, i.e. two almost identical genes except of one basepair in Cx43G138R relative to Cx43 wild-type, is responsible for the very rare homologous recombination. This assumption is supported by observations of Robert Requardt during his PhD thesis. He used a very similar construct to that one used for the generation of the Cx43G138R expressing mice. Despite an extension of the homology regions he ascertained a similar low recombination rate of 0.5%.

The clone no.234 which had undergone correct homologous recombination was used for blastocyst injection and, after transduction with the biologically active Cre peptide (Nolden et al., 2006), for other *in vitro* analyses, e.g. microinjections of dyes to test channel function or ATP release assay to check hemichannel activities.

5.2 Cx43G138R expressing mice represent a new conditional mouse model for ODDD

The G138R mutation is localized in the cytoplasmic loop of the membrane-embedded Cx43 protein, i.e. the receptor domain for the C-terminal tail in the ball-and-chain model describing the opening and closing of a gap junction channels (GJC) (Delmar et al., 2004). This mutation was characterized in transfected cells as a dominant-negative one inhibiting the gap junctional function of wild-type Cx43 (Roscoe et al., 2005). Thus, this mutation leads to a lack of GJC activity, although the Cx43 protein is still expressed in the cell membrane. These properties clearly distinguish the Cx43G138R mutation from Cx43 null mutant mice that do not express the Cx43 protein and both, the Cx43G60S and Cx43I130T mutations, where the mutated protein is largely excluded from the plasma membrane (Flenniken et al., 2005; Kalcheva et al., 2007). This PhD work confirms the dominance of the G138R mutation using embryonic cardiomyocytes from heterozygous mice and showed a strong (approx. 94%) reduction in cell-to-cell permeability of tracer molecules.

Because of high embryonic lethality of the ubiquitously expressed mutant and the necessity to compare mice of the same gender and age for bone morphological studies, only male mice were tested. Here, significant osteopenia with reduced bone volume and increased trabecular spacing was observed. This is most likely due to a decreased number of osteoblasts in the ODDD mutant mice, although the difference in osteoblast number was not statistically significant. Notably, expression of Cx43G138R, as well as other ODDD mutants in osteoblast-enriched calvaria cells, does not seem to alter the ability of these cells to differentiate and produce mineralized matrix *in vitro* (McLachlan et al., 2005). Therefore, the dominant-negative effect of the mutant proteins may not be sufficient to completely inhibit wild-type Cx43 in committed osteoblasts, but it may be sufficient to interfere with earlier commitment of stromal cell precursors. A reduced number of osteoblasts in the ODDD transgenic mice would be consistent with this notion and would require precise examination of osteoblast's differentiation process. Analyses concerning the expression of crucial developmental proteins will be discussed in subsequent chapters (5.6 and 5.7).

5.3 Spontaneous ventricular arrhythmias in Langendorff and *in vivo* recordings of mutated adult hearts

The cardiac function in adult mice was determined by surface and intracardiac ECG, Langendorff and *in vivo* ECG measurements.

5.3.1 Ventricular arrhythmias in ODDD mutated mice are mainly due to the strongly decreased gap junctional coupling

Suppressed impulse propagation in the ventricle recognized by the broadening of the QRS complex and the lowering of its amplitude are similar to the situation in the Cx43-deficient heart (Eckardt et al., 2006). The Cx43-mediated coupling in the heterozygous mouse mutant described in this article is maintained by Cx43G138R-Cx43WT heterotypic (103 pS in open state) and Cx43WT-Cx43WT homotypic channels. Furthermore, the impulse propagation in working myocardium of the heterozygously mutated hearts can be maintained by heterotypic Cx45-Cx43 channels (55 pS) (Tab. 5.1) in working myocardium. In atria, the co-expressed Cx40 cannot generate functional heterotypic channels with Cx43, i.e. Cx40 mediated coupling is not affected by the Cx43G138R mutation. The impulse propagation via the recently described Cx30.2 (Kreuzberg et al., 2006), is not changed in Cx43G138R mutated hearts. That is because Cx30.2 is not co-expressed with Cx43.

	Cx30.2	**Cx40**	**Cx43**	**Cx45**
Cx30.2	9	18	18	17
Cx40	18	180	Not functional	45-50
Cx43	18	Not functional	115	55
Cx45	17	45-50	55	32

Table 5.1: Single channel conductances in pS of cardiac gap junction channels (homo- and heterotypic configurations). Except Cx40 and Cx43, all cardiac connexin can generate heterotypic channels with a different single channel conductance (Kreuzberg et al., 2006).

Thus, Cx43 mediated coupling can be maintained by Cx43G138R-Cx43WT heterotypic channels. However, the probability to generate these channels is low.

The most striking findings in the Cx43G138R transgenic mice were the development of severe ventricular tachycardias, the missing influence of the mutation on heart morphology, as seen in the Cx43-deficient mice, and the increased activity of ATP-releasing channels.

In fact, the predisposition to arrhythmia in Cx43G138R mice can be explained by the uncoupling of ventricular cardiomyocytes, resulting in the loss of directed electrical conduction. This has been discussed for adult Cx43-deficient hearts (Eckardt et al., 2006; van Rijen et al., 2004), exhibiting ventricular arrhythmias that occur less frequently than in Cx43+/floxG138R: alphaMyHC-Cre mice. In this context, van Rijen et al. (van Rijen et al., 2004) showed that only a low percentage of cardiac Cx43-depleted animals developed spontaneous arrhythmias, whereas all of the Cx43G138R mice exhibited spontaneous VTs implicating an enhanced arrhythmogeneity of the G138R mutation versus the Cx43-deficient heart. The previously published Cx43 mutants by Flenniken et al. (2005) and Kalcheva (2007) showed no relevant QRS-prolongation, low-voltage ECG or spontaneous long-lasting ventricular arrhythmias, but significantly prolonged P-waves and AV nodal conduction blocks. Analogous conduction defects of the atria and AV node, i.e. prolongation and first-degree AV nodal block, occurred in Cx43+/floxG138R: alphaMyHC-Cre mice.

In vitro analyses revealed a strong reduction of Cx43 mediated coupling in primary mouse cardiomyocytes, ES cells and HeLa cells (Fig. 4.21). The residual coupling was highest in cultured ES cells which can be explained by the expression of Cx31 and Cx45. Also in ventricular cardiomyocytes Cx45 is expressed besides Cx43. These cells showed a 94% reduction of tracer transfer in comparison to wild-type cells. In order to determine the Cx43 coupling in G138R mutants, connexin deficient HeLa cells were transfected with CX43WT and the mutated isoform. Neither Cx43G138R cells, nor Cx43G138R-Cx43WT transfectants showed very low transfer of the injected dye. These data prove the dominant behavior of the Cx43G138R mutation and suggest that the observed residual coupling in ES cell or primary cardiomyocytes are due to the co-expressed connexins.

Compared to other mouse strains with alterations of Cx43 expression and function, the Cx43G138R mutant seems to have the strongest impact on cardiac arrhythmogeneity,

resulting in prominent alterations of the electrical conduction in atria, AV node and ventricular myocardium accompanied by severely enhanced arrhythmogeneity in vivo and in the isolated heart.

These findings point toward more severe alterations of intercellular coupling, conduction properties and other Cx43 functions when compared with all other Cx43 mutants described to date.

5.3.2 Ventricular arrhythmias in Cx43G138R mice can be aggravated by increased activity of ATP releasing channels which can be stimulated by hypoxia

A possible molecular basis for the striking arrhythmogeneity of G138R mutated hearts may be an enhanced activity of the ATP-releasing channels, which form a leak across the plasma membrane. This could lead to a reduction in the resting potential, as already proposed for mCx30.2 (Bukauskas et al., 2006). This may contribute to enhanced automaticity and initiation of extra-systolic activity. This notion is supported by aggravation of cardiac arrhythmia during short hypoxic phases (Fig. 4.11 and 4.12). Here, the opening times of ATP-releasing channels may be extended (Fig. 4.23C and D), leading to increased uncoupling of cardiomyocytes and thus to ventricular arrhythmia. The increased activity of ATP-releasing channels was observed in transgenic ES cells and embryonic cardiomyocytes expressing the same amount of both Cx43WT and Cx43G138R proteins. Under hypoxic conditions an 80% increased ATP release in oxygen-dependent cardiomyocytes (ED 16.5) could be found, but not in oxygen-independent ones (ED 12.5) (Fig. 4.23D). The physiological relevance of this gain-of-function mutation regarding the ATP-releasing channel activity was studied in cultured cardiomyocytes. Here, the increased beating frequency of mutated cells could be lowered to the wildtype level using Gap26, a mimetic peptide with an amino acid sequence corresponding to the region of the first extracellular loop of Cx43, as a blocker of ATP-releasing channels. Furthermore, this experiment clearly shows that the blockade of ATP-releasing channels in wild-type cells does not influence the beating frequency of wild-type ventricular cardiomyocytes. It can be hypothesized that the increased activity of ATP-releasing channels and the associated increased release of ions could depolarize the membrane potential of the mutated cells. Under this aspect, the ATP-releasing channels

in Cx43G138R mutated cells show some analogy to the mutated cardiac potassium channel KCNQ1 (Chen et al., 2003). This gain-of-function mutation in the *KCNQ1* gene, associated with the long-QT syndrome in a Chinese family, was shown to be the molecular basis for the autosomal-dominant atrial fibrillation of the corresponding patients. However, this hypothesis needs to be corroborated by further experiments. The results suggest that increased activity of ATP-releasing channels in patients with ODDD mutations can aggravate the predisposition to arrhythmias, which is due to the strong reduction of gap junctional communication (van Rijen et al. 2004).

5.4 The mortality of ODDD mutated mice is due to the proarrhythmic action of the mutated Cx43 protein

The conditional approach allowed to investigate the influence of the G138R mutation in each cell type, where the Cre-recombinase can be specifically activated. Thus, the heart could be determined as the causative tissue for the embryonic lethality observed in the mutant, further underlining the importance of Cx43 for normal heart function. In humans, only few ODDD patients have been reported to suffer from a cardiac phenotype. However, the Cx43G60S, Cx43I130T and, even to a stronger degree, the Cx43G138R mutant mice exhibit cardiac dysfunctions, which have not been reported for ODDD patients. Currently, it cannot be excluded that the mouse heart is more sensitive to Cx43 ODDD like mutations than the human heart. On the basis of this work as well as the study by Flenniken et al. (2005) and Kalcheva et al. (2007), it appears possible that some ODDD patients may exhibit a cardiac phenotype during hypoxic stress that has not been detected yet. It is also possible that up-regulation of other connexins such as Cx45 in human heart failure (Yamada et al., 2003) can partially compensate for the loss of Cx43 coupling. However, such an up-regulation of Cx45 in the Cx43G138R mouse mutant could not be found (Fig. 4.7). Because of the embryonic lethality due to cardiac expression of the Cx43G138R mutation, a detailed investigation of the cardiac phenotype and its molecular basis was carried out. To exclude the influence of any other organs such as the central nervous system, all cardiac analyses were performed with mice specifically expressing the Cx43G138R mutation in cardiomyocytes (Cx43+/floxG138R:

alphaMyHC-Cre). In addition to the heart-related embryonic lethality, premature lethality could be observed in adult mutants during 2–6.5 months after birth, as determined by the Kaplan–Meier survival curve (Fig. 4.5). The observed *in vivo* arrhythmias (Fig. 4.11 and), which are particularly pronounced during hypoxic periods (Fig. 4.12), could be responsible or at least be associated with the high lethality of ODDD-mutated mice.
In summary, this data imply the pro-arrhythmic action of G138R mutated Cx43 and underlines the importance of Cx43 containing gap junction channels in cardiac physiology as recently shown in engraftment experiments of Cx43 expressing cells into post-infarct mouse hearts (Roell et al., 2007).

5.4.1 Disturbed gap junctional coupling is possibly caused by a partial lack of phosphorylation of the Cx43G138R protein

The loss of the P2 phosphorylation band that was observed in the mutated mouse hearts under *in vitro* and *in vivo* conditions has been suggested to be associated with the loss of Cx43 channel function (Oh et al., 1993; Solan et al., 2007). A new potential phosphorylation site on the tyrosine 137 (Y137) localized in the amino acid sequence of Cx43 before the G138R mutation was predicted during my diploma thesis using the NetPhos 2.0 algorithm (Fig.4.7 in Dobrowolski, 2004, diploma thesis). In order to check the assumption that the G138R mutation could disturb the phosphorylation on Y137, a potentially critical site for generation of the P2 band, a Cx43 Y137F mutation was generated and expressed in HeLa cells (data not shown). The amino acid exchange from tyrosine to the not-phosphorylatable phenylalanine has only negligible effects on the secondary structure of the protein. Indeed, Cx43 Y137F were significantly less phosphorylated than the Cx43 wild-type proteins in the parallel analyses to those described in chapter 4.3.6. However, the P2 phosphorylation band could still be generated in HeLa cells expressing these proteins. These data suggest Y137 as a new phosphorylation site, the first one located in the cytoplasmic loop of Cx43. However, this amino acid residue is not the key site for the generation of the P2 band. Thus, the glycine residue at position 138 of Cx43 seems to contribute to the occurrence of the P2 phosphorylation state and the function of GJCs. A possible explanation for this could be the influence of glycine 138 on the structure of the cytoplasmic loop, which contains two

distinct alpha helical regions promoting the binding to the channel closing C-terminal tail (Duffy et al., 2002). Interestingly, two human mutations, G138R and G143S, are located at the boundaries of the two alpha helices respectively, and lead to closure of Cx43 containing gap junction channels in HeLa cells. Glycine is known to act as an alpha helix blocker, arginine or serine do not influence this structure. An extension of the predicated alpha helices in the G138R or G143S mutated loops could increase the binding to the C-terminus and promote channel closure.

5.4.2 The increased activity of ATP releasing channels in Cx43G138R expressing cells can be correlated with the increased half-life of the protein

The expression of increased activity of ATP releasing channels by Cx43 mutants as seen in I31M, G138R and G143S cells (Dobrowolski et al., 2007) is similar to that found with other connexin isoforms, such as Cx32F235C (Lin Liang et al., 2005) and Cx26G45E (Stong et al., 2006) mutants, resulting in ‘‘leaky’’ hemichannels (also called ATP releasing channels because of their doubtful molecular identity). However, some ODDD associated Cx43 mutations (Y17S, G21R, A40V, F52dup, L90V and I130T; Lai et al., 2006) show a functional loss of these channels. The enhanced activity of ATP releasing channels in some mutants (G138R and G143S) can be explained by an obvious degradation defect seen in pulse-chase analyses (Fig. 4.26). The increased function of these channels observed in the I31M mutant showing a normal half-time cannot be explained by an increased amount of Cx43 hemichannels in the membrane. Thus, it is possible that the I31M mutation localized in the first transmembrane domain, which is an important determinant of conductance (Hu et al., 2006), changes the properties of Cx43 and activity of ATP releasing channels. Data regarding the H194P mutant are similar to those reported for the Cx43 cysteine-less mutant (Bao et al., 2004), which also revealed a lack of gap junction plaques but still indicated functional hemichannels.

It is possible that mutations in the cytoplasmic loop of Cx43 like the G143S or G138R may favor the binding of the C-terminus to the loop disturbing the degradation of these proteins. The importance of the C-terminus for Cx43 degradation could be shown in the characterization of its truncated mutant, the Cx43K258stop (Maass et al., 2004). A

degradation impairment leads to an enrichment of the protein in distinct cell compartments. One of these compartments is the plasma membrane. Here, the increasing amount of connexin proteins results in an increased number of hemichannels. The properties of the hemichannels themselves may not be altered by these mutations. The Cx43 localization in G138R mutated hearts supports this assumption. Here, the Cx43 positive staining could be detected in intercalated discs between two cardiomyocytes but also shows a tendency to accumulate in lateral membranes (see Fig. 4.6G-H).

5.5 Different ODDD mouse models and Cx43G138R expressing mice

Until now, three mouse models have been generated, showing ODDD like phenotypes, the Cx43G61S (Flenniken et al., 2005), Cx43G138R (Dobrowolski et al., 2008) and Cx43I130T (Kalcheva et al., 2007) expressing mice.

Besides the development of diverse ODDD characteristics, striking cardiac phenotypes are present in all models, although only for one of the three mutations, the I130T, cardiac arrhythmias were described in the corresponding patients (Paznekas et al.., 2003). Unfortunately, it is uncertain whether the cardiac phenotype in Cx43I130T expressing mice is specific for this mutation or shares a similar mechanism to the other two mutations also leading to arrhythmias.

In human, ODDD associated cardiac symptoms are relatively rare. This discrepancy between human and mice could be explained by intra- and interfamiliar variability as already seen in other symptoms of ODDD like syndactylies (Debeer et al., 2005). The individual genetic background in each patient could be responsible for the variability. This aspect has already been proposed for the high variability in symptoms of Cloustron syndrome caused by Cx30 mutations (van Steensel et al., 2004) or caractogenesis in Cx50 null mutated mice (Gerido et al., 2003). Thus, variability between the different ODDD mouse models regarding the cardiac phenotype does not occur, since they have a similar genetic background.

It is hard to predict a potential genetic modifier altering the severity or appearance of cardiac arrhythmia in ODDD as already described for calpain 3 in caractogenesis

(Baruch et al., 2001). However, recently *KCNJ2* gene coding for Kir2.1, a K^+ subunit important for the maintenance of resting potential in cardiomyocytes, has been described to be closely regulated with Cx43 by the microRNA miR-1 (Yang et al., 2007). Until now, however, a defined connection between ODDD associated cardiac symptoms and the *KCNJ2* gene expression has not been reported.

A possible explanation for the interfamiliar variability could also be due to functional differences between the single mutations. Recently, different potency of the G21R and G138R mutations has been described: the G21R mutated Cx43 is twice as potent in inhibiting the wild-type Cx43 function as the G138R mutant protein (Gong et al., 2007).

There are obvious differences between the Cx43G138R expressing mice and the other two ODDD mouse models, the most striking are cardiac phenotypes. The three ODDD mutants as well as the cardiac specific Cx43 deficient mice are precisely compared in Table 5.2 on the following page. It can be affirmed that G138R mutated mice show the strongest cardiac phenotype by developing severe spontaneous VTs to 100%, whereas such events could be detected in only 25% of the investigated I130T or in none G60S mutants. Furthermore, the Cx43G138R expressing mice showed Cx43 positive staining in the intercalated discs, while the other ODDD mutants did not, nevertheless, the G138R mutated cardiomyocytes exhibit a strong reduction of coupling.

The activity of hemichannels in mutated hearts was only investigated and described in the Cx43G138R mice. In primary cardiomyocytes these channels could be stimulated by zero calcium conditions and hypoxia, hypoxic periods resulted *in vivo* in clear increase of arrhythmic events. Moreover, the observed embryonic lethality in these mutants was due to the cardiac expression of the mutation and emerged during ED 13-16.5, a period in which cardiomyocytes fully adopt their metabolism to oxygen. These facts underline the importance of the action of these ATP releasing channels in the cardiac physiology and remain to be checked in the other ODDD mouse models.

	Cx43fl/fl:alphaMyHC-Cre Eckardt et al., 2006		Cx43 +/floxG138R:alphaMyHC-Cre Dobrowolski et al., 2008		Cx43 +/G60S Flenniken, Osborne et al., 2005		Cx43 +/I130T Kalcheva et al., 2007	
Genetic conspicuousness	Heterozygous: rezessive	Homozygous: phenotype	Heterozygous: dominant	Homozygous: not viable	Heterozygous: dominant	Homozygous: lethal	Heterozygous: dominant	Homozygous: lethal
lifespan	-	16 days after birth (PD)	4 – 6.5 months	ED 13 – 16.5	normal	-	normal	-
Embrynonic lethality	-	32 % (25% expected,17% born)	44 % (25% expected, 14% born)	100 %	-	100 %	36% (50% expected, 32% born)	100 %
QRS (ms)	n.s.	676 % (85.9±14.1 vs +/fl: 12.7±1.6)	170 % (23.8±4.4 vs +/+: 14.0±0.8)	-	2 out of 9 mutants: prolonged	-	n.s. (p=0.1) (12.3±1.0 vs +/+10.5±0.3;)	-
Ampl. R (mV)	n.s.	5.8 % (0.18±0.06 vs +/fl: 3.12±0.97)	22 % (0.12±0.02 vs +/+: 0.55± 0.07)	-	n.s.	-	30 % (1.4 vs 4.6)	-
PQ (ms)	n.s.	n.s.	124 % (53.0±2.0 vs 42.8±6.3)	-	n.s.	-	n.s.	-
Cx43 trafficking	reduced by 50%, normal	No protein in cardiomyocytes	plasma membrane (widely normal)	-	Widely not localized in plasma membrane	-	Widely not localized in plasma membrane	-
Reduction of coupling	50% in cardiomyocytes	100 % in cardiomyocytes (Cx43 ablation, immunfluorescence data)	94 % in cardiomyocytes (microinjection data)	-	Very weakly coupled	-	50% (7.9±2.4 vs 15.7±1.4)	-
Hemichannel activity in cardiomyocytes	50% in cardiomyocytes	0 % in cardiomyocytes loss-of-function mutation	200 % gain-of-function mutation	200 %	Not known	-	Not known	-
Heart morphology	n.s.	hypertrophy in subpulmonal region of the outflow tract	n.s.	-	Patent foramen ovale	-	n.s.	-
Echocardiography	n.s.	n.s.	n.s.	-	Preejection + ejection time elevated, diastolic chamber dimension + thickness reduced	-	n.s.	-
Arrhythmogeneity	n.s.	0 % spontaneous VTs Small amplitudes + broadening of the complexes => diffuse ventricular activation => strong reduction of QRS amplitudes	100 % spontaneous ventricular tachycardias (VTs)	-	0 % spontaneous VTs 56 % bradycardia 44 % sinus arrest 11 % sinus arrest 11 % sinus dissociation	-	25 % spontaneous VTs 75 % inducible VTs	-
Cause of death	-	Irregular ventricular activation suspected	Ventricular tachycardia (VT) favored by hypoxic stimulation	Not known	Bradycardia suspected	Not known	Not known	Not known

Table 5.2: Comparison of cardiac function in ODDD mouse models vs conditional Cx43 mutant (Cx43fl/fl:alphaMyHC-Cre). All ODDD mutated mice developed cardiac anomalies in a dominant manner. Notice the lack of Cx43 expression in all except the Cx43G138R mutant, as well as strong penetrance of sustained spontaneous ventricular tachycardias (VTs) in this ODDD mouse model.

5.6 The morphological ODDD phenotype can be explained by a reduced Bmp2 and Shh expression

After ubiquitous activation of the mutated Cx43G138R gene in the transgenic mice, all morphological ODDD phenotypic manifestations described in patients including syndactyly, craniofacial and bone abnormalities were found. These abnormalities demonstrate the importance of Cx43 during embryonic development and confirm the identity of this ODDD mouse model.

The reduced expressions of the two key morphogens, not only for the limb and bone formation, Shh and Bmp2 (see Fig. 4.17 and 4.19), can explain the phenotypes in ODDD mutated mice and patients.

The bone phenotype observed in heterozygously mutated mice (Fig. 4.3) could be explained by the obviously reduced osteoblast number, which, however, did not reach significance because of the strongly variable phenotype of the male mutants. The reduced expression of Bmp2 could be the reason for the reduced osteoblast's portion in mutant bone. Bmp2 is described to be crucial for the differentiation of mesenchymal precursor cells to osteoblasts (Thies et al., 1992).

The craniofacial malformations seen in ODDD mutants (Fig. 4.2H) are similar to those described for mouse embryos with a reduced Shh expression. These wild-type embryos were cultured in a cyclopamine conditioned solution, a Shh signaling antagonist (Nagase et al., 2005) and present an animal model for holoprosencephaly (HPE). This cephalic disorder is characterized by an impaired development of the embryonic forebrain, prosencephalon, causing facial and sometimes brain defects. HPE is known to be mainly caused by Shh mutations or to have environmental causes in man (Roessler et al., 1996). An extremely high intra- and interfamiliar variability is reported in HPE patients which ranges from cyclopia and perinatal lethality to hypotelorism (abnormal closeness of the eyes), microcephaly and dental malformations (Cohen et al., 1989a,b and 1992). Interestingly, malformations described for mild forms of HPE equal those in ODDD patients. The cause for this analogy could be a reduction of the Shh induced signaling and its influence of the downstream affected pathways like that of Bmp2.

Also the observed enamel hypoplasia in Cx43+/G138R mice (Fig. 4.2G) can be explained with a reduction of the Bmp2 expression in mutants. Bmp2, besides other

members of this gene family, was found in the enamel knot, the putative signaling center regulating tooth shape, and is expressed there by the dentin-forming odontoblasts and the enamel forming ameloblasts (Aberg et al., 1997). However, a reduction of Bmp2 expression does not result in a dental patterning defect but reduces the enamel thickness (Zhao et al., 2000).

The disturbed interdigital apoptosis in the G138R mutated mice leading to the observed syndactylies is most likely due to a decreased Bmp2 level and not an excessive expression of its antagonist Noggin in the developing limb (Fig. 4.17). Bmp2 is known to induce cell death between the digits and separating them from each other (Ganan et al., 1996; Yokouchi et al., 1999; Zou and Niswander, 1996). An immoderate blockade of apoptosis could be excluded because no differences in Noggin expression in the developing hands or feet were seen between the two genotypes. In order to further quantify the amount of Bmp2 in the limb bud, cultures were assessed and western blot analyses were provided. The reduction of Bmp2 levels already seen in fused neural tube or head in whole mount embryos (Fig. 4.17) could also be confirmed in the limb bud (ED11.5 and ED13.5) (Fig. 4.19).

It has been hypothesized that the amount of certain morphogen is crucial for a proper development of the distinct tissue, as described by Bandyopadhyay et al. (2007) for Bmp2, 4 and 7. The lowered quantity of Shh, Bmp2 or their downstream signaling could lead to the observed phenotypic variability in the heterozygously mutated Cx43G138R mice, ODDD and HPE patients.

Thus, ODDD patients may show a reduction in Bmp2 and Shh expression which would lead to the known morphological anomalies. Because Bmps are expressed in adult bone (Daluiski et al., 2001) a biopsy of bone matter from an affect person would be sufficient to quantify the transcripts of the mentioned genes.

5.7 Cx43 mediated coupling modulate morphogen expression in limb bud and bone

In order to investigate the molecular reasons for the morphological malformations in the ODDD mice hemizygous mutants were used. These Cx43LacZ/G138R mice showed a high penetrance of the ODDD phenotype. The immunohistochemical analyses of whole mount embryos (ED10.5 – ED13.5) and limb bud culture experiments revealed an alteration of two major morphogens in the mutant mice, i.e. proteins with an ability to induce proliferation and regulate tissue patterning. These two morphogens were sonic hedgehog (Shh) and bone morphogenic protein 2 (Bmp2), whereas all other tested proteins (Bmp4, FGF8 or Noggin) showed no changes between the genotypes. Furthermore, the combination of control animals (wild-type and Cx43 deficient mice) allows to conclude that the decreased expression of Shh and Bmp2 is due to a disruption of Cx43 mediated gap junctional coupling. This assumption is supported by the appearance of morphologic ODDD specific symptoms in heterozygously mutated mice or human patients carrying other Cx43 mutations. The occurrence of the syndactylies or craniofacial alterations in patients with *GJA1* gene mutations not altering the activity of ATP releasing channels (Lai et al., 2006), exclude their action as the reason for these symptoms.

Function, expression pattern and signaling pathways of both morphogens are well described. It is also known that Shh signaling acts upstream of Bmp2 (Laufer et al., 1994) (see Fig. 1.8). This fact suggests that the reduced expression of Shh seen in ODDD mice is the cause for the reduced Bmp2 expression in these mutants.

However, the precise molecular mechanism how Cx43 influences the expression of these morphogens is not known. The link between Cx43 and Shh or Bmp2 transcription could be provided by studies using Cx43-antisense nucleotides in chick limbs. Here, the knock-down of Cx43 expression led to a reduction of both morphogens mRNA levels. Recently, Shh signaling has been described to be associated with an increase of intracellular Ca^{2+} concentration which mediates proliferation signals in mouse ES cells (Heo et al., 2007).

Since it is well known that Cx43 containing gap junction channels are able to transfer Ca^{2+} or inositol-1,4,5-trisphosphate (IP_3) (Saez et al., 1989), calcium imaging studies of wild-type and mutated primary limb bud cells were performed. During these analyses it

could be observed that neither Cx43LacZ/G138R nor Cx43 deficient cells could propagate spontaneous Ca^{2+} oscillations to neighboring cells. This behavior was contrary to wild-type cells (Fig. 4.20F-J). Thus, it is possible that Ca^{2+} acts as a morphogen modulator and the disturbed Ca^{2+} propagation results in a reduced Shh signaling which in turn leads to a diminished Bmp2 expression. This hypothesis will be further clarified in ongoing analyses.

However, it cannot be excluded that small molecular messengers other than proteins are involved in this processes. Serotonin is such a molecule which signaling is crucial for patterning of the left-right axis (Fukumoto et al., 2005). The transfer of serotonin and possibly other small morphogens through long-range gap junctional channels is apparently driven by an electrophoretical mechanism (Esser et al., 2006). This signaling process influence the lateral expression of the marker proteins Nodal and sonic hedgehog, i.e. acts upstream of the corresponding genes (Levin and Mercola, 1999).

5.8 Impact of the Cx43G138R mutation on the brain

The Cx43G138R mutated gene is driven by the endogenous Cx43 promoter which allows its expression in astrocytes of the adult brain (Fig. 4.13). The G138R mutation leads to a gap junction channel blockade and increased activity of ATP releasing channels. Both effects influence processes in the brain. Specific deletion of Cx43 in astrocytes results in deceleration of spreading depression and locomotory activity, whereas the resulting reduction of gap junctional coupling appears to be compensated by Cx30 up-regulation (Theis et al., 2003).

The activity of Cx43 hemichannels was recently described to play a central role in the hypoxic preconditioning in the brain (Lin et al., 2008). Cx43 supported or mediated ATP release and an accumulation of its metabolic product and a neuroprotective agent adenosine elevate cellular resistance to subsequent hypoxic events (Lin et al., 2008).

During this PhD work two ODDD mutants were analyzed which could be very helpful to further reveal the influence of connexin mediated intercellular coupling and increased activity of ATP releasing channels on processes in the brain. The Cx43flox/floxG138R:Nestin-Cre mice are the only living homozygous ODDD mutants.

Since the heterozygously G138R mutated mice show in comparison to wild-type ones a doubled activity of the ATP releasing channels, it can be expected that the homozygous mutants show a fourfold increased activity of these channels. Consequently, these homozygous brain specific mutants are suitable to further analyze the impact of hemichannels *in vivo*. An increased adenosine concentration and an associated neuroprotection can be expected. However, a gain-of-function mutation regarding the ATP releasing channels in the brain has not been described till now, the consequences of an increased efflux of signaling molecules and ions remain unpredictable. In this homozygous mutant the Cx43 mediated coupling is similar to Cx43 deficient mice. As shown in Figure 4.21 the Cx43G138R mutation dominantly inhibits Cx43 coupling in stably transfected HeLa cells, also the generation of the functional Cx43G138R/Cx43WT heterotypic channels is not possible in astrocytes of these mice. Furthermore, the gap junctional coupling seems to be compensated by Cx30 up-regulation in the homozygous, brain specific ODDD mutants (see Fig. 4.15 bottom right). Hence, conditional Cx43 knock-out mice (for example Cx43flox/floxLacZ:Nestin-Cre) are the adequate controls for the subsequent analyses (see chapter 5.9 Future perspectives).

The second interesting mutant are the hemizygous Cx43LacZ/G138R mice. The connexin expression in these mice is strongly decreased (see Fig. 4.15). Cx43 expression is reduced to 15%, whereas the amount of Cx30 is not significantly altered. The missing compensation by Cx30 could provide for widely pronounced phenotype.

5.9 Future perspectives

The Cx43G138R mouse model of ODDD will be further used to analyze the effects of increased activity of ATP-releasing channels and reduction of gap junctional function on bone formation, syndactyly and astrocytic functions. In addition, the Cx43G138R mutated mice may serve as a useful platform to test therapies against Cx43 dephosphorylation, gap junction channel closure and increased activity of ATP releasing channels.

5.9.1 Bone morphogenesis in Cx43G138R mice

Further analyses of bone morphogenesis will be provided in cooperation with the group of Prof. Roberto Civitelli (St. Louis, USA). In order to define the impact of the Cx43G138R on the development of bone several histological stainings will be done. Thus, tartrate-resistant acid phosphatase (TRAP) analyses for osteoclasts, trichrome staining for osteoblasts as well as calcein injections for whole mineralized tissue are planed. Furthermore, the dominant-negative effect of the mutant Cx43 protein will be investigated in reference to early osteoblast commitment of stromal cell precursors. A possible impairment of the differentiation of these cells would explain the obviously decreased number of osteoblasts in ODDD mutated bones. The use of different Cx43G138R mutants like hemizygous Cx43G138R/LacZ mice or the homozygous Cx43flox/floxG138R:Dermo1-Cre and Runx2-Cre mediated ubiquitous or specific activation in osteoblasts will help to resolve this problem.

5.9.2 The impact of the Cx43G138R mutation in brain

In cooperation with groups of Prof. Maiken Nedergaard (Rochester, NY, USA) and Dr. Martin Theis (Bonn, Germany) the impact of the increased activity of ATP releasing channels and reduction of gap junctional coupling in the brain will be investigated.
The use of two photon microscopy allows real-time imaging of cellular processes in living brains such as neuronal degeneration or neuroprotection. Specific excitation of eGFP, which is expressed in Cx43G138R positive cells, allows to distinguish astrocytes

releasing ATP *in vivo* and precisely examine their cellular behavior as well as their influence on other direct cell neighbors. As already mentioned above, Cx43 mediated release of ATP and an accumulation of adenosine during hypoxic preconditioning is described to protect cells from subsequent hypoxic stress (Lin et al., 2007). The gain-of-function of these ATP releasing channels will be further analyzed using the G138R expressing mice in the hypoxia model.

Furthermore, hemizygous mutants as well as early neuron specific homozygous ODDD mutants will be investigated during kainate induced epilepsy. The determination of the status epilepticus in Cx43G138R mice should elucidate the function of hemichannels in the brain.

5.9.3 Modulation of morphogen expression by gap junctional coupling

To further understand the molecular mechanisms behind the modulation of morphogen expression by gap junctional coupling diverse *in vitro* and *in vivo* experiments are planed. The possible modulation of Shh and Bmp2 expression by Ca^{2+} or IP_3 signaling will be investigated in limb bud cultures. Here, an increase of the frequency of intercellular Ca^{2+} oscillations will be provided by long-term application of carbachol (up to 3 days). Because carbachol's maximal action last only for an average of 8 hours, the drug has to be reapplied after this time. The expression of the morphogens will be subsequently tested in quantitative real-time PCR analyses in cooperation with the group of Prof. Michael Hoch (Bonn, Germany).

The possible involvement of small morphogenic molecules, like serotonin, on the expression of Shh and Bmp2 can also be examined in the primary cell cultures. Thus, serotonin can be applied over a long time and is easy to handle because of its relatively long half-life time of up to 48 h. In addition, serotonin has also been described to be involved in craniofacial development (Lauder et al., 1988) by regulation of cranial neural crest migration (Moiseiwitsch et al., 1995). However, a direct influence of serotonin on Shh or Bmp2 expression has not been described. The transcripts of these two genes will also be quantified in real-time PCR analyses.

Subsequent *in vivo* and *in vitro* imaging of Ca^{2+} or IP_3 propagation in the developing mouse limb buds will be performed in cooperation with Dr. Hartmann Hartz (Munich,

Germany). *In vivo* studies can be performed using two photon microscopy. These analyses will further illuminate the possible interaction of Ca^{2+} and morphogen signaling.

6. Summary

The Cx43G13R expressing mice present a new conditional mouse model for ODDD, carrying the human G138R point mutation. The main findings of this study are the occurrence of all common phenotypes of the human-inherited disease ODDD, like syndactylies, craniofacial anomalies, enamel hypoplasia, and the heart related mortality of Cx43G138R heterozygously mutated mice. The mortality of the mice is likely due to the strongly decreased gap junctional function, supporting the proarrhythmic action of the G138R-mutated Cx43 protein. This appears to be associated with a strongly diminished phosphorylation (P2 band) of this protein. The expression of the mutant Cx43 in HeLa and ES cell as well as the use of primary cardiomyocytes derived from mutant embryonic hearts revealed besides a strong decrease of Cx43 mediated gap junctional coupling and increased activity of ATP releasing channels. The physiological relevance of both effects could be ascertained in vivo. Impulse propagation and activation pattern could be determined in Langendorff recordings and surface ECGs showing a striking broadening of the QRS complex and chaotic appearance of field potentials in heterozygously mutated hearts. These data are similar to those obtained with conditional Cx43 deficient mice, suggesting the loss Cx43 mediated coupling to be responsible for the observed alterations. However, also the increased activity of ATP releasing channels in mutant hearts was physiologically relevant. In order to investigate the impact of the ATP releasing channels in the heart, primary cultures of cardiomyocytes were established and further characterized. Noticeably, beating frequency of mutated cardiomyocytes was faster than that recorded in wild-type cells. Using the gap junction blocker flufenaminic acid (FFA) at a concentration inhibiting ATP-releasing hemichannels or the mimetic peptide Gap26 as a specific blocker of these channels reduced the increased beating frequency of mutated cardiomyocytes in culture to the same level as observed in wild-type cells. This suggests that the spontaneous ventricular arrhythmias observed in Langendorff and *in vivo* recordings of mutated adult hearts are mainly due to the strongly decreased gap junctional coupling and could be aggravated by the increased release of cellular ATP or other small molecules.

Furthermore, the morphological anomalies of the ODDD mutated mice could be referred to a obviously reduced expression of two key morphogens: sonic hedgehog (Shh) and

bone morphogenic protein 2 (Bmp2). Diminished levels of these proteins lead to a deficient induction of interdigital apoptosis by Bmp2 causing syndactylies. In addition, impaired development of the embryonic forebrain by Shh, may cause facial defects.

7. References

Aberg T, Wozney J, Thesleff I. Expression patterns of bone morphogenetic proteins (Bmps) in the developing mouse tooth suggest roles in morphogenesis and cell differentiation. Dev Dyn. 4:383-96. 1997

Agah, R., Frenkel, P.A., French, B.A., Michael, L.H., Overbeek, P.A. and Schneider, M.D. Gene recombination in postmitotic cells. Targeted expression of Cre recombinase provokes cardiac-restricted, site-specific rearrangement in adult ventricular muscle in vivo. J Clin Invest., 100, 169-179. 1997

Alberts, B.,Johnson, A., Lewis, J., Raff, M., Roberts, K., Walter, P., Molecular Biology of THE CELL, fourth edition, 2002

Attal J, Theron MC, Houdebine LM. The optimal use of IRES (internal ribosome entry site) in expression vectors. Genet Anal. 15:161-5. 1999

Axelsen LN, Haugan K, Stahlhut M, Kjølbye AL, Hennan JK, Holstein-Rathlou NH, Søberg Petersen J and Nielsen MS. Increasing Gap Junctional Coupling: A Tool for Dissecting the Role of Gap Junctions. J Memb Biol 216:1: 23-35, 2007

Baruch A, Greenbaum D, Levy ET, Nielsen PA, Gilula NB, Kumar NM, and Bogyo M. Defining a link between gap junction communication, proteolysis, and cataract formation. J Biol Chem 276:28999-9006. 2001.

Bauer,R., Loer,B., Ostrowski,K., Martini,J., Weimbs,A., Lechner,H., and Hoch,M. Intercellular communication: the Drosophila innexin multiprotein family of gap junction proteins. Chem. Biol. 12, 515-526. 2005

Bandyopadhyay A, Tsuji K, Cox K, Harfe BD, Rosen V, Tabin CJ. Genetic analysis of the roles of BMP2, BMP4, and BMP7 in limb patterning and skeletogenesis. PLoS Genet. 2:e216. 2006

Bani-Yaghoub M, Felker JM, Sans C, Naus CC. The effects of bone morphogenetic protein 2 and 4 (BMP2 and BMP4) on gap junctions during neurodevelopment. Exp Neurol. 162:13-26. 2000

Bao X, Chen Y, Reuss L, Altenberg GA. Functional expression in Xenopus oocytes of gap-junctional hemichannels formed by a cysteine-less connexin 43. J Biol Chem 279:9689–9692. 2004

Bao X, Lee SC, Reuss L, Altenberg GA. Change in permeant size selectivity by phosphorylation of connexin 43 gap-junctional hemichannels by PKC. Proc Natl Acad Sci USA 104:4919–4924. 2007

Bayly RD, Ngo M, Aglyamova GV, Agarwala S. Regulation of ventral midbrain patterning by Hedgehog signaling. Development. 11:2115-24. 2007

Beardslee, MA, Lerner, DL, Tadros, PN, Laing, JG, Beyer, EC, Yamada, KA, Kléber, AG, Schuessler, RB, Saffitz, JE. Circ Res. 87:656-667. 2000

Bedner,P., Niessen,H., Odermatt,B., Kretz,M., Willecke,K., and Harz,H. Selective permeability of different connexin channels to the second messenger cyclic AMP. J. Biol. Chem. 281, 6673-6681. 2006

Bennett, M.V.L. and Verselis, V.K. Biophysics of gap junctions. Semin. Cell. Biol., 3, 29-47.1992

Bennett,M.V., Contreras,J.E., Bukauskas,F.F., and Saez,J.C. New roles for astrocytes: gap junction hemichannels have something to communicate. Trends Neurosci. 26, 610-617. 2003

Bergoffen J, Scherer SS, Wang S, Scott MO, Bone LJ, Paul DL, Chen K, Lensch MW, Chance PF, and Fischbeck KH. Connexin mutations in X-linked Charcot-Marie-Tooth disease. Science 262:2039-42, 1993.

Beyer EC, Kistler J, Paul DL, Goodenough DA. Antisera directed against connexin43 peptides react with a 43-kD protein localized to gap junctions in myocardium and other tissues.

J Cell Biol. 2:595-605. 1989

Bijlsma MF, Spek CA, Zivkovic D, van de Water S, Rezaee F, Peppelenbosch MP. Repression of smoothened by patched-dependent (pro-)vitamin D3 secretion. PLoS Biol. 8:e232. 2006

Brink,P.R., Cronin,K., Banach,K., Peterson,E., Westphale,E.M., Seul,K.H., Ramanan,S.V., and Beyer,E.C. Evidence for heteromeric gap junction channels formed from rat connexin43 and human connexin37. Am. J. Physiol. 273, C1386-C1396. 1997

Bruce AF, Rothery S, Dupont E, Severs NJ. Gap junction remodelling in human heart failure is associated with increased interaction of connexin43 with ZO-1. Cardiovasc Res. 4:757-65. 2008

Bruzzone, S., Guida, L., Zocchi, E., Franco, L. and De Flora, A. Connexin 43 hemi channels mediate Ca2+-regulated transmembrane NAD+ fluxes in intact cells. FASEB J., 15, 10-12. 2001

Bruzzone R, Veronesi V, Gomès D, Bicego M, Duval N, Marlin S, Petit C, D'Andrea P, White TW.Loss-of-function and residual channel activity of connexin26 mutations associated with non-syndromic deafness.FEBS Lett. 1-3:79-88. 2003

Buchholz, F., Angrand, P.O. and Stewart, A.F. A simple assay to determine the functionality of Cre or FLP recombination targets in genomic manipulation constructs. Nucleic. Acids. Res., 24, 3118–3119. 1996

Buchholz F, Angrand PO, und Stewart AF. Improved properties of FLP recombinase evolved by cycling mutagenesis. Nat Biotechnol 16:657-662. 1998

Bugiani M, Al SS, Lamantea E, Bizzi A, Bakhsh E, Moroni I, Balestrini MR, Uziel G, and Zeviani M. GJA12 mutations in children with recessive hypomyelinating leukoencephalopathy. Neurology 67:273-79, 2006.

Bukauskas, F.F., Angele, A.B., Verselis, V.K. and Bennett, M.V. Coupling asymmetry of heterotypic connexin 45/ connexin 43-EGFP gap junctions: properties of fast and slow gating mechanisms. Proc. Natl. Acad. Sci. U. S. A., 99, 7113-7118. 2002

Bukauskas, F.F. and Verselis, V.K. Gap junction channel gating. Biochim Biophys Acta, 1662, 42-60. 2004

Bukauskas, F.F., Kreuzberg, M.M., Rackauskas, M., Bukauskiene, A., Bennett, M.V.L., Verselis, V.K. and Willecke, K. Properties of mouse connexin 30.2 and human connexin 31.9 hemichannels: Implications for atrioventricular conduction in the heart. Proc. Nat. Acad., U.S.A., 103, 9726–9731. 2006

Capdevila J, Johnson RL. Endogenous and ectopic expression of noggin suggests a conserved mechanism for regulation of BMP function during limb and somite patterning. Dev Biol. 197:205-17. 1998

Castro, C. H., Shin, C. S., Stains, J. P., Cheng, S. L., Sheikh, S., Mbalaviele, G., Szejnfeld, V. L. and Civitelli, R. Targeted expression of a dominant-negative N-cadherin in vivo delays peak bone mass and increases adipogenesis. J. Cell Sci., 117, 2853-2864. 2004

Chen, Y.H., Xu, S.J., Bendahhou, S., Wang, Y., Xu W.Y., Jin, H.W., Sun, H., Zhuang, Q.N., Yang, Y.Q., Li, Y.B., et al. KCNQ1 gain-of-function mutation in familial atrial fibrillation. Science, 299, 251-254. 2003

Chiang C, Litingtung Y, Lee E, Young KE, Corden JL, et al. Cyclopia and defective axial patterning in mice lacking Sonic hedgehog gene function. Nature 383: 407–413. 1996

Chiang C, Litingtung Y, Harris MP, Simandl BK, Li Y, Beachy PA, Fallon JF. Manifestation of the limb prepattern: limb development in the absence of sonic hedgehog function. Dev Biol. 236:421-35. 2001

Cohen,M.M.,Jr. Perspectives on holoprosencephaly, Part I. Epidemiology, genetics, and syndromology. Teratology, 40, 211–235. 1989a

Cohen,M.M.,Jr. Perspectives on holoprosencephaly, Part III. Spectra, distinctions, continuities, and discontinuities. Am. J. Med. Genet., 34, 271–288. 1989b

Cohen,M.M.,Jr and Sulik,K.K. Perspectives on holoprosencephaly. Part II. Central nervous system, craniofacial anatomy, syndrome commentary, diagnostic approach, and experimental studies. J. Craniofacial Genet. Dev. Biol., 12, 196–244. 1992

Cohen MM Jr, Shiota K. Teratogenesis of holoprosencephaly. Am J Med Genet. 1:1-15. 2002

Coppen,S.R., Kodama,I., Boyett,M.R., Dobrzynski,H., Takagishi,Y., Honjo,H., Yeh,H.I., and Severs,N.J. Connexin45, a major connexin of the rabbit sinoatrial node, is coexpressed with connexin43 in a restricted zone at the nodal-crista terminalis border. J. Histochem. Cytochem. 47, 907-918.1999a

Coppen,S.R., Severs,N.J., and Gourdie,R.G. Connexin45 (alpha 6) expression delineates an extended conduction system in the embryonic and mature rodent heart. Dev. Genet. 24, 82-90.1999b

Cordero D, Marcucio R, Hu D, Gaffield W, Tapadia M, Helms JA. Temporal perturbations in sonic hedgehog signaling elicit the spectrum of holoprosencephaly phenotypes.J Clin Invest. 114:485-94. 2004

Daluiski A, Engstrand T, Bahamonde ME, Gamer LW, Agius E, Stevenson SL, Cox K, Rosen V, Lyons KM. Bone morphogenetic protein-3 is a negative regulator of bone density. Nat Genet. 1:84-8. 2001

Debeer P, Van Esch H, Huysmans C, Pijkels E, De Smet L, Van de Ven W, Devriendt K, Fryns JP. Novel GJA1 mutations in patients with oculo-dento-digital dysplasia (ODDD). Eur J Med Genet. 4:377-87, 2005

Degen, J., Meier, C., Van Der Giessen, R.S., Söhl, G., Petrasch-Parwez, E., Urschel, S., Dermietzel, R., Schilling, K., De Zeeuw, C.I. and Willecke, K. Expression pattern of lacZ reporter gene representing connexin36 in transgenic mice. J. Comp. Neurol., 473, 511-525. 2004

Degen, J. “Erzeugung und Charakterisierung von konditionalen Knock-In Reportergen-Mäusen des Connexin36”, PhD thesis, University of Bonn, 2004

Delmar, M., Coombs, W., Sorgen, P., Duffy, H.S. and Taffet, S.M. Structural bases for the chemical regulation of Connexin43 channels. Cardiovasc Res., 62, 268-275. 2004

Dent JA, Polson AG, Klymkowsky MW. A whole-mount immunocytochemical analysis of the expression of the intermediate filament protein vimentin in Xenopus. Development. 1:61-74. 1989

Dobrowolski, R. “Expression einer Connexin 43 Mutation, die im Menschen Oculodentodigitale Dysplasie verursacht, in HeLa-Zellen und embryonalen Stammzellen der Maus”, diploma thesis, University of Bonn, 2004

Dobrowolski, R., Sommershof, A. and Willecke, K. Some oculodentodigital dysplasia-associated Cx43 mutations cause increased hemichannel activity in addition to deficient gap junction channels. J. Membr. Biol., doi 10.1007/s00232-007-9055-7. 2007

Dobrowolski R, Sasse P, Schrickel JW, Watkins M, Kim JS, Rackauskas M, Troatz C, Ghanem A, Tiemann K, Degen J, Bukauskas FF, Civitelli R, Lewalter T, Fleischmann BK, and Willecke K. The conditional connexin43G138R mouse mutant represents a new model of hereditary oculodentodigital dysplasia in humans. Hum Mol Genet, 4:539-54. 2008

Dobrowolski R and Willecke K, Connexin caused genetic diseases and corresponding mouse models. . Antioxid Redox Signal. Submitted, 2008

Dobrzynski,H., Nikolski,V.P., Sambelashvili,A.T., Greener,I.D., Yamamoto,M., Boyett,M.R.,and Efimov,I.R. Site of origin and molecular substrate of atrioventricular junctional rhythm in the rabbit heart. Circ. Res. 93, 1102-1110.2003

Duffy, H.S., Sorgen, P.L., Girvin, M.E., O'Donnell, P., Coombs, W., Taffet, S.M., Delmar, M. and Spray, D.C. pH-dependent intramolecular binding and structure involving Cx43 cytoplasmic domains. J. Biol. Chem., 277, 36706-36714.2002

Ebihara,L. New roles for connexons. News Physiol Sci. 18:100-3., 100-103. 66. Stout,C., Goodenough,D.A., and Paul,D.L. Connexins: functions without junctions. Curr. Opin. Cell Biol. 16, 507-512. 2004

Eckardt, D., Kirchhoff, S., Kim, J.S., Degen, J., Theis, M., Ott, T., Wiesmann, F., Doevendans, P.A., Lamers, W.H., de Bakker, J.M. et al. Cardiomyocyte-restricted deletion of connexin43 during mouse development. J Mol Cell Cardiol., 41, 963-971. 2006

Eloff,B.C., Gilat,E., Wan,X., and Rosenbaum,D.S. Pharmacological modulation of cardiac gap junctions to enhance cardiac conduction: evidence supporting a novel target for antiarrhythmic therapy. Circulation. 108, 3157-3163. 2003

Esser AT, Smith KC, Weaver JC, Levin M. Mathematical model of morphogen electrophoresis through gap junctions. Dev Dyn. 8:2144-59. 2006

Evans,W.H. and Martin,P.E. Gap junctions: structure and function. Mol. Membr. Biol. 19, 121-136. 2002

Evans, W.H., De Vuyst, E. and Leybaert, L. The gap junction cellular internet: connexin hemichannels enter the signalling limelight. Biochem. J., 397, 1-14. 2006

Fara, M., Horak, I., Hrivnakova, J., Kapras, J., Nova, M. and Stloukalova, M. Oculodentodigital dysplasia. Acta Chir. Plast., 19, 110-122. 1977

Fernandes M, Gutin G, Alcorn H, McConnell SK, Hébert JM. Mutations in the BMP pathway in mice support the existence of two molecular classes of holoprosencephaly. Development, 21:3789-94. 2007

Flenniken, A.M., Osborne, L.R., Anderson, N., Ciliberti, N., Fleming, C., Gittens, J.E., Gong, X.Q., Kelsey, L.B., Lounsbury, C., Moreno, L., et al. A Gja1 missense mutation in a mouse model of oculodentodigital dysplasia. Development, 132, 4375-4386. 2005

Foppiano S, Hu D, Marcucio RS. Signaling by bone morphogenetic proteins directs formation of an ectodermal signaling center that regulates craniofacial development. Dev Biol. 312:103-14. 2007

Francis PH, Richardson MK, Brickell PM, Tickle C Bone morphogenetic proteins and a signalling pathway that controls patterning in the developing chick limb. Development 120: 209–218. 1994

Fukumoto T, Kema IP, Levin M. Serotonin signaling is a very early step in patterning of the left-right axis in chick and frog embryos. Curr Biol. 9:794-803. 2005

Ganan Y, Macias D, Duterque-Coquillaud M, Ros MA, Hurle JM Role of TGF beta s and BMPs as signals controlling the position of the digits and the areas of interdigital cell death in the developing chick limb autopod. Development 122: 2349–2357. 1996

Gerido DA, Sellitto C, Li L, and White TW. Genetic background influences cataractogenesis, but not lens growth deficiency, in Cx50-knockout mice. *Invest Ophthalmol Vis Sci* 44:2669-74, 2003.

Giepmans BN, Verlaan I, Moolenaar WH. 2001. Connexin-43 interactions with ZO-1 and alpha- and betatubulin. Cell Commun Adhes. 8:219-23.

Gillepsie, F.D. A hereditary syndrome: „Dysplasia oculodentodigitalis.“ Arch. Ophthalmol., 71, 187-192. 1964

Gollob MH, Jones DL, Krahn AD, Danis L, Gong XQ, Shao Q, Liu X, Veinot JP, Tang AS, Stewart AF, Tesson F, Klein GJ, Yee R, Skanes AC, Guiraudon GM, Ebihara L, and Bai D. Somatic mutations in the connexin 40 gene (GJA5) in atrial fibrillation. N Engl J Med 354:2677-88, 2006.

Gourdie,R.G., Severs,N.J., Green,C.R., Rothery,S., Germroth,P., and Thompson,R.P. The spatial distribution and relative abundance of gap-junctional connexin40 and connexin43 correlate to functional properties of components of the cardiac atrioventricular conduction system. J. Cell Sci. 105, 985-991.1993

Gilula NB, Epstein ML, Beers WH. Cell-to-cell communication and ovulation. A study of the cumulus-oocyte complex. J Cell Biol. 1:58-75. 1978

Gong, X.Q., Shao, Q., Langlois, S., Bai, D. and Laird, D.W. Differential potency of dominant negative connexin43 mutants in oculodentodigital dysplasia. J. Biol. Chem., 26, 19190-19202. 2007

Groenewegen WA, Firouzi M, Bezzina CR, Vliex S, van L, I, Sandkuijl L, Smits JP, Hulsbeek M, Rook MB, Jongsma HJ, and Wilde AA. A cardiac sodium channel mutation cosegregates with a rare connexin40 genotype in familial atrial standstill. Circ Res 92:14-22. 2003.

Heathcote K, Syrris P, Carter ND, and Patton MA. A connexin 26 mutation causes a syndrome of sensorineural hearing loss and palmoplantar hyperkeratosis (MIM 148350). J Med Genet 37:50-51. 2000

Hennemann, H., Schwarz, H.J. and Willecke, K. Characterization of gap junction genes expressed in F9 embryonic carcinoma cells: molecular cloning of mouse connexin31 and -45 cDNAs. Eur. J. Cell. Biol., 57, 51–58. 1992

Heo JS, Lee MY, Han HJ. Sonic hedgehog stimulates mouse embryonic stem cell proliferation by cooperation of Ca2+/protein kinase C and epidermal growth factor receptor as well as Gli1 activation. Stem Cells. 12:3069-80. 2007

Herr, C., Smyth, N., Ullrich, S., Yun, F., Sasse, P., Hescheler, J., Fleischmann, B., Lasek, K., Brixius, K., Schwinger, R.H., et al. Loss of annexin A7 leads to alterations in frequency-induced shortening of isolated murine cardiomyocytes. Mol. Cell. Biol., 21, 4119-4128. 2001

Hesse, M., Kondo, C.S., Clark, R.B., Su, L., Allen, F.L., Geary-Joo, C.T., Kunnathu, S., Severson, D.L., Nygren, A., Giles, W.R. and Cross, J.C. Dilated cardiomyopathy is associated with reduced expression of the cardiac sodium channel Scn5a. Cardiovasc. Res., 75, 498-509. 2007

Hu X, Ma M, Dahl G. Conductance of connexin hemichannels segregates with the first transmembrane segment. Biophys J 90:140–150. 2006

Juang JM, Chern YR, Tsai CT, Chiang FT, Lin JL, Hwang JJ, Hsu KL, Tseng CD, Tseng YZ, and Lai LP. The association of human connexin 40 genetic polymorphisms with atrial fibrillation. Int J Cardiol 116:107-12. 2007

Judisch, G.F., Martin-Casals, A., Hanson, J.W. and Olin, W.H. Oculodentodigital dysplasia; four new reports and a literature review. Arch. Ophthal., 97, 878-884. 1979

Kalcheva N, Qu J, Sandeep N, Garcia L, Zhang J, Wang Z, Lampe PD, Suadicani SO, Spray DC, and Fishman GI. Gap junction remodeling and cardiac arrhythmogenesis in a murine model of oculodentodigital dysplasia. Proc Natl Acad Sci U S A. 2007.

Kaprielian,R.R., Gunning,M., Dupont,E., Sheppard,M.N., Rothery,S.M., Underwood,R., Pennell,D.J., Fox,K., Pepper,J., Poole-Wilson,P.A., and Severs,N.J. Downregulation of immunodetectable connexin43 and decreased gap junction size in the pathogenesis of chronic hibernation in the human left ventricle. Circulation. 97, 651-660.1998

Kim HK, Lee YS, Sivaprasad U, Malhotra A, Dutta A. Muscle-specific microRNA miR-206 promotes muscle differentiation. J Cell Biol. 5:677-87. 2006

Kirchhoff S, Nelles E, Hagendorff A, Kruger O, Traub O, and Willecke K. Reduced cardiac conduction velocity and predisposition to arrhythmias in connexin40-deficient mice. Curr Biol 8:299-302, 1998.

Kirchhoff S, Kim JS, Hagendorff A, Thonnissen E, Kruger O, Lamers WH, and Willecke K. Abnormal cardiac conduction and morphogenesis in connexin40 and connexin43 double-deficient mice. Circ Res 87:399-405. 2000.

Kreuzberg,M.M., Söhl,G., Kim,J.S., Verselis,V.K., Willecke,K., and Bukauskas,F.F. Functional properties of mouse connexin30.2 expressed in the conduction system of the heart. Circ. Res. 96, 1169-1177. 2005

Kreuzberg,M.M., Schrickel,J.W., Ghanem,A., Kim,J.S., Degen,J., Janssen-Bienhold,U., Lewalter,T., Tiemann,K., and Willecke,K. Connexin30.2 containing gap junction channels decelerate impulse propagation through the atrioventricular node. Proc. Natl. Acad. Sci. U. S. A. 103, 5959-5964. 2006

Kreuzberg MM, Willecke K, Bukauskas FF. Connexin-mediated cardiac impulse propagation: connexin 30.2 slows atrioventricular conduction in mouse heart. Trends Cardiovasc Med. 2006 16:266-72

Krüger,O., Plum,A., Kim,J.S., Winterhager,E., Maxeiner,S., Hallas,G., Kirchhoff,S., Traub,O., Lamers,W.H., and Willecke,K. Defective vascular development in connexin 45- deficient mice. Development. 127, 4179-4193. 2000

Kühn R, Schwenk F, Aguet M, und Rajewsky K. Inducible gene targeting in mice. Science 269:1427- 1429. 1995

Kumar,N.M. and Gilula,N.B. The gap junction communication channel. Cell. 84, 381- 388. 1996

Lai, A., Le, D.-N., Paznekas, W.A., Gifford, W.S., Wang Jabs, E. and Charles, A.C. Oculodentodigital dysplasia connexin43 mutations result in non-functional connexin hemichannels and gap junctions in C6 glioma cells. J. Cell. Sci., 119, 532-541. 2006

Laird DW. Life cycle of connexins in health and disease. Biochem J 394:527-43. 2006.

Lallemand, Y., Luria, V., Haffner-Krausz, R. and Lonai, P. Maternally expressed PGK-Cre transgene as a tool for early and uniform activation of the Cre site-specific recombinase. Transgenic Res., 7, 105–112. 1998

Lamartine J, Munhoz EG, Kibar Z, Lanneluc I, Callouet E, Laoudj D, Lemaitre G, Hand C, Hayflick SJ, Zonana J, Antonarakis S, Radhakrishna U, Kelsell DP, Christianson AL, Pitaval A, Der Kaloustian V, Fraser C, Blanchet-Bardon C, Rouleau GA, and Waksman G. Mutations in GJB6 cause hidrotic ectodermal dysplasia. Nat Genet 26:142-44. 2000.

Lammers, W.J., Schalij, M.J., Kirchhof, C.J. and Allessie, M.A. Quantification of spatial inhomogeneity in conduction and initiation of reentrant atrial arrhythmias. Am J Physiol.,259, 1254-1263. 1990

Lampe PD, Lau AF. The effects of connexin phosphorylation on gap junctional communication. Int J Biochem Cell Biol 36:1171-1186. 2004

Lauder JM, Tamir H, Sadler TW. Serotonin and morphogenesis. I. Sites of serotonin uptake and -binding protein immunoreactivity in the midgestation mouse embryo. Development. 4:709-20. 1988

Laufer E, Nelson CE, Johnson RL, Morgan BA, Tabin C. Sonic hedgehog and Fgf-4 act through a signaling cascade and feedback loop to integrate growth and patterning of the developing limb bud. Cell. 79:993-1003. 1994

Law LY, Lin JS, Becker DL, Green CR. Knockdown of connexin43-mediated regulation of the zone of polarizing activity in the developing chick limb leads to digit truncation. Dev Growth Differ. 6:537-47. 2002

LeMotte PK, Kuroiwa A, Fessler LI, Gehring WJ. The homeotic gene Sex Combs Reduced of Drosophila: gene structure and embryonic expression. EMBO J. 1:219-27. 1989

Levin M, Mercola M. Gap junction-mediated transfer of left-right patterning signals in the early chick blastoderm is upstream of Shh asymmetry in the node. Development. 21:4703-14. 1999

Lewandoski,M. Conditional control of gene expression in the mouse. Nat. Rev. Genet. 2, 743-755. 2001

Li QY, Newbury-Ecob RA, Terrett JA, Wilson DI, Curtis AR, Yi CH, Gebuhr T, Bullen PJ, Robson SC, Strachan T, Bonnet D, Lyonnet S, Young ID, Raeburn JA, Buckler AJ, Law DJ, Brook JD. Holt-Oram syndrome is caused by mutations in TBX5, a member of the Brachyury (T) gene family. Nat Genet. 15:21-9. 1997

Li, D., Fareh, S., Leung, T.K. and Nattel, S. Promotion of atrial fibrillation by heart failure in dogs: atrial remodeling of a different sort. Circulation, 100, 87-95. 1999

Lin JH, Lou N, Kang N, Takano T, Hu F, Han X, Xu Q, Lovatt D, Torres A, Willecke K, Yang J, Kang J, Nedergaard M. A central role of connexin 43 in hypoxic preconditioning. J Neurosci. 3:681-95. 2008

Lin Liang SG, de Miguel M, Gomez-Hernandez JM, Glass JD, Scherer SS, Mintz M, Barrio LC, Fischbeck KH. Severe neuropathy with leaky connexin32 hemichannels. Ann Neurol 57:749–754. 2005

Loddenkemper, T., Grote, K., Evers, S., Oelerich, M. and Stogbauer, F. Neurological manifestations of the oculodentodigital dysplasia syndrome. J. Neurol., 249, 584-595. 2002

Lopez-Bigas N, Olive M, Rabionet R, Ben-David O, Martinez-Matos JA, Bravo O, Banchs I, Volpini V, Gasparini P, Avraham KB, Ferrer I, Arbones ML, and Estivill X. Connexin 31 (GJB3) is expressed in the peripheral and auditory nerves and causes neuropathy and hearing impairment. Hum Mol Genet 10:947-52. 2001.

Macari F, Landau M, Cousin P, Mevorah B, Brenner S, Panizzon R, Schorderet DF, Hohl D, and Huber M. Mutation in the gene for connexin 30.3 in a family with erythrokeratodermia variabilis. Am J Hum Genet 67:1296-301. 2000.

Mackay D, Ionides A, Kibar Z, Rouleau G, Berry V, Moore A, Shiels A, and Bhattacharya S. Connexin46 mutations in autosomal dominant congenital cataract. Am J Hum Genet 64:1357-64. 1999.

Maestrini E, Korge BP, Ocana-Sierra J, Calzolari E, Cambiaghi S, Scudder PM, Hovnanian A, Monaco AP, and Munro CS. A missense mutation in connexin26, D66H, causes mutilating keratoderma with sensorineural deafness (Vohwinkel's syndrome) in three unrelated families. Hum Mol Genet 8:1237-43. 1999.

Magin, T.M., McWhir, J. and Melton, D.W. A new mouse embryonic stem cell line with good germ line contribution and gene targeting frequency. Nucleic. Acids. Res., 20, 3795-3796.

Makarenkova H, Patel K. Gap junction signalling mediated through connexin-43 is required for chick limb development. Dev Biol. 2:380-92. 1999

Mazgalev,T.N. and Tchou,P.J. Surface potentials from the region of the atrioventricular node and their relation to dual pathway electrophysiology. Circulation. 101, 2110-2117. 2000

McLachlan, E., Manias, J.L., Gong, X.Q., Lounsbury, C.S., Shao, Q., Bernier, S.M., Bai, D. and Laird, D.W. Functional characterization of oculodentodigital dysplasia-associated Cx43 mutants. Cell Commun Adhes., 5-6, 279-292. 2005

Maass K, Ghanem A, Kim JS, Saathoff M, Urschel S, Kirfel G, Grummer R, Kretz M, Lewalter T, Tiemann K, Winterhager E, Herzog V, and Willecke K. Defective epidermal barrier in neonatal mice lacking the C-terminal region of connexin43. Mol Biol Cell 15:4597-608, 2004.

Moiseiwitsch JR, Lauder JM. Serotonin regulates mouse cranial neural crest migration. Proc Natl Acad Sci U S A. 16:7182-6. 1995

Moorman,A.F. and Christoffels,V.M. Cardiac chamber formation: development, genes, and evolution. Physiol Rev. 83, 1223-1267. 2003

Musil,L.S., Le,A.C., Van Slyke, J.K., and Roberts,L.M. Regulation of connexin degradation as a mechanism to increase gap junction assembly and function. J. Biol. Chem. 275, 25207-25215. 2000

Nagase T, Nagase M, Osumi N, Fukuda S, Nakamura S, Ohsaki K, Harii K, Asato H, Yoshimura K. Craniofacial anomalies of the cultured mouse embryo induced by inhibition of sonic hedgehog signaling: an animal model of holoprosencephaly. J Craniofac Surg. 16:80-8. 2005

Nagy JI, Patel D, Ochalski PAY, Stelmack GJ: Connexin 30 in rodent, cat and human brain: selective expression in grey matter astrocytes, co-localization with connexin 43 at gap junctions and late developmental appearance. Neuroscience, 88:447–468. 1999

Nagy JI, Ionescu AV, Lynn BD, und Rash JE. Connexin29 and connexin32 at oligodendrocyte and astrocyte gap junctions and in myelin of the mouse central nervous system. J Comp Neurol 464:356-370. 2003

Niessen,H., Harz,H., Bedner,P., Kramer,K., and Willecke,K. Selective permeability of different connexin channels to the second messenger inositol 1,4,5-trisphosphate. J. Cell Sci. 113, 1365-1372. 2000

Neijssen J, Herberts C, Drijfhout JW, Reits E, Janssen L, and Neefjes J. Cross-presentation by intercellular peptide transfer through gap junctions. Nature 434:83-88. 2005.

Netter,F.H. Atlas der Anatomie des Menschen. Ciba Geigy, fourth edition.1993

Nishii,K., Kumai,M., Egashira,K., Miwa,T., Hashizume,K., Miyano,Y., and Shibata,Y. Mice lacking connexin45 conditionally in cardiac myocytes display embryonic lethality similar to that of germline knockout mice without endocardial cushion defect. Cell Commun. Adhes. 10, 365-369. 2003

Nivelon-Chevallier, A., Audry, D., Audry, F. and Dumas, R. Dysplasie oculodento-digital: A propos d'un cas avec paraplégie spasmodique. J. Genet. Hum., 29, 171-179. 1981

Nolden, L., Edenhofer, F., Haupt, S., Koch, P., Wunderlich, F.T., Siemen, H. and Brüstle, O. Site-specific recombination in human embryonic stem cells induced by cell-permeant Cre recombinase. Nat. Methods., 3, 461-467. 2006

Oh, S.Y., Dupont, E., Madhukar, B.V., Briand, J.P., Chang, C.C., Beyer, E. and Trosko, J.E. Characterization of gap junctional communication-deficient mutants of a rat liver epithalial cell line. Eur. J. Cell. Biol., 60, 250-255. 1993

Paznekas, W.A., Boyadjiev, S.A., Shapiro, R.E., Daniels, O., Wollnik, B., Keegan, C.E., Innis, J.W., Dinulos, M.B., Christian, C., Hannibal, M.C., et al. Connexin 43 (GJA1) mutations cause the pleiotropic phenotype of oculodentodigital dysplasia. Am. J. Hum. Genet., 72, 408-418. 2003

Penuela S, Bhalla R, Gong XQ, Cowan KN, Celetti SJ, Cowan BJ, Bai D, Shao Q, Laird DW. Pannexin 1 and pannexin 3 are glycoproteins that exhibit many distinct characteristics from the connexin family of gap junction proteins. J Cell Sci. 2007 120:3772-83.

Peters,N.S., Green,C.R., Poole-Wilson,P.A., and Severs,N.J. Reduced content of connexin43 gap junctions in ventricular myocardium from hypertrophied and ischemic human hearts. Circulation. 88, 864-875.1993

Pizette S, Niswander L Early steps in limb patterning and chondrogenesis. Novartis Found Symp 232: 23–36; discussion 36–46. 2001

Rackauskas, M., Kreuzberg, M.M., Pranevicius, M., Willecke, K., Verselis, V.K. and Bukauskas, F.F. Gating properties of heterotypic gap junction channels formed of connexins 40, 43, and 45. Biophys J., 92, 1952-1965. 2007

Reaume, A.G., de Sousa, P.A., Kulkarni, S., Langille, B.L., Zhu, D., Davies, T.C., Juneja, S.C., Kidder, G.M. and Rossant, J. Cardiac malformation in neonatal mice lacking connexin43. Science, 267, 1831-1834.1995

Reddi AH, Huggins C. Biochemical sequences in the transformation of normal fibroblasts in adolescent rats. Proc Natl Acad Sci U S A 69: 1601– 1605. 1972

Revel JP, Karnovsky MJ. Hexagonal array of subunits in intercellular junctions of the mouse heart and liver. J Cell Biol.3:C7-C12.1967

Richard G, White TW, Smith LE, Bailey RA, Compton JG, Paul DL, and Bale SJ. Functional defects of Cx26 resulting from a heterozygous missense mutation in a family with dominant deaf-mutism and palmoplantar keratoderma. Hum Genet 103:393-99, 1998.

Richard G. Connexins: a connection with the skin. Exp Dermatol 9:77-96, 2000.

Richard G, Rouan F, Willoughby CE, Brown N, Chung P, Ryynanen M, Jabs EW, Bale SJ, DiGiovanna JJ, Uitto J, Russell J. Missense mutations in GJB2 encoding connexin-26 cause the ectodermal dysplasia keratitis-ichthyosis-deafness syndrome. Am J Hum Genet 70:1341-48, 2002.

Riddle RD, Johnson RL, Laufer E, Tabin C. Sonic hedgehog mediates the polarizing activity of the ZPA. Cell. 75:1401-16. 1993

Roell W, Lewalter T, Sasse P, Tallini YN, Choi BR, Breitbach M, Doran R, Becher UM, Hwang SM, Bostani T, von Maltzahn J, Hofmann A, Reining S, Eiberger B, Gabris B, Pfeifer A, Welz A, Willecke K, Salama G, Schrickel JW, Kotlikoff MI, Fleischmann BK. Engraftment of connexin 43-expressing cells prevents post-infarct arrhythmia. Nature. 7171:819-24. 2007

Roessler E, Belloni E, Gaudenz K, Jay P, Berta P, Scherer SW, Tsui LC, Muenke M. Mutations in the human Sonic Hedgehog gene cause holoprosencephaly. Nat Genet. 3:357-60. 1996

Roscoe, W., Veitch, G.I., Gong, X.Q., Pellegrino, E., Bai, D., McLachlan, E., Shao, Q., Kidder, G.M. and Laird, D.W. Oculodentodigital dysplasia-causing connexin43 mutants are non-functional and exhibit dominant effects on wild-type connexin43. J. Biol.Chem., 280, 11458-11466. 2005

Rose B und Loewenstein WR. Calcium ion distribution in cytoplasm visualised by aequorin: diffusion in cytosol restricted by energized sequestering. Science 190:1204-1206. 1975

Sáez JC, Connor JA, Spray DC, Bennett MV. Hepatocyte gap junctions are permeable to the second messenger, inositol 1,4,5-trisphosphate, and to calcium ions. Proc Natl Acad Sci U S A. 8:2708-12. 1989

Salviati L, Trevisson E, Baldoin MC, Toldo I, Sartori S, Calderone M, Tenconi R, and Laverda A. A novel deletion in the GJA12 gene causes Pelizaeus-Merzbacher-like disease. Neurogenetics 8:57-60, 2007.

Schnichels M, Worsdorfer P, Dobrowolski R, Markopoulos C, Kretz M, Schwarz G, Winterhager E, and Willecke K. The connexin31 F137L mutant mouse as a model for the human skin disease erythrokeratodermia variabilis (EKV). Hum Mol Genet 16:1216-24, 2007.

Seki, A., Coombs, W., Taffet, S.M. and Delmar, M. Loss of electrical communication, but not plaque formation, after mutations in the cytoplasmic loop of connexin43. Heart Rhythm, 1, 227-233. 2004

Severs,N.J., Coppen,S.R., Dupont,E., Yeh,H.I., Ko,Y.S., and Matsushita,T. Gap junction alterations in human cardiac disease. Cardiovasc. Res. 62, 368-377. 2004

Shibayama, J., Paznekas, W., Seki, A., Taffet, S., Jabs, E.W., Delmar, M. and Musa, H. Functional characterization of connexin43 mutations found in patients with oculodentodigital dysplasia. Circ. Res., 96, 83-91. 2005

Shiels A, Mackay D, Ionides A, Berry V, Moore A, and Bhattacharya S. A missense mutation in the human connexin50 gene (GJA8) underlies autosomal dominant "zonular pulverulent" cataract, on chromosome 1q. Am J Hum Genet 62:526-32, 1998.

Smith JH, Green CR, Peters NS, Rothery S, Severs NJ. Altered patterns of gap junction distribution in ischemic heart disease. An immunohistochemical study of human myocardium using laser scanning confocal microscopy. Am J Pathol. 4:801-21. 1991

Söhl, G. and Willecke, K. An update on connexin genes and their nomenclature in mouse and man. Cell. Commun. Adhes., 10, 173-180. 2003

Söhl,G. and Willecke,K. Gap junctions and the connexin protein family. Cardiovasc.Res. 62, 228-232. 2004

Söhl,G., Maxeiner,S., and Willecke,K. Expression and functions of neuronal gap junctions. Nat. Rev. Neurosci. 6, 191-200. 2005

Solan JL, Lampe PD. Key connexin 43 phosphorylation events regulate the gap junction life cycle. J Membr Biol. 1-3:35-41. 2007

Spray, D.C., Ye, Z.C. and Ransom, B.R. Functional connexin ‘‘Hemichannels’’: A critical appraisal. Glia, 54, 758–773. 2006

Stergiopoulos K, Alvarado JL, Mastroianni M, Ekvitorin JF, Taffet SM, und Delmar M. Hetero-domain interactions as a mechanism for the regulation of connexin channels. Circ Res 84:1144-1155. 1999

Sternberg N, Sauer B, Hoess R, Abremski K. Bacteriophage P1 cre gene and its regulatory region. Evidence for multiple promoters and for regulation by DNA methylation. J Mol Biol.

187:197-212. 1986

Stong BC, Chang Q, Ahmad S, Lin X. A novel mechanism for connexin 26 mutation linked deafness: cell death caused by leaky gap junction hemichannels. Laryngoscope 116:2205–2210. 2006

Stout, C.E., Costantin, J.L., Naus, C.C.G. and Charles, A.C. Intercellular Calcium Signaling in Astrocytes via ATP Release through Connexin Hemichannels. J. Biol. Chem., 12, 10482-10488. 2002

Sun X, Mariani FV, Martin GR. Functions of FGF signalling from the apical ectodermal ridge in limb development.Nature. 6897:501-8. 2002

Theis, M., Magin, T.M., Plum, A. and Willecke, K. General or cell type-specific deletion and replacement of connexin-coding DNA in the mouse. Methods, 20, 205–218. 2000

Theis M, de Wit C, Schlaeger TM, Eckardt D, Krüger O, Döring B, Risau W, Deutsch U, Pohl U, Willecke K. Endothelium-specific replacement of the connexin43 coding region by a lacZ reporter gene. Genesis. 1:1-13. 2001

Theis M, Jauch R, Zhuo L, Speidel D, Wallraff A, Frisch C, Söhl G, Teubner B, Euwens C, Huston J, Steinhauser C, Messing A, Heinemann U, Willecke K: Accelerated hippocampal spreading depression and enhanced locomotory activity in mice with astrocyte-directed inactivation of connexin43. J Neurosci, 23:766–776. 2003

Thies RS, Bauduy M, Ashton BA, Kurtzberg L, Wozney JM, Rosen V. Recombinant human bone morphogenetic protein-2 induces osteoblastic differentiation in W-20-17 stromal cells. Endocrinology. 3:1318-24. 1992

Toyofuku T, Yabuki M, Otsu K, Kuzuya T, Hori M, Tada M. Direct association of the gap junction protein connexin-43 with ZO-1 in cardiac myocytes. J Biol Chem. 273:12725-31. 1998

Traub, O., Eckert, R., Lichtenberg-Frate, H., Elfgang, C., Bastide, B., Scheidtmann, K.H., Hülser, D.F. and Willecke, K. Immunochemical and electrophysiological characterization of murine connexin40 and -43 in mouse tissues and transfected human cells. Eur. J. Cell. Biol., 64, 101-112. 1994

Tronche, F., Kellendonk, C., Kretz, O., Gass, P., Anlag, K., Orban, P.C., Bock, R., Klein, R. and Schutz, G. Disruption of the glucocorticoid receptor gene in the nervous system results in reduced anxiety. Nat. Genet., 23, 99 –103. 1999

Uhlenberg B, Schuelke M, Ruschendorf F, Ruf N, Kaindl AM, Henneke M, Thiele H, Stoltenburg-Didinger G, Aksu F, Topaloglu H, Nurnberg P, Hubner C, Weschke B, and Gartner J.

Mutations in the gene encoding gap junction protein alpha 12 (connexin 46.6) cause Pelizaeus-Merzbacher-like disease. Am J Hum Genet 75:251-60, 2004.

Urist MR. Bone: Formation by autoinduction. Science 150: 893–899. 1965

Uyguner O, Tukel T, Baykal C, Eris H, Emiroglu M, Hafiz G, Ghanbari A, Baserer N, Yuksel-Apak M, and Wollnik B. The novel R75Q mutation in the GJB2 gene causes autosomal dominant hearing loss and palmoplantar keratoderma in a Turkish family. Clin Genet 62:306-09. 2002.

van Rijen, H.V., Eckardt, D., Degen, J., Theis, M., Ott, T., Willecke, K., Jongsma, H.J., Opthof, T. and de Bakker, J.M. Slow conduction and enhanced anisotropy increase the propensity for ventricular tachyarrhythmias in adult mice with induced deletion of connexin43. Circulation, 109, 1048-1055. 2004

van Steensel MA. Gap junction diseases of the skin. Am J Med Genet C Semin Med Genet 131C:12-19. 2004.

van Steensel, M.A.M., Spruijt, L., van der Burgt, I., Bladergroen, R.S., Vermeer, M., Steijlen, P.M. and vanGeel, M. A 2-bp deletion in the GJA1 gene is associated with oculo-dento-digital dysplasia with palmoplantar keratoderma. Am. J. Med. Genet. A., 132, 171-174. 2005

van Zeijl L, Ponsioen B, Giepmans BN, Ariaens A, Postma FR, Várnai P, Balla T, Divecha N, Jalink K, Moolenaar WH. Regulation of connexin43 gap junctional communication by phosphatidylinositol 4,5-bisphosphate. J Cell Biol. 5:881-91. 2007

Wang,Y.S., Scheinman,M.M., Chien,W.W., Cohen,T.J., Lesh,M.D., and Griffin,J.C. Patients with supraventricular tachycardia presenting with aborted sudden death: incidence, mechanism and long-term follow-up. J. Am. Coll. Cardiol. 18, 1711-1719. 1991

Wang X, Li L, Peracchia LL, Peracchia C. Chimeric evidence for a role of the connexin cytoplasmic loop in gap junction channel gating. Pflugers Arch. 431: 844-52. 1996

Weintraub, D.M., Baum, J.L. and Pashayan, H.M. A fimily with oculodentodigital dysplasia. Cleft Palate J., 12, 323-329. 1975

Wilgenbus, K.K., Kirkpatrick, C.J., Knuechel, R., Willecke, K. and Traub, O. Expression of Cx26, Cx32 and Cx43 gap junction proteins in normal and neoplastic human tissues. Int. J. Cancer, 51, 522-529. 1992

Willecke K, Eiberger J, Degen J, Eckardt D, Romualdi A, Guldenagel M, Deutsch U, and Sohl G. Structural and functional diversity of connexin genes in the mouse and human genome. Biol

Chem 383:725-37. 2002.

Winnier G, Blessing M, Labosky PA, Hogan BL Bone morphogenetic protein-4 is required for mesoderm formation and patterning in the mouse. Genes Dev 9: 2105–2116. 1995

Wolf NI, Cundall M, Rutland P, Rosser E, Surtees R, Benton S, Chong WK, Malcolm S, Ebinger F, Bitner-Glindzicz M, and Woodward KJ. Frameshift mutation in GJA12 leading to nystagmus, spastic ataxia and CNS dys-/demyelination. Neurogenetics 8:39-44. 2007.

Wozney JM, Rosen V, Celeste AJ, Mitsock LM, Whitters MJ, et al. Novel regulators of bone formation: Molecular clones and activities. Science 242: 1528–1534. 1988

Yamada, K.A., Rogers, J.G., Sundset, R., Steinberg, T.H. and Saffitz, J.E. Up-regulation of connexin45 in heart failure. J. Cardiovasc. Electrophysiol., 11, 1205-1212. 2003

Yang Y, Drossopoulou G, Chuang PT, Duprez D, Marti E, et al. Relationship between dose, distance and time in Sonic Hedgehog-mediated regulation of anteroposterior polarity in the chick limb. Development 124: 4393–4404. 1997

Yang B, Lin H, Xiao J, Lu Y, Luo X, Li B, Zhang Y, Xu C, Bai Y, Wang H, Chen G, Wang Z. The muscle-specific microRNA miR-1 regulates cardiac arrhythmogenic potential by targeting GJA1 and KCNJ2. Nat Med. 4:486-91. 2007

Yokouchi Y, Vogan KJ, Pearse RV 2nd, Tabin CJ Antagonistic signaling by Caronte, a novel Cerberus-related gene, establishes left-right asymmetric gene expression. Cell 98: 573–583. 1999

Zhang H, Bradley A Mice deficient for BMP2 are nonviable and have defects in amnion/chorion and cardiac development. Development 122: 2977–2986. 1996

Zhang W, Green C, Stott NS. Bone morphogenetic protein-2 modulation of chondrogenic differentiation in vitro involves gap junction-mediated intercellular communication. J Cell Physiol. 193:233-43. 2002

Zhao X, Zhang Z, Song Y, Zhang X, Zhang Y, Hu Y, Fromm SH, Chen Y. Transgenically ectopic expression of Bmp4 to the Msx1 mutant dental mesenchyme restores downstream gene expression but represses Shh and Bmp2 in the enamel knot of wild type tooth germ. Mech Dev. 1-2:29-38. 2000

Zou H, Niswander L Requirement for BMP signaling in interdigital apoptosis and scale formation. Science 272: 738–741. 1996

8. List of abbreviations

A	adenin
A	Ampere
AER	apical ectodermal ridge
alphaMyHC	alpha myosin heavy chain
ATP	adenosine triphosphate
BSA	bovine serum albumin
bp	base pairs
Bmp	bone morphogenic protein
bpm	beats per minute
C	cytosin
Ca	calcium
cAMP	cyclic 3',5'-adenosine monophosphate
cDNA	copy DNA, reverse transcribed mRNA
CFP	cyan fluorescent protein
ChAT	choline acetyltransferase
Cl	chloride
C-terminus	carboxy-terminus
Cx	connexin
Da	Dalton
DNA	desoxy ribonucleic acid
dNTP	2'-desoxy-nucleoside-5'-triphosphate
ECG	electrocardiogram
E. coli	Escherichia coli
EB	embryoid body
ED	embryonic day
EF	left ventricular ejection fraction
e.g.	for example (Latin: exempli gratia)
eGFP	enhanced green fluorescent protein
ES cell	embryonic stem cell
EtBr	ethidium bromide
FFA	Flufenaminic acid
Fig	figure
FITC	fluorescein isothiocyanate
g	gram
G	guanin
GFAP	glial fibrillary acidic protein
gj	unitary conductance
Gj	transjunctional conductance
GJC	gap junction channel
h	hour
HF	heart frequency
HPE	holoprosencephaly
Hz	Hertz
i.e.	that is (Latin: id est)
IgG	immunoglobulin G
Ij	transjunctional current
IP_3	inositol 1,4,5-trisphosphate
IRES	internal ribosomal entry site
isoOMPA	tetraisopropylpyrophosphoamide
kb	kilo base pairs
KO	knock-out
l	liter
LVM	left ventricular muscle mass
LVEDV	left ventricular enddiastolic volume
m	meter
M	molar
Mg	magnesium
min	minute
Na	sodium
NAD	nicotinamide adenine dinucleotide
neurobiotin	N-(2-aminoethyl)biotinamide
neo	neomycin resistance gene
NGS	normal goat serum
NLS	nuclear localization signal
ODDD	oculodento digital dysplasia
PB	phosphate buffer
PBS	phosphate buffered saline
PCR	polymerase chain reaction
PFA	paraform aldehyde
PGK	phosphoglycerate kinase promoter
PI	propidium iodide
PIP_2	phosphatidylinositol bisphosphate
pH	negative decadic logarithm of hydrogen ion concentration
PLCß3	phosphatidylinositol bisphosphate hydrolyzing receptors
PKC	protein kinase C
RNA	ribonucleic acid
RT-PCR	reverse transcriptase-polymerase chain reaction
s	second
S	Siemens
Shh	sonic hedgehog
T	thymidin
Tab.	Table
UTR	untranslated region
V	volt
VES	ventricular extra systole
Vj	transjunctional voltage
vol	volume
VT	ventricular tachycardia
ZO-1	zonula occludens protein 1
ZPA	zone of polarizing activity
Ω	Ohm
°C	degree Celsius

9. Supplement

9.1 Cloning of the conventional Cx40A96S construct

In order to investigate the molecular mechanisms and to develop strategies how to avoid idiopathic atrial fibrillations in patients carrying the Cx40 A96S point mutation (Gollob et al., 2006), the decision has been made to generate a mouse model expressing this mutated protein. The following figures present the generation of the non-conditional Cx40A96S construct.

The resulting Cx40A96S conventional mouse vector has a total size of 13253 bp including a 5' homology region of 5031 bp and a 3' homology region of 1560 bp.

As already described for the conditional Cx43G138R mouse vector the use of eGFP allows to in vivo label the cells expressing the mutated form of Cx40 without affect the expression of the Cx40 proteins. The PGK-Neomycin cassettes are flanked by frt sites and have to be excised using the deleter/Flp mice to avoid the strong PGK promoter activity.

The Cx40A96S vector has been used in cooperation with the diploma student Indra Luebkemeier for homologous recombination in mouse ES cells and will be further analyzed *in vivo*.

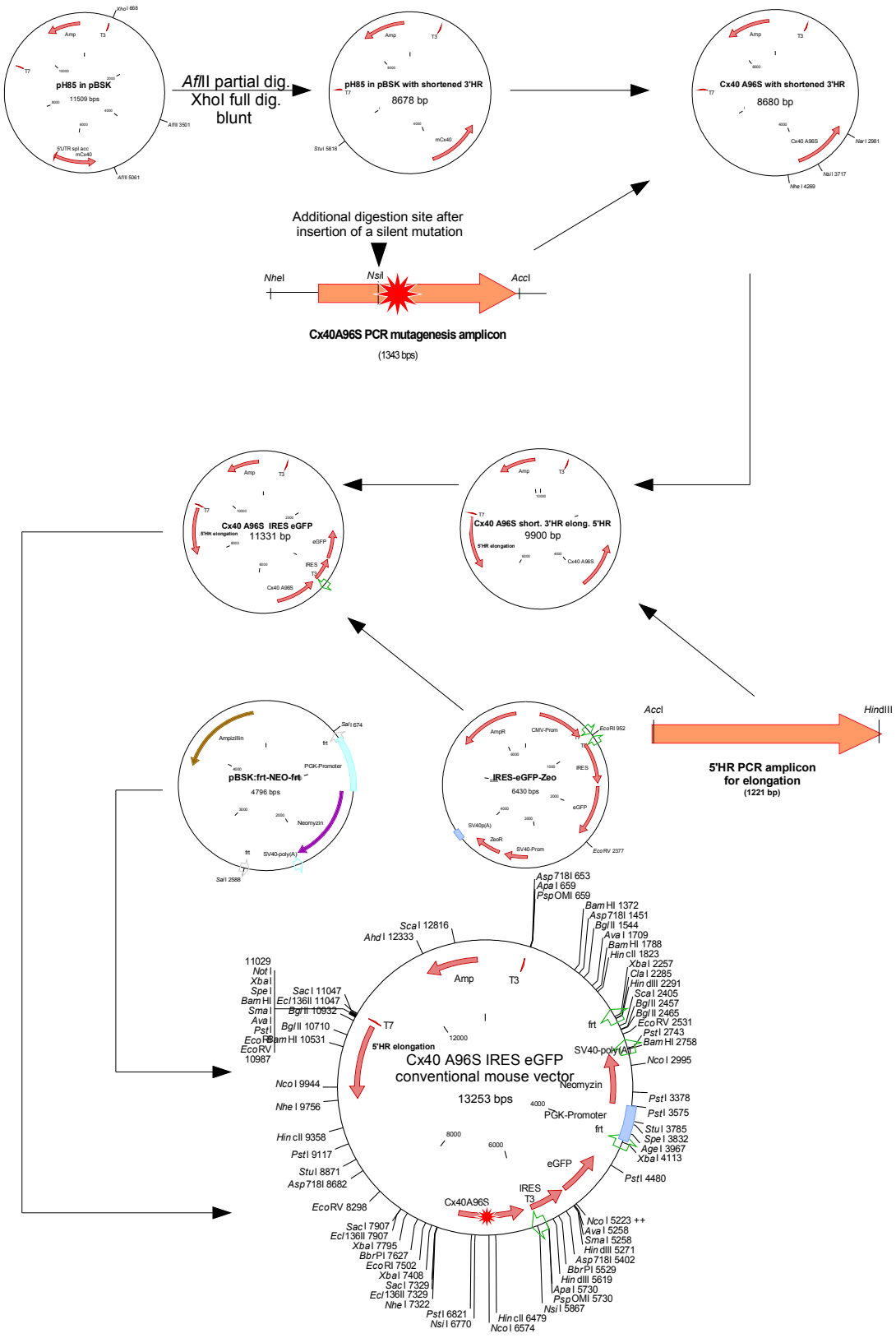

Figure 9.1: The cloning strategy for the conventional Cx40A96S mouse construct consists of at last five cloning steps and result in the 13.3 kb mouse vector.

A

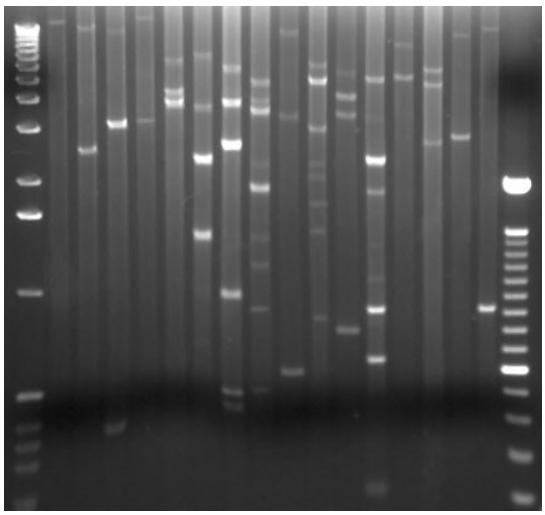

Enzyme	NotI	NheI	HindIII	ClaI	AvaI	NcoI	BamHI	XbaI	SacI	HincII	KpnI	PstI	StuI	EcoRV	ScaI	NsiI
Expected fragment sizes	13253	10819	9925	13253	5747	6304	5277	4487	9535	5718	5224	4997	8167	5767	10411	12350
		2434	2980		3957	3370	3614	3295	3140	4656	3951	2341	5086	4797	2842	903
			348		3549	2228	2496	3228	578	2879	3280	2296		2689		
						1351	970	1856			798	1882				
							480	387				905				
							416					635				
												197				

B

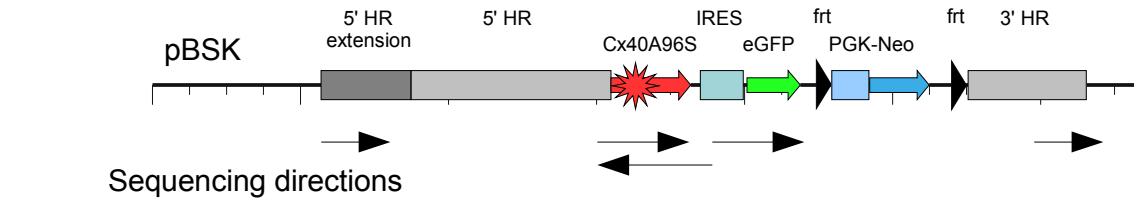

Figure 9.2: Control digestions of the Cx40A96S mouse vector. (A) All used restriction enzymes showed a expected digestion pattern (see table) as could be detected on the shown agarose gel. (B) The sequencing of the final vector was performed by 4baseLab (Reutlingen, Germany) and approved the proper sequence of regions marked by arrows.

9.2 Vector maps

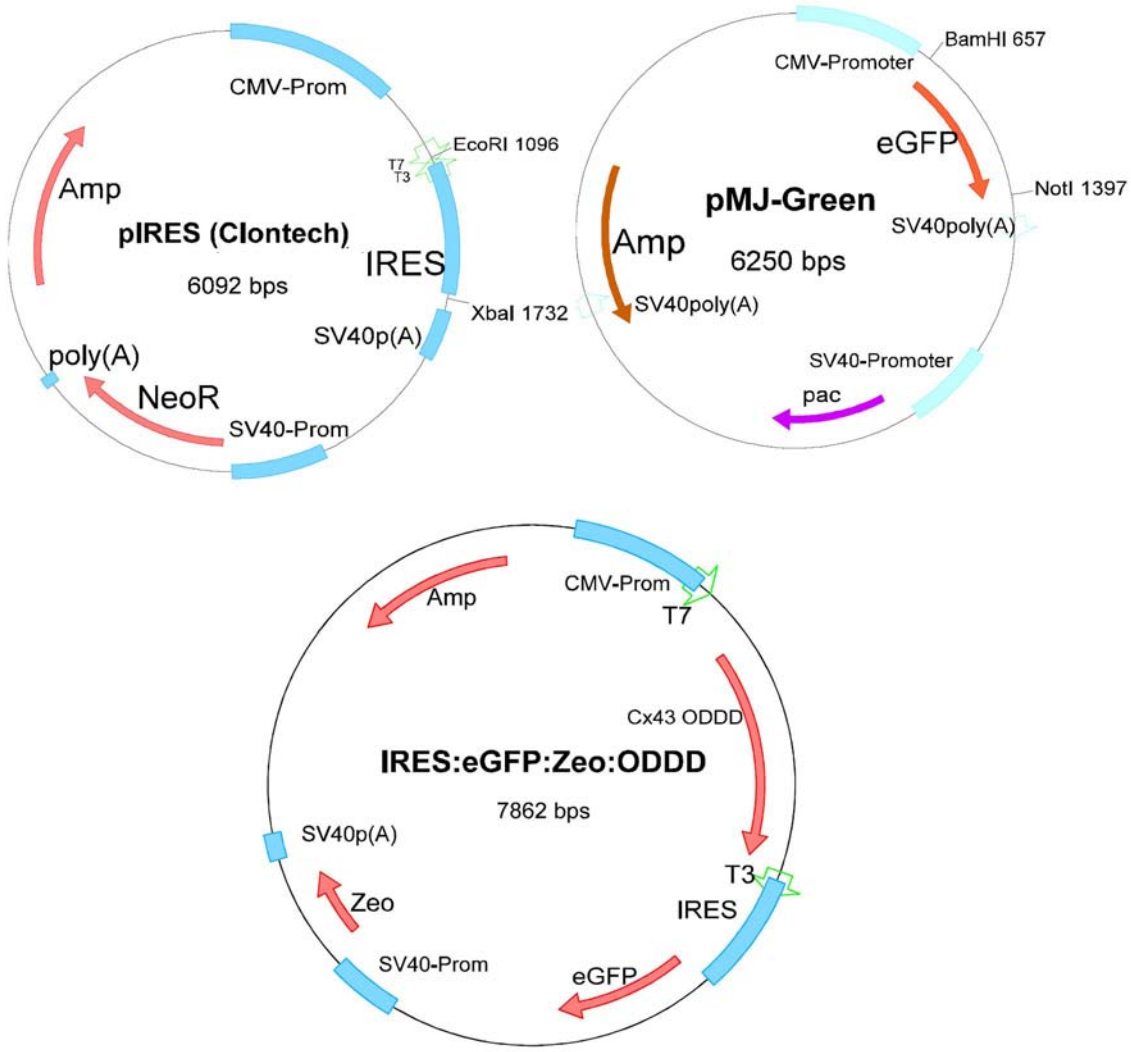

Figure 9.3: The vectors pIRES (clontech) and pMJ-Green (Maxeiner et al., 2005) and PCR amplicons containing mutated Cx43 coding regions were used to clone the eukaryotic IRES:eGFP:Zeo:ODDD vectors. These vectors were used to express the mutated Cx43 G138R, I31M, I143S and H194P proteins in HeLa cells. In these cells CMV promoter drives the Cx43 ODDD mutations followed by the IRES cassette (internal ribosomal entry site) and eGFP. This combination of gene cassettes facilitated the expression of the eGFP reporter in cytoplasm of cells expressing the mutant proteins.